Fermion Mass Generation without Spontaneous Symmetry Breaking

by

Venkitesh P Ayyar

Department of Physics
Duke University

Date: _____

Approved:

_____
Shailesh Chandrasekharan, Supervisor

_____
Mark Kruse

_____
Ronen Plesser

_____
Harold Baranger

_____
Joshua Socolar

Dissertation submitted in partial fulfillment of the requirements for the degree of
Doctor of Philosophy in the Department of Physics
in the Graduate School of Duke University
2016

Abstract

Fermion Mass Generation without Spontaneous Symmetry Breaking

by

Venkitesh P Ayyar

Department of Physics
Duke University

Date: _____

Approved:

_____
Shailesh Chandrasekharan, Supervisor

_____
Mark Kruse

_____
Ronen Plesser

_____
Harold Baranger

_____
Joshua Socolar

An abstract of a dissertation submitted in partial fulfillment of the requirements for the degree of Doctor of Philosophy in the Department of Physics in the Graduate School of Duke University
2016

Abstract

The conventional mechanism of fermion mass generation in the Standard Model involves Spontaneous Symmetry Breaking (SSB). In this thesis, we study an alternate mechanism for the generation of fermion masses that does not require SSB, in the context of lattice field theories. Being inherently strongly coupled, this mechanism requires a non-perturbative approach like the lattice approach.

In order to explore this mechanism, we study a simple lattice model with a four-fermion interaction that has massless fermions at weak couplings and massive fermions at strong couplings, but without any spontaneous symmetry breaking. Prior work on this type of mass generation mechanism in 4D, was done in the late 1980's using either mean-field theory or Monte-Carlo calculations on small lattices. In this thesis, we have developed a new computational approach that enables us to perform large scale quantum Monte-Carlo calculations to study the phase structure of this theory. In 4D, our results confirm prior results, but differ in some quantitative details of the phase diagram. In contrast, in 3D, we discover a new second order critical point using calculations on lattices up to size 60^3. Such large scale calculations are unprecedented. The presence of the critical point implies the existence of an alternate mechanism of fermion mass generation without any SSB, that could be of interest in continuum quantum field theory.

To my parents

Contents

List of Tables

List of Figures

List of Abbreviations and Symbols

Symbols

$\not{\partial}$	$\gamma_\mu \partial_\mu$.

Abbreviations

SSB	Spontaneous Symmetry Breaking.
QFT	Quantum Field theory.
QCD	Quantum Chromodynamics.
PMW	Paramagnetic weak.
PMS	Paramagnetic strong.
FM	Ferromagnetic.
RG	Renormalization Group.
PBC	Periodic Boundary conditions.
APBC	Anti-periodic Boundary conditions.

Acknowledgements

I owe most thanks to my research advisor, Shailesh Chandrasekharan, for guiding me through this research and helping my growth as a physicist. I would like to express my gratitude to Duke University for giving me this wonderful opportunity to pursue research in physics and providing excellent resources to help me grow as a researcher. I would like to thank the Department of Energy[1] for sponsoring this research. I would like to thank other members of the Duke LEFT group, fellow graduate students Arman Margaryan, Emilie Huffman, Reginald Bain and Yiannis Makris and professors Thomas Mehen and Roxanne Springer, for useful discussions and guidance. I would also like to thank Prof. Berndt Mueller for providing research guidance during my early graduate years.

Such computationally intensive research cannot be carried out without the help of computing resources and I owe thanks to the Open Science Grid[2](OSG) and Duke Research Computing for providing computing resources, knowledge and assistance. A special thanks goes out to Duke IT staff members Jimmy Dorff and Barry Wilson for all their help in setting up the computing environment. I would also like to thank fellow graduate students Jonah Bernhard, Forrest Friesen and Leo Fang for helpful discussions. A special thanks to graduate students Jonathan Mueller, Sean Finch, Chris Pollard, Kevin Claytor, Ting Ke and Marco Bertolini for making graduate

[1] This work has been supported by the U.S. Department of Energy, Office of Science, Nuclear Physics program under Award No. DE-FG02-05ER41368.

[2] The Open Science Grid is supported by the National Science Foundation and the U.S. Department of Energy's Office of Science.

student life a such a wonderful experience.

Last but not least, I owe thanks to my parents Mr. and Mrs. Ayyar and my sister Priya, for all they have done over the years. None of this would have been possible without their sacrifice and support.

1

Introduction

The origin of fermion mass is a fundamental problem in particle physics [1]. Fermion mass terms in a free theory break certain symmetries which we call generically as 'chiral symmetries'. One way to produce fermion masses is by explicitly breaking these symmetries. Fermion masses can also be produced dynamically, through the physics of Spontaneous Symmetry Breaking (SSB) [2]. This latter scenario is realized in the Standard Model. The action of a system undergoing SSB preserves the symmetries of interest, however the vacuum is not invariant under the full symmetry. In the Standard Model, SSB occurs in two different sectors:

i) The Higgs mechanism in the Electro-weak sector.

ii) Chiral symmetry breaking in the Strong sector.

The electro-weak sector of the Standard Model has an $SU(2)_L \times U(1)_Y$ gauge symmetry [3]. Fermion mass terms break this symmetry and are hence not allowed in the action. In order to give fermions their mass, a Higgs field is introduced that couples to the fermions via Yukawa couplings. The Higgs field gets an expectation value that spontaneously breaks the $SU(2)_L \times U(1)_Y$ symmetry thus giving masses

to the fermions. This results in the formation of fermion bilinear condensates. This mechanism also provides masses to the W^+, W^- and Z gauge bosons.

In contrast, in the strong sector of the Standard Model SSB is achieved without the introduction of a Higgs field. The QCD Lagrangian with gluons and two flavors of massless quarks has an $SU(2)_L \times SU(2)_R$ chiral symmetry in addition to an SU(3) color gauge symmetry. The chiral symmetry breaks spontaneously due to non-perturbative dynamics. This results in the formation of fermion bilinear condensates that make the quarks massive. This phenomenon is often referred to as 'dynamical symmetry breaking' [4, 5].

In this thesis work, we explore an alternate mechanism for fermion mass generation that does not involve any SSB. Starting with an action that forbids fermion bilinear mass terms, we find that fermions become massive without breaking any symmetries at strong couplings .

1.1 Review of SSB

The mechanism of SSB can be elucidated by a simple toy model of fermions interacting with a complex scalar field. Consider a model with one flavor of four-component Dirac fermions represented by the Grassman fields $\overline{\psi}$ and ψ, coupled to a complex scalar field ϕ. The Euclidean action for this theory is given by

$$S_E = \int d^4x \left\{ \overline{\psi}\gamma_\mu\partial_\mu\psi + (\partial_\mu\phi^*)(\partial_\mu\phi) + V(\phi) - g\overline{\psi}\ \rho e^{i\gamma_5\varphi}\ \psi \right\} \tag{1.1}$$

where $V(\phi) = m^2|\phi|^2 + \frac{\lambda}{4}|\phi|^4$ ($\lambda > 0$) and the complex field ϕ is written as $\phi = \rho e^{i\varphi}$. The Dirac matrices γ_μ are 4×4 Hermitian matrices that satisfy the algebra $\{\gamma_\mu, \gamma_\nu\} = 2\delta_{\mu,\nu}$. This action is symmetric under the transformation $U_V(1) \times U_A(1)$ given by

$$\begin{aligned} U_V(1) &: \psi \to e^{-i\theta_V}\psi\ ,\ \overline{\psi} \to \overline{\psi}e^{i\theta_V}, \phi \to \phi \\ U_A(1) &: \psi \to e^{-i\gamma_5\theta_A}\psi\ ,\ \overline{\psi} \to \overline{\psi}e^{-i\gamma_5\theta_A}, \phi \to \phi\ e^{2i\theta_A} \end{aligned} \tag{1.2}$$

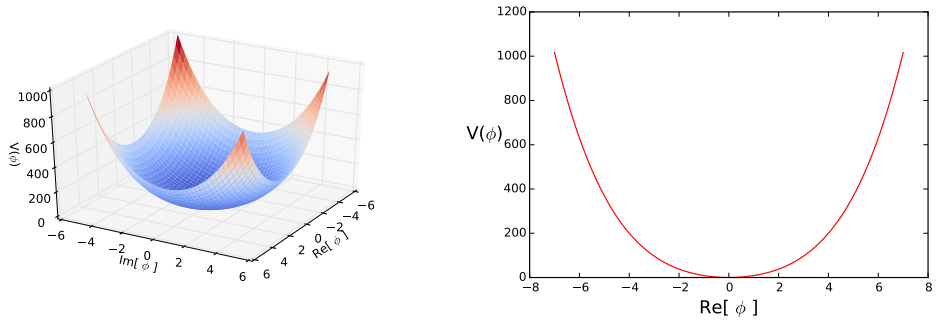

FIGURE 1.1: Plot of the potential $V(\phi)$ for $m^2 > 0$ as a function of ϕ. The left figure shows the variation of $V(\phi)$ in the complex ϕ plane while the right figure shows this variation along $\phi_I = 0$. For $m^2 > 0$, we have a global minimum at $|\phi| = 0$. This corresponds to a single complex massive scalar particle.

where γ_5 is defined as $\gamma_5 = \gamma_1\gamma_2\gamma_3\gamma_4$. From the action, it is clear that a fermion mass term of the form $m\overline{\psi}\psi$ explictly breaks the $U_A(1)$ symmetry. In fact, one can argue that no fermion bilinear term that is invariant under all the symmetries of the action exists.

The action in Eq. (1.1) can be rewritten in terms of left and right handed fields given by $\psi_L = (\frac{1-\gamma_5}{2})\psi$, $\psi_R = (\frac{1+\gamma_5}{2})\psi$, $\overline{\psi_L} = \overline{\psi}(\frac{1+\gamma_5}{2})$, $\overline{\psi_R} = \overline{\psi}(\frac{1-\gamma_5}{2})$. The action now takes the form

$$S_E = \int d^4x \left\{ \overline{\psi_L}\not{\partial}\psi_L + \overline{\psi_R}\not{\partial}\psi_R + (\partial_\mu\phi^*)(\partial_\mu\phi) + V(\phi) - g\overline{\psi_L}\psi_R\phi - g\overline{\psi_R}\psi_L\phi^* \right\} \quad (1.3)$$

where $\not{\partial} = \gamma_\mu\partial_\mu$. In this form, it can be seen that the action has an explicit $U_L(1) \times U_R(1)$ symmetry given by

$$\psi_L \to e^{i\theta_L}\psi_L \;\; ; \psi_R \to e^{i\theta_R}\psi_R \; ; \;\; \overline{\psi_L} \to e^{-i\theta_L}\overline{\psi_L} \; ; \;\; \overline{\psi_R} \to e^{-i\theta_R}\overline{\psi_R} \; ; \;\; \phi \to e^{i(\theta_L-\theta_R)}\phi$$

This is related to the $U_V(1) \times U_A(1)$ symmetry in Eq. (1.2). $\theta_L = \theta_R$ corresponds to the $U_V(1)$ symmetry while $\theta_L = -\theta_R$ corresponds to the $U_A(1)$ symmetry.

For $m^2 > 0$, the potential has a minimum at $\phi = 0$. This is shown in Fig. (1.1). In this regime, the action describes a theory of massless fermions interacting with a

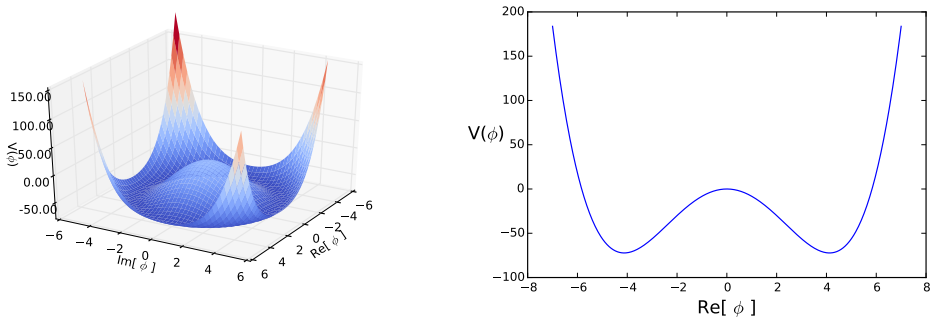

FIGURE 1.2: Plot of the potential $V(\phi)$ for $m^2 < 0$ as a function of ϕ. The left figure shows the variation of $V(\phi)$ vs ϕ in the complex plane while the right figure shows this variation along $\phi_I = 0$. In addition to a local maximum at $|\phi| = 0$, there exist an infinite number of minima at $|\phi|^2 = v$. This corresponds to a massless scalar π and a massive scalar σ.

complex boson ϕ of mass m. On the other hand, if $m^2 < 0$, $V(\phi)$ is the well known Mexican-hat potential. It has a local maximum at $\phi = 0$ and an infinite number of minima along $|\phi|^2 = v$ with $v = \sqrt{\frac{-2m^2}{\lambda}}$ as shown in Fig. (1.2). Without loss of generality, we can expand ϕ about one of these minima as $\phi = v + \frac{1}{\sqrt{2}}(\sigma + i\pi)$ and write the above action as

$$S_E = \int d^4x \left\{ \overline{\psi}\partial\!\!\!/\psi + \frac{1}{2}(\partial_\mu\sigma)^2 + \frac{1}{2}(\sqrt{2}m)^2\sigma^2 + \frac{1}{2}(\partial_\mu\pi)^2 - gv\overline{\psi}\psi + ... \right\} \tag{1.4}$$

where the dots denote higher order interaction terms. Thus, although the action preserves the axial symmetry, the choice of the vacuum v has broken this symmetry. This is the phenomenon of SSB. The theory now describes fermions interacting with two fields σ and π. The field σ describes a real massive scalar particle of mass $\sqrt{2}m$. The field π describing a massless scalar particle is called a Goldstone boson. According to Goldstone's theorem [6], SSB creates a massless boson for every generator of a continuous symmetry broken by the vacuum. In this case, since the vacuum v breaks the $U_A(1)$ symmetry, we have a single Goldstone boson π. Interestingly, the term $gv\overline{\psi}\psi$ resembles a mass term for the fermion. Thus, the fermions have acquired

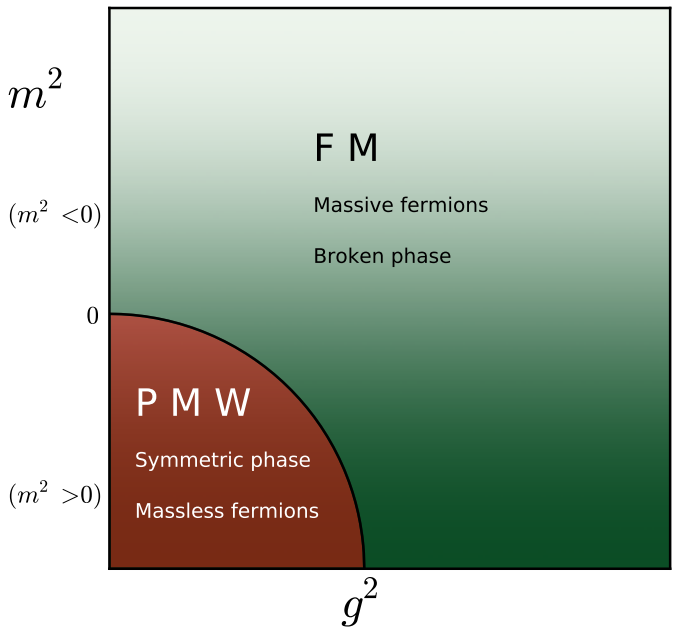

FIGURE 1.3: The Phase diagram showing the phase transition between the massless and massive fermionic phases. The red region represents a symmetric massless phase called the PMW phase. The grey region represents the spontaneously broken massive phase called the FM phase. m^2 is negative at the top and positive at the bottom.

a mass gv through the SSB of the axial symmetry $U_A(1)$. It can be shown that the fermion bilinear condensate $\langle\overline{\psi}\psi\rangle$ is non-zero.

It is interesting to look at the phase diagram in the $m^2 - g^2$ plane for a fixed value of $\lambda > 0$. When $m^2 > 0$, for small Yukawa couplings, we get massless fermions. However, as the coupling g crosses a threshold, previous work shows that the fermions become massive via SSB [7]. The phase with massless fermions at weak couplings is symmetric and hence called the Paramagnetic Weak phase (PMW), while the massive fermion phase is spontaneously broken and hence referred to as the Ferromagnetic phase (FM). This general phase diagram in the $m^2 - g^2$ plane is qualitatively shown in Fig. (1.3).

1.2 Alternate mechanism of mass generation

As explained above, SSB provides a way to generate fermion masses without explicitly breaking chiral symmetries. However, the vacuum does break the symmetry. Can there be other mechanisms to generate fermion masses that do not require SSB?

Lattice field theories are a good place to look for such alternate mechanisms, since they can be studied non-perturbatively and hence often show a much richer phase structure. Indeed, previous studies of lattice Yukawa models have shown the existence of a more interesting phase structure than that in Fig. (1.3) [8, 9]. These studies have found that, in addition to the symmetric massless (PMW) phase and the spontaneously broken massive (FM) phase obtained in the continuum, there can be an additional exotic phase at strong Yukawa couplings [10, 11]. In this phase, all fermion bilinear condensates vanish, but fermions are still massive. This exotic phase is thus a massive symmetric phase and is hence referred to as the Paramagnetic Strong phase (or the PMS phase). This qualitative phase structure is shown in Fig. (1.2).

The presence of the PMS phase indicates an alternate mechanism for fermion mass generation without SSB in lattice field theories. But, such a phase could very well be a lattice artifact without a continuum analog. However, if we could find a lattice model in which PMW and PMS phase boundaries touch each other at a second-order critical point, this would imply the existence of a continuum limit for the PMS phase and thus make this alternate mechanism of fermion mass generation of interest even in continuum field theory. In this thesis, we discover one such critical point in a specific lattice model in three dimensions. Further, it is a second order transition between two phases with the same symmetries that cannot be distinguished by a local order parameter.

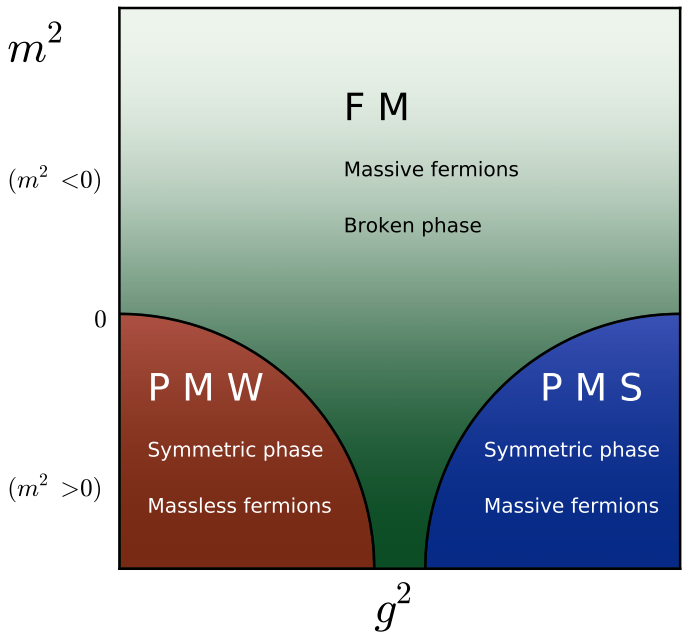

FIGURE 1.4: The complex phase structure obtained in some lattice field theories. In addition to the PMW and FM phases, these lattice theories show an exotic symmetric massive phase at strong couplings called the strong paramagnetic phase or PMS phase.

1.3 Four-fermion field theories

So far, we have focused on Yukawa models. However, we can also discuss the same physics using four-fermion models where the Higgs field is absent. For example, the action of one such four-fermion model that reproduces the physics of the Yukawa model in Eq. (1.5) is given by

$$S_{4f} = \int d^4x \left\{ \overline{\psi_L} \not{\partial} \psi_L + \overline{\psi_R} \not{\partial} \psi_R - U(\overline{\psi_L} \psi_R \overline{\psi_R} \psi_L) \right\} \tag{1.5}$$

Since the four-fermion coupling is perturbatively irrelevant, for small couplings we expect massless fermions. Previous studies of similar four-fermion models in the continuum using mean-field analysis [12, 13] have shown the existence of the spontaneously broken FM phase at larger values of the coupling U. Since we expect

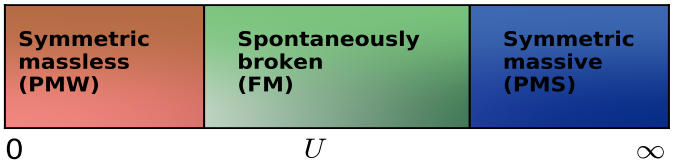

FIGURE 1.5: The three phase structure seen in four-fermion lattice models. The exotic PMS phase is expected as in Yukawa models.

the four-fermion theory to capture the physics along the horizontal line at large values of m^2 in Fig. (1.2), we also expect a PMS phase in an appropriate lattice four-fermion model at large U. The expected qualitative phase diagram in the space of the coupling constant U for these four-fermion lattice theories is shown in Fig. (1.5). The exotic scenario where the PMW phase touches the PMS phase is shown in Fig. (1.6).

In addition to retaining the rich phase structure of the Yukawa models, four-fermion models have become easier to study, thanks to recent Monte Carlo techniques like the Fermion Bag approach [14, 15]. In this thesis, we study a simple four-fermion lattice model in order to explore the phenomenon of fermion mass generation without SSB. While the phase diagram in 3D is consistent with Fig. (1.6), in 4D we find the phase diagram to be consistent with Fig. (1.5). Our results in 3D have also been observed recently using similar models motivated in both particle physics [16] and [17, 18, 19] condensed matter physics.

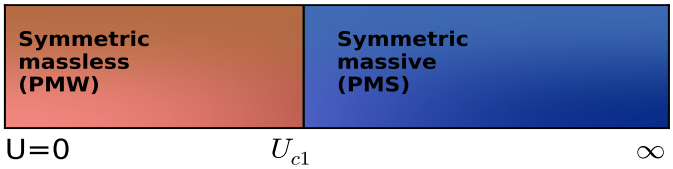

FIGURE 1.6: The phase structure seen in our four-fermion lattice model in 3D. The presence of a second-order critical point at U_{c1} separating the PMW and PMS phases points to a continuum theory that exhibits fermion mass generation without SSB.

1.4 Organization of thesis

The thesis is organized as follows. Section 2 introduces the lattice field theory approach and its connection to continuum quantum field theory. Section 3 introduces the model we study, its symmetry properties, and the approach we use to solve it. Section 4 discusses the concept of Monte-Carlo methods used in lattice field theories. It also discusses the computational methods used. Sections 5 and 6 present the results in 3D and 4D. Section 7 summarises the conclusions and the implications of this work.

2

The Lattice Approach

The standard method for solving continuum quantum field theories (QFTs) is by using perturbation theory. In this approach, one computes quantities analytically using Feynman diagrams up to a certain order in the coupling constants. When loop diagrams arise, they can diverge and so one needs to develop a renormalization procedure with an appropriate regulator so that physical observables are finite, when the regulator is removed. Further, due to the sharp rise in the number of Feynman diagrams with the order of perturbation theory, computations are not practical beyond 4th or 5th order. In most cases, the perturbative expansion is also an asymptotic series. Hence, while the perturbative approach is very useful to compute a large number of quantities like scattering cross-sections, decay rates, etc., it only works for weakly coupled theories. For strongly coupled theories like QCD, one needs to turn to non-perturbative approaches like lattice field theory.

A lattice field theory can be understood from two different perspectives:

i) As a regularization of a continuum QFT.

In this perspective, a lattice field theory is constructed to study a continuum

QFT with an ultraviolet momentum cut-off, obtained by discretizing it in position space. If Λ is the usual ultraviolet cut-off of the continuum theory, the lattice spacing a of the lattice theory acts as this cut-off and is related to it as $a \sim \frac{1}{\Lambda}$. The continuum theory with a momentum cutoff and the lattice theory can be matched in perturbation theory. However, the lattice theory can also explore the strong coupling regime of the theory. In other words, the lattice theory helps to define the original continuum QFT even in the strong coupling regime.

ii) As an interesting quantum many-body theory in its own right.

In this perspective, the lattice theory is taken to be a quantum many-body theory in its own right that can be studied non-perturbatively to explore interesting phase structures and continuum limits, if they exist. For example, the theory may model a condensed matter system, which has a natural lattice spacing. Such lattice theories often exhibit a rich phase structure. Moreover, if the phase diagram harbors second-order critical points, then a continuum limit of the lattice theory exists, where a continuum QFT should emerge. This will be explained later in this chapter.

2.1 Lattice field theory as a regularized continuum QFT

Let us first explain the view point that lattice field theory is a way to nonperturbatively regulate a continuum QFT using examples of free field theory. For this purpose we start with simple, free continuum field theories containing either bosons or fermions, and discretize them and compare their properties with the corresponding continuum theory. The discussion below follows [20].

2.1.1 Lattice bosons

Our aim is to discretize a simple continuum field theory with a single scalar field $\phi(x)$. Its continuum action in Euclidean space is given by

$$S_b = \frac{1}{2}\int d^4x \left[\phi(x)(-\partial_\mu\partial_\mu + m^2)\phi(x)\right]. \tag{2.1}$$

In the path integral approach in Euclidean space, the propagator is defined as the two point correlation function of the statistical mechanical system defined by the above action. It is given by

$$D_B(x,y) = \langle\phi(x)\phi(y)\rangle = \frac{\int[d\phi]\ (\phi(x)\phi(y))\ e^{-S}}{\int[d\phi]\ e^{-S}} \tag{2.2}$$

The expression for the bosonic propagator in position space for the action defined in Eq. (2.1) is given by

$$D_B(x,y) = \int \frac{d^4k}{(2\pi)^4}\ e^{-ik\cdot(x-y)}\frac{1}{k^2+m^2} \tag{2.3}$$

Let us now see how this propagator is reproduced from a lattice regulated theory. Using a lattice spacing a, we can discretize space-time on a hypercubic lattice so that the fields are defined on the space-time lattice site na. We can then discretize the second derivative term as

$$\partial_\mu\partial_\mu\phi(x) \to \frac{1}{a^2}\sum_{\mu=1}^{4}(\phi(na+\hat{\mu}) + \phi(na-\hat{\mu}) - 2\phi(na)) \tag{2.4}$$

where $\hat{\mu}$ represents the unit vector along the direction $\mu = 1,2,3,4$. With this substitution the continuum action is transformed into the lattice action

$$S_{b(lattice)} = \frac{a^4}{2}\sum_{n,m}\phi_n K_{n,m}\phi_m \tag{2.5}$$

$$K_{n,n'} = \frac{1}{a^2}\left[-\sum_{\mu}(\delta_{n+\hat{\mu},n'} + \delta_{n-\hat{\mu},n'} - 2\delta_{n,n'}) + m^2a^2\delta_{n,n'}\right] \tag{2.6}$$

where $\phi_n = \phi(na)$ is the lattice field. The bosonic propagator in the lattice theory can be calculated easily and one gets

$$D_B(n,n') \;=\; \langle\phi_n\phi_{n'}\rangle = a^2\int_{\frac{-\pi}{a}}^{\frac{\pi}{a}}\frac{d^4k}{(2\pi)^4}\frac{e^{ik\cdot(n-n')\ a}}{\sum_\mu 4\sin^2\left(\frac{k_\mu a}{2}\right) + a^2m^2} \tag{2.7}$$

In the above expression, it is clear that, $2\sin\left(\frac{k_\mu a}{2}\right) \to k_\mu a$ as $a \to 0$, and we recover the continuum expression in Eq. (2.3). Thus, the lattice propagator yields the continuum propagator in the continuum limit ($a \to 0$). When $a \neq 0$, it gives a regulated theory with a momentum cut-off π/a.

2.1.2 Lattice fermions

We would like to repeat this procedure for free fermions. Let us consider the Dirac action representing one flavor of free massive fermions.

$$S_f = \int d^4x\left[\overline{\psi}(x)(\gamma_\mu\partial_\mu + m)\psi(x)\right] \tag{2.8}$$

where the γ_μ are the Dirac matrices defined in Section 1.1. In analogy with Eq. (2.2), the fermionic propagator is defined as

$$D_F(x,y) = \langle\psi(x)\overline{\psi}(y)\rangle = \frac{\int[d\psi][d\overline{\psi}]\ (\psi(x)\overline{\psi}(y))\ e^{-S}}{\int[d\psi][d\overline{\psi}]\ e^{-S}} \tag{2.9}$$

where the path integral is defined over Grassmann valued fields ψ and $\overline{\psi}$. Note $D_F(x,y)$ is a 4×4 matrix in the Dirac space. Performing the Grassmann integration with the action given in Eq. (2.8), one obtains

$$D_F(x,y) = \int\frac{d^4k}{2\pi^4}e^{-ik\cdot x}\frac{-i\gamma_\mu k_\mu + m}{k^2+m^2} \tag{2.10}$$

Discretizing space-time on a hypercubic lattice as before and using the symmetric lattice derivative with lattice spacing a given by

$$\partial_\mu \psi(x) \to \frac{1}{2a} \sum_{\mu=1}^{4} (\psi(na + \hat{\mu}) - \psi(na - \hat{\mu})) \tag{2.11}$$

we obtain the lattice fermion action

$$S_{f\,(lattice)} = a^4 \sum_{n,m,\alpha,\beta} \overline{\psi}_{n,\alpha} K_{n,n'} \psi_{n',\beta} \ , \tag{2.12}$$

where

$$K_{n,n'} = \frac{1}{a} \left[\sum_{\mu} \frac{1}{2} (\gamma_\mu)_{\alpha\beta} \left(\delta_{n+\hat{\mu},n'} - \delta_{n-\hat{\mu},n'} \right) + ma \delta_{n,n'} \delta_{\alpha,\beta} \right] \ , \tag{2.13}$$

and α, β denote spinor indices. The lattice fermionic propagator is given by

$$D_F(n,n') = \langle \psi_x \overline{\psi_y} \rangle = a \int_{\frac{-\pi}{a}}^{\frac{\pi}{a}} \frac{d^4k}{(2\pi)^4} \frac{e^{ik\cdot(n-n')a} \left(-i \sum_\mu \gamma_\mu \sin(k_\mu a) + ma \right)}{\left(\sum_\mu \sin^2(k_\mu a) + m^2 a^2 \right)} \tag{2.14}$$

Since the sine function has zeros at all points where $k_\mu = 0$ or π/a, in the limit $a \to 0$, the above propagator gets contributions from a total of 16 poles in momentum space. Close to these poles, the propagator in momentum space looks exactly the same as the continuum propagator given in Eq. (2.10). In other words, there exists a 16-fold degeneracy in the ground-state physics and this can be interpreted as though the lattice theory describes 16 flavors of fermions. Thus, discretization has created multiple flavors of fermions. This phenomenon is called *Fermion doubling*. In general, discretizing a fermionic theory in a d dimensional Euclidean space produces 2^d fermion flavors.

The phenomenon of fermion doubling has significant implications when relating the lattice theory back to the continuum theory. For bosons, the lattice theory will reproduce the continuum physics in the limit $a \to 0$. In contrast, for fermions,

the lattice theory now needs to be mapped to a continuum theory having 2^d times the original number of fermion flavors. There are ways to circumvent this doubling problem at the cost of breaking the chiral symmetry using what are called *Wilson fermions* [20]. Other formulations that retain the chiral symmetry at the cost of making the action non-local are *Domain wall fermions*, *SLAC fermions* [21, 22].

2.2 Lattice field theory as an interesting quantum many-body theory.

Let us now explain the second view point that lattice field theories can be studied as quantum many-body theories that are interesting in their own right. This is especially true in the presence of fermions, due to the phenomenon of fermion doubling. Examples of such interesting lattice field theories often arise in condensed matter physics. A simple example is the tight binding model of graphene, where electrons hop on a honeycomb lattice. In this model, massless Dirac fermions appear naturally at low energies. In the action formulation, they are similar to staggered fermions [23] discussed below.

2.2.1 Staggered fermions

We begin with the lattice fermion action in Eq. (2.13) representing 16 fermion flavors and set $a = 1$. In this new notation, all lengths are measured in terms of the lattice spacing. The resulting action has the form

$$S = \frac{1}{2} \sum_{n,\hat{\mu}} \overline{\psi}_n \left[\gamma_\mu \psi_{n+\hat{\mu}} - \gamma_\mu \psi_{n-\hat{\mu}} \right] + m \overline{\psi_n} \psi_n \tag{2.15}$$

where $n \equiv (n_1, n_2, n_3, n_4)$ represents the lattice site. We then perform the variable transformation

$$\psi_n = \gamma_1^{n_1} \gamma_2^{n_2} \gamma_3^{n_3} \gamma_4^{n_4} \ \chi_n \tag{2.16}$$

and rewrite the action as

$$S = \frac{1}{2}\sum_{n,\hat{\mu}} \overline{\chi}_n \eta_{\mu,n} \left[\chi_{n+\hat{\mu}} - \chi_{n-\hat{\mu}}\right] + m\overline{\chi_n}\chi_n \tag{2.17}$$

where $\eta_{1,n} = 1 \;\; \eta_{2,n} = (-1)^{n_1} \;\; \eta_{3,n} = (-1)^{n_1+n_2} \;\; \eta_{4,n} = (-1)^{n_1+n_2+n_3}$ and χ and $\overline{\chi}$ are four-component Grassmann variables. Since the spinor space has been diagonalized, we obtain four identical copies of fermions. We throw away three of these to get the Staggered fermion action

$$\begin{aligned} S_{staggered} &= \sum_{x,y} \overline{\psi}_x M_{x,y} \psi_y + m\overline{\psi}_x \psi_x \\ M_{x,y} &= \sum_{\hat{\alpha}=1,2,3,4} \frac{1}{2}\eta_{x,\hat{\alpha}} \left[\delta_{x,y+\hat{\alpha}} - \delta_{x,y-\hat{\alpha}}\right] \\ \eta_{x,1} &= 1 \;\; \eta_{x,2} = (-1)^{x_1} \;\; \eta_{x,3} = (-1)^{x_1+x_2} \;\; \eta_{x,4} = (-1)^{x_1+x_2+x_3} \end{aligned} \tag{2.18}$$

where we now define the one-component Grassmann fields $\overline{\psi}$ and ψ on each lattice site. As opposed to the 16 flavors in the naive lattice fermion action, the staggered fermion action has only four extra flavors in 4D. The Staggered fermion formulation preserves some remnants of the continuum symmetries that keep fermions massless at the cost of retaining some of the extra flavors obtained due to fermion doubling. For completeness, we present the form of the staggered fermion propagator below.

$$D_{n,n'} = \frac{1}{L^3}\sum_k \frac{-\sin k.(n'-n)(\sum_\alpha \eta_{\alpha,n} \sin k_\alpha) + m\cos k.(n'-n)}{\sum_\beta \sin^2 k_\beta + m^2} \tag{2.19}$$

2.2.2 Reduced staggered fermions

In the above section, we defined the action for one flavor of staggered fermions with two Grassmann fields $\overline{\psi}$ and ψ defined at every point on the lattice. A slight redefinition of the fields yields the reduced staggered fermion action [24, 25] given by

$$S_{reduced\ staggered} = \frac{1}{2}\sum_{i=1}^{2}\sum_{x,y} \psi_{x,i} M_{x,y} \psi_{y,i} + m\psi_{x,1}\psi_{x,2} \tag{2.20}$$

where, the $\overline{\psi}$ and ψ at each site have been replaced by the two flavors $\psi_{x,1}$ and $\psi_{x,2}$. Thus, one flavor of staggered fermions is equivalent to 2 flavors of reduced staggered fermions. In the massless limit, the two flavors decouple from each other. In our work, we will use 4 flavors of reduced staggered fermions.

2.3 Continuum limit

Let us consider a lattice field theory with spacing a and some coupling Y which can be tuned to a second-order critical point $Y = Y_c$. From the theory of second-order phase transitions, we know that correlation functions diverge at Y_c. If ξ is one such physical correlation length, since all lengths are measured in terms of the lattice spacing a,

$$\lim_{Y \to Y_c} \frac{\xi}{a} \to \infty \tag{2.21}$$

In condensed matter physics, the lattice spacing is natural and hence, one can interpret the physical correlation length ξ to diverge as we approach Y_c. On the other hand, in particle physics, the correlation length ξ is related to m^{-1}, where m is mass of a particle, which is a physical quantity. Hence one can interpret the approach to the critical point as though the lattice spacing a vanishes as $Y \to Y_c$. This implies that as Y approaches Y_c, the physics of the lattice theory is described by a renormalizable continuum theory.

Wilson has argued that the divergence of the correlation length is related to the renormalization group (RG) flows near a fixed point in the space of coupling constants of a continuum QFT [26]. In particular, a diverging correlation length is related to a relevant (or marginally relevant) direction at the fixed point. Using the dimensionless variable $y = \frac{Y - Y_c}{Y_c}$, an RG calculation shows that the correlation length

for relevant couplings diverges as

$$\xi \sim \frac{1}{y^{\nu}} \tag{2.22}$$

where ν is called a critical exponent [27]. We can use the above expression to derive a finite size scaling relation for a general observable O in the critical region. In a lattice theory with lattice size L, the only length scales in the critical region are L and ξ. Hence, the observable O can only depend on L through the relation

$$O \sim L^{p}\ f(L/\xi) \tag{2.23}$$

where p is the length dimension of O. Using $\xi \sim \frac{1}{y^{\nu}}$ from Eq. (2.22), the above equation becomes

$$O \sim L^{p}\ f(y^{\nu}\ L) \tag{2.24}$$

This can be simplified to give

$$O \sim L^{p}\ \tilde{f}(y\ L^{1/\nu}) \tag{2.25}$$

where $\tilde{f}(x)$ is a function that must be analytic near $x = 0$. Eq. (2.25) expresses the observable O in terms of the coupling Y and lattice size L. We will use this form later in Chapter 5 to estimate the critical exponents close to the transition.

Since it is the only currently known technique to study strongly interacting systems ab initio, the lattice method has been used extensively to study QCD. These have provided accurate theoretical predictions of experimentally measured quantities like hadron spectrum, form factors, etc. [28, 29, 30, 31, 32]. In addition, lattice field theories with critical points are by themselves very interesting. At these points, different lattice systems are expected to flow to the same fixed points at long distances and hence describe the same low-energy physics. This leads to the concept of universality classes that are classified by the fixed points [27].

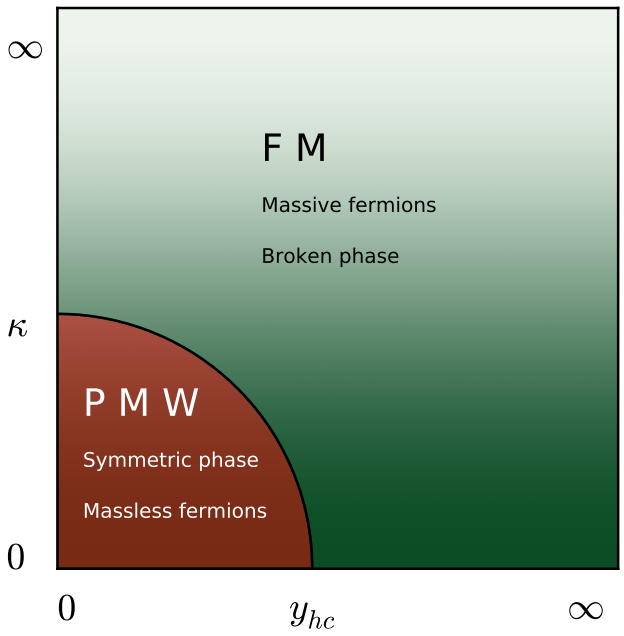

FIGURE 2.1: The Phase diagram for the hypercubic Yukawa model. This model contains the PMW phase and the FM phase.

2.4 Lattice Yukawa models

As explained in the Introduction, lattice field theories with Yukawa couplings have been studied extensively on the lattice and these show a rich phase structure. Here, we discuss two such models that give qualitatively different phase diagrams.

These models were first studied by Lee, Shigemitsu and Shrock in [10] with staggered fermions interacting with a scalar field ϕ in 4 Euclidean dimensions. Two types of interactions were explored: a local and a hypercubic Yukawa interaction. The actions for these two models are given by

$$S = S_B + S_F + S_Y \tag{2.26}$$

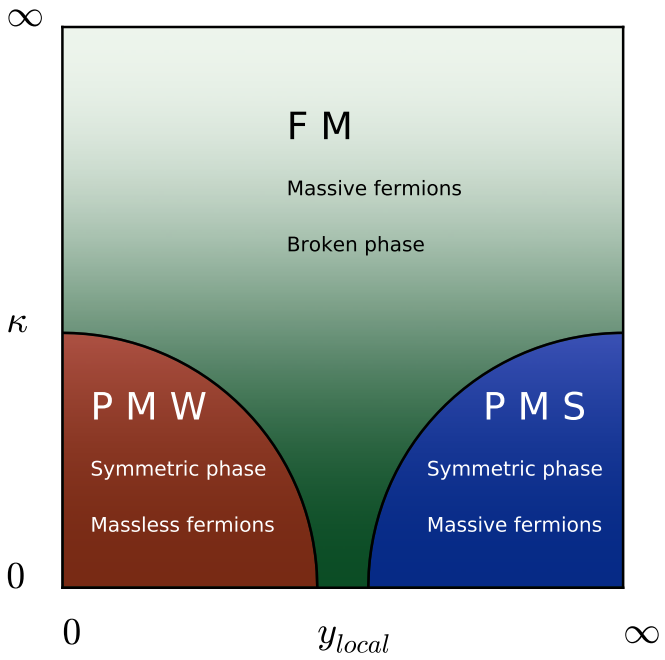

FIGURE 2.2: The phase diagram for the local Yukawa model. It shows the strong paramagnetic phase (PMS) phase in addition to the PMW and FM phases seen in the hypercubic Yukawa model.

where S_B and S_F are the same for both models and are given by

$$S_B = \sum_n \phi_n^2 - 2\kappa \sum_{n,\mu} \phi_n \phi_{n+\hat{\mu}} + \lambda \sum_n (\phi_n^2 - 1)^2 \tag{2.27}$$

$$S_F = \frac{1}{2} \sum_{n,\mu,f} \overline{\chi}_{n,f} \eta_{n,\mu} (\chi_{n+\hat{\mu}} - \chi_{n-\hat{\mu}}) + \sum_{n,f} m_f \overline{\chi}_n \chi_{n,f} \tag{2.28}$$

The two models differ in their Yukawa interactions. In one model, the bosonic field is associated with the center of a hypercube (hc) and couples to the fermion fields at all the corners of the hypercube, while in the other model, it is associated with a lattice site (local) and only couples to the fermion fields on that site. The hypercubic and local Yukawa interactions are given by

$$S_Y = S_{Y,hc} = 2^{-d} y_{hc} \sum_n \phi_n \sum_{n' \epsilon hc(n);f} \overline{\chi}_{n',f} \chi_{n',f} \tag{2.29}$$

$$S_Y = S_{Y,local} = y_l \sum_n \phi_n \sum_f \overline{\chi}_{n,f} \chi_{n,f} \tag{2.30}$$

where $hc(n)$ denotes the corners associated with the hypercube centered at n, f donotes fermion flavor and as before, $\hat{\mu}$ denotes the unit vector in the direction μ.

It was discovered in [10] that the hypercubic Yukawa model shows a phase structure with just PMW and FM phases as shown in Fig. (2.1), while the phase diagram of the local Yukawa model contains the exotic PMS phase at strong couplings in addition to the PMW and FM phases discussed in the Introduction as shown in Fig. (2.2). In fact, some mean field calculations for the local Yukawa coupling [33, 34] have predicted a direct first order transition between the PMW and PMS phases in 3D. In this thesis, we find a single second-order critical point separating the PMS and PMW phases in 3D at $\kappa = 0$.

3

Model and Symmetries

In this thesis, we wish to use lattice field theory in order to explore if the PMW and PMS phases, introduced in Chapter 1, may be connected through a direct phase transition as suggested in Fig. (1.6). If this phase transition turns out to be second order, we would establish that the PMS phase is of interest in continuum quantum field theory since we can use the critical point to define a continuum limit. To simplify our computations, instead of studying the Yukawa model discussed in the previous chapter, we study its four-fermion limit. While earlier work was done in 4D mostly using mean field theory, here we study the theory in both 3D and 4D.

3.1 Model

Our model contains 4 flavors of massless reduced staggered fermions interacting via an on-site four-fermion interaction. The action of our model is given by

$$S = S_0 - U \sum_x \left(\psi_{x,1}\psi_{x,2}\psi_{x,3}\psi_{x,4}\right), \tag{3.1}$$

where S_0 is the free part of the action and is given by

$$S_0 = \frac{1}{2}\sum_{i=1}^{4}\sum_{x,y}\psi_{x,i}M_{x,y}\psi_{y,i}. \tag{3.2}$$

Here, $\psi_{x,i},\ i = 1,2,3,4$ are four independent Grassmann valued fields that represent the four flavors of reduced staggered fermions, x represents the sites of a cubic (3D) or hypercubic (4D) lattice, and the free staggered fermion matrix M has been defined in Eq. (2.18). Four flavors of reduced staggered fermions are equivalent to two flavors of regular staggered fermions as described in Chapter 2. More details can be found in [35]. The partition function for this system can be written as

$$Z = \int \left[d\psi_1 d\psi_2 d\psi_3 d\psi_4\right] e^{-S_0} e^{-U\sum_x \psi_{x,1}\psi_{x,2}\psi_{x,3}\psi_{x,4}}. \tag{3.3}$$

The functional integration is over all the four independent Grassmann fields $\psi_{x,i},\ i = 1,2,3,4$.

We define the parity of each site as $\epsilon_x = (-1)^{x_1+x_2+x_3}$. Sites with $\epsilon_x = 1$ are called even sites and those with $\epsilon_x = -1$ are called odd sites. In our work, we use symmetrical lattices of equal size L in each direction and take the large L limit to explore ground state properties. In order to extract results using finite lattices, we need to define boundary conditions. The most common ones are periodic boundary conditions (PBC) or anti-periodic boundary conditions (APBC). These give rise to momenta of the form

$$p_\mu = \begin{cases} \frac{2\pi}{L}\ k_\mu & \text{for PBC} \\ \frac{2\pi}{L}\ (k_\mu + \frac{1}{2}) & \text{for APBC} \end{cases};\ k_\mu = 0,1,2...(L-1). \tag{3.4}$$

where $\mu = 1,2,3,4$ represents the direction. Since, imposing PBCs in every direction results in zero modes, in the massless limit, Eq. (2.19) shows that the resulting propagators will be singular. To avoid this, APBCs are often imposed in at least one direction. In this work, we impose anti-periodic boundary conditions in all directions.

3.2 Symmetries

The action given in Eq. (3.1) is symmetric under the usual space-time lattice transformations and an internal $SU(4)$ transformation in 3D and 4D [25, 36]. For three dimensions, these are listed below.

(i) Shift Symmetry:

$$\psi_{x,i} \to \xi_{x,\hat{\alpha}} \psi_{x+\hat{\alpha},i}, \tag{3.5}$$

where $\xi_{x,\hat{1}} = (-1)^{x_2+x_3}$, $\xi_{x,\hat{2}} = (-1)^{x_3}$, and $\xi_{x,\hat{3}} = 1$.

(ii) Space-time rotations:

$$\psi_{x,i} \to S_R(R^{-1}x)\psi_{R^{-1}x,i}, \tag{3.6}$$

where $R \equiv R^{(\rho\sigma)}, \rho \neq \sigma$ is the rotation $x_\rho \to x_\sigma$,$x_\sigma \to -x_\rho$, and $x_\tau \to x_\tau$ when $\tau \neq \rho, \sigma$ and $S_R(x) = \frac{1}{2}(1 \pm \eta_{\hat{\rho}}(x)\eta_{\hat{\sigma}}(x) \mp \xi_\rho(x)\xi_\sigma(x) + \eta_{\hat{\rho}}(x)\eta_{\hat{\sigma}}(x)\xi_\rho(x)\xi_\sigma(x))$ where the two signs represent the cases $\rho > \sigma$ and $\rho < \sigma$ respectively.

(iii) Axis reversal:

$$\psi_{x,i} \to (-1)^{x_\rho}\psi_{(I^\rho x),i} \tag{3.7}$$

where $I^\rho x$ is the axis reversal operation on x which changes $x_\rho \to -x_\rho$ and $x_\sigma \to x_\sigma, \sigma \neq \rho$.

(iv) Global $SU(4)$ transformations:

$$\begin{pmatrix} \psi_{x_e,1} \\ \psi_{x_e,2} \\ \psi_{x_e,3} \\ \psi_{x_e,4} \end{pmatrix} \to V \begin{pmatrix} \psi_{x_e,1} \\ \psi_{x_e,2} \\ \psi_{x_e,3} \\ \psi_{x_e,4} \end{pmatrix} \tag{3.8a}$$

$$\begin{pmatrix} \psi_{x_o,1} \\ \psi_{x_o,2} \\ \psi_{x_o,3} \\ \psi_{x_o,4} \end{pmatrix} \to V^* \begin{pmatrix} \psi_{x_o,1} \\ \psi_{x_o,2} \\ \psi_{x_o,3} \\ \psi_{x_o,4} \end{pmatrix} \tag{3.8b}$$

where x_e and x_o refer to even and odd lattice sites respectively, and V is an $SU(4)$ matrix in the fundamental representation.

Similar transformations exist even in 4D. In addition, the free action S_0 is also symmetric under the $U(1)$ symmetry given by

$$\psi_{x,i} \to e^{i\theta\epsilon_x}\psi_{x,i} \tag{3.9}$$

where ϵ_x is the site-parity of site x. In many four-fermion models, spontaneous breaking of this symmetry results in massive fermions. However in our model, although this symmetry is broken explicitly by the interaction, the fermions remain massless at weak couplings because the other symmetries forbid fermion bilinear mass terms. The corresponding mass order parameters were constructed in [25, 36] and are given by

$$O^0_{a,b}(x) = \psi_{x,a}\psi_{x,b} \tag{3.10a}$$

$$O^1_{\mu,a}(x) = \epsilon_x\xi_{\mu,x}\psi_{x,a}S_\mu\psi_{x,a} \tag{3.10b}$$

$$O^{2A}_{\mu\nu,a}(x) = \xi_{\mu,x}\xi_{\nu,x+\hat{\mu}}\psi_{x,a}S_\mu S_\nu\psi_{x,a} \tag{3.10c}$$

$$O^{2B}_{\mu\nu,a}(x) = \epsilon_x\xi_{\mu,x}\xi_{\nu,x+\hat{\mu}}\psi_{x,a}S_\mu S_\nu\psi_{x,a} \tag{3.10d}$$

$$O^3_{\mu\nu\lambda,a}(x) = \xi_{\mu,x}\xi_{\nu,x+\hat{\mu}}\xi_{\nu,x+\hat{\mu}+\hat{\nu}}\psi_{x,a}S_\mu S_\nu S_\lambda\psi_{x,a} \tag{3.10e}$$

where $S_\mu\psi_{x,a} = \psi_{x+\hat{\mu},a} + \psi_{x-\hat{\mu},a}$. For fermions to become massive through the conventional mechanism, one or more of these order parameters must acquire a non-zero expectation value. This can only occur when one or more of the lattice symmetries are spontaneously broken. In this work, we only focus on the order parameter $O^0_{a,b}(x)$

given in Eq. (3.10a) which is the order parameter for the $SU(4)$ symmetry. Some of the other order parameters were studied recently in [16]. In our recent paper [37], we argue why all bilinear order parameters will vanish at sufficiently strong couplings. We repeat some of these arguments in Section 3.5.

3.3 General observables of interest

Since four-fermion couplings are perturbatively irrelevant and the lattice symmetries of the action do not allow the formation of bilinear condensates, the theory remains massless at weak couplings. This is the PMW phase. At strong couplings, as we will explain later in Section 3.5, one expects fermions to become massive without breaking any lattice symmetries. This is the PMS phase. However, at intermediate couplings, there could be a spontaneously broken FM phase where one or more of the symmetries of the action are broken spontaneously and fermions become massive due to the formation of fermion bilinear condensates. To study if such an intermediate phase exists, we need to compute masses of the particles in the theory and the mass order parameters that distinguish the spontaneously broken phase from the symmetric phase. A brief discussion of how to choose an order parameter is given in Appendix A. Observables that are of interest include

- Fermion bilinear (bosonic) correlators and susceptibilities:

  To infer the presence of non-zero fermion bilinear order parameters, we can compute correlators of the form

  $$C(x,y) = \langle O_x O_y \rangle \tag{3.11}$$

  where O is one of the fermion bilinear mass order parameters defined in Eq. (3.10). Using the cluster property, we expect

  $$\lim_{|x-y|\to\infty} \langle O_x O_y \rangle \sim \langle O_x \rangle^2. \tag{3.12}$$

This implies that $C(x,y) \sim \langle O_x \rangle^2$ as $|x-y| \to \infty$. The expectation value of such an order parameter is also referred to as a condensate (Φ). Thus, the presence of a condensate can be inferred if $C(x,y)$ approaches a constant at large separations. However, if the correlation function vanishes at large separations, then the corresponding condensate is zero. In the PMS phase, since we expect all lattice symmetry order parameters to vanish, all these correlators must decay to zero at large separations.

From the bosonic correlator $C(x,y)$, we can also compute the susceptibility

$$\chi = \frac{1}{2}\sum_x C(0,x) = V\Phi^2 \tag{3.13}$$

In a massive theory, where the correlation functions decay exponentially, the susceptibilities saturate to a constant value at large volumes. On the other hand, when the correlation function decays like a power, depending on the power, the susceptibility could grow, but the growth will not be proportional to the volume. For a non-zero condensate, the corresponding susceptibility will grow with the volume V. In the PMS phase, we expect the susceptibility to saturate to a constant.

- Fermionic correlators:

  To infer the mass of the fermions we can measure fermionic correlators of the form

  $$F(x,y) = \langle \psi_{x,a}\ \psi_{y,a} \rangle \tag{3.14}$$

  As explained in Appendix B, exponential decay of such a correlator indicates that the particle is massive, while a power-law decay indicates that the particle is massless. In the PMS phase, we expect massive fermions, while in the PMW phase the fermions will be massless.

- Four-fermion condensates:

  Four-fermion condensates measure the explicit breaking of the $U(1)$ symmetry discussed in Eq. (3.9) by the interaction term. We define this condensate through the relation

$$\rho_m = \frac{U}{V} \sum_x \langle \psi_{x,1} \psi_{x,2} \psi_{x,3} \psi_{x,4} \rangle \tag{3.15}$$

  This order parameter is non-zero for all values of U. We will argue that these serve as pseudo-order parameters.

3.4 The Fermion Bag approach

The conventional way to solve four-fermion models is to introduce an auxiliary scalar field [38]. This approach involves the conversion of the four-fermion coupling into a Yukawa coupling by introducing the auxiliary field. This allows one to perform the Grassmann integral and write the partition function as an integral purely over the auxiliary field. The fermionic physics is encoded as a determinant of a fermion matrix that depends on the auxiliary field. If this determinant is positive, one can use the Hybrid Monte-Carlo Method [39] to solve the problem. While such methods have been used by other groups, we employ a different method that deals directly with the fermionic degrees of freedom, called the Fermion Bag Approach [14].

The Fermion Bag Approach was proposed a few years ago and has enabled the solution of many problems that could not be solved earlier [40, 41]. A review of this approach is given in [42]. We will illustrate this method by applying it to our model. In the fermion bag approach, we expand the partition function in Eq. (3.3) as follows

$$\begin{aligned} Z &= \int \left\{ \prod_{i=1}^{4} [d\psi_i] \right\} \; e^{-S_0} e^{U \sum_x \psi_{x,1} \psi_{x,2} \psi_{x,3} \psi_{x,4}} \\ &= \int \left\{ \prod_{i=1}^{4} [d\psi_i] \right\} \; e^{-S_0} \prod_x \left(1 + U \psi_{x,1} \psi_{x,2} \psi_{x,3} \psi_{x,4} \right). \end{aligned} \tag{3.16}$$

We define a binary field m_x that takes values 0 or 1 on each site x. Sites with $m_x = 0$ are called *free sites* and sites with $m_x = 1$ are called *monomers*. In terms of this field, we can re-write the partition function as :

$$Z = \sum_{[m]} \int \left\{ \prod_{i=1}^{4} [d\psi_i] \right\} e^{-S_0} \prod_x \left(U \psi_{x,1} \psi_{x,2} \psi_{x,3} \psi_{x,4} \right)^{m_x} \tag{3.17}$$

where $[m]$ denotes a configuration of monomers m_x at all the sites x and the summation denotes a sum over all possible monomer configurations. Thus each monomer contributes a $U\psi_{x,1}\psi_{x,2}\psi_{x,3}\psi_{x,4}$ to the Grassmann integration. On a lattice with V number of sites, there are 2^V monomer configurations. One such configuration is illustrated on a 2D lattice in Fig. (3.1). Performing a sum over all configurations gives us the exact value of the partition function. Let us consider a configuration C with k monomers. Let $[x_m]$ and $[x_f]$ denote the sets of lattice sites containing the monomer sites and free sites respectively. If the lattice contains V sites, then $[x_m]$ contains k sites and $[x_f]$ contains $(V-k)$ sites. The contribution of this configuration C to the partition function in Eq. (3.17) is given by

$$\begin{aligned} Z(C) &= \int \left\{ \prod_{i=1}^{4} [d\psi_i] \right\} e^{-S_0} \left(U^k \right) \prod_{x \ \epsilon \ x_m} \left(\psi_{x,1} \psi_{x,2} \psi_{x,3} \psi_{x,4} \right) \\ &= U^k \prod_{i=1}^{4} \left[\int [d\psi_i] e^{-\frac{1}{2} \sum_{x,y} \psi_{x,i} M_{x,y} \psi_{y,i}} \prod_{x \ \epsilon \ x_m} \psi_{x,i} \right] \end{aligned} \tag{3.18}$$

Note that the four flavors of the reduced staggered fermions have been decoupled in the partition function.

The matrix M has some special properties that help us simplify this expression even further. Let n_{odd}, n_{even} be the number of odd and even monomer sites in a configuration. From Eq. (2.18), it can be seen that the matrix M has non-zero values only when connecting an odd site to an even site or an even site to an odd site. Let us write M in the form

$$M = \begin{array}{c} \\ even \\ odd \end{array} \begin{array}{c} \begin{array}{cc} even & odd \end{array} \\ \left[\begin{array}{c|c} 0 & A \\ \hline -A^T & 0 \end{array}\right] \end{array} \tag{3.19}$$

Hence, the inverse matrix $G = M^{-1}$, which gives the propagator between any two sites, also has the same property and can be written in the form

$$G = \begin{array}{c} \\ even \\ odd \end{array} \begin{array}{c} \begin{array}{cc} even & odd \end{array} \\ \left[\begin{array}{c|c} 0 & -W^T \\ \hline W & 0 \end{array}\right] \end{array} \tag{3.20}$$

where $W = A^{-1}$. It can be shown that any configuration with $n_{even} \neq n_{odd}$ does not contribute to the partition function. This has been discussed in Appendix C. For configurations with $n_{even} = n_{odd}$, the matrices A and W are square matrices. In this case, we can use the properties of the matrix M and the rules of Grassmann integration to prove the following two relations [43] for one flavor of reduced staggered fermion ψ:

$$\int [d\psi] e^{-\frac{1}{2}\sum_{x,y}\psi_x M_{x,y}\psi_y}\ \psi_{x'}\psi_{y'} \quad = \quad \sigma \times (DetA)\ W_{y',x'} \tag{3.21}$$

$$\int [d\psi] e^{-\frac{1}{2}\sum_{x,y}\psi_x M_{x,y}\psi_y}\ \psi_{x'}\psi_{y'} \quad = \quad \sigma \times (Det\tilde{A}) \tag{3.22}$$

where x' and y' have opposite parity i.e. one is even (odd) and the other is odd (even). The matrix $\tilde{A}$ is a sub-matrix of A obtained by removing one row and one

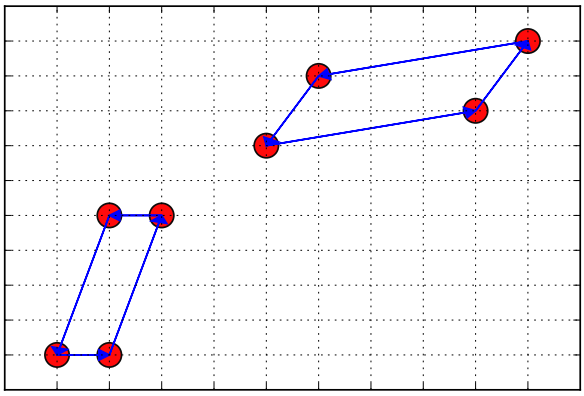

FIGURE 3.1: Fermion bag configuration with the circles indicating the presence of monomers. In the weak coupling picture, when there are very few monomers, observables can be expressed in terms of propagators between monomers. The fermions at the monomer sites can hop on to other monomer sites.

column corresponding to the sites x' and y' and σ is a sign factor that depends on the ordering of the Grassmann variables. Since we have four flavors of reduced staggered fermions, this sign factor will eventually get cancelled. Using these relations, we can perform the Grassmann integral in Eq. (3.18) in two dual ways. We call these the weak coupling and the strong coupling approach as discussed below.

3.4.1 Weak coupling approach

Using the relation in Eq. (3.21) and Wick's theorem [44], we can simplify the expression in Eq. (3.18) in terms of propagators linking the monomer sites to get

$$Z(C) = U^k \; Det A^4 \; Det {W_0}^4 \tag{3.23}$$

where A has been defined in Eq. (3.19) and W_0 is a sub-matrix of the matrix W defined in Eq. (3.20). The matrix W_0 depends on the monomer configuration, connects odd monomers to even monomers and has dimensions $(k/2 \times k/2)$. The matrix A is independent of the monomer configuration and will cancel out in all observables.

Configurations with large number of monomers are suppressed for small values of the coupling, due to the presence of the term U^k in Eq. (3.18). In this limit, configuration weights are easier to compute using Eq. (3.23) since W is a small matrix. In this picture, fermions can be viewed as existing on the monomer sites and hopping onto other monomer sites through the free propagator. The collection of monomer sites can be thought of as a fermion bag, within which fermions can hop. Fig. (3.1) shows this view point.

For completeness, we list expressions similar to Eq. (3.23) for some important observables. The four-point condensate ρ_m defined in Eq. (3.15) is simply the density of monomer sites. For each monomer configuration C, the contribution to ρ_m is given by

$$\rho_m(C) = \frac{k}{V} \tag{3.24}$$

where $k = n_{even} + n_{odd}$ is the total number of monomers in the configuration. Two other important observables of interest are the bosonic and fermionic correlators defined in Eqs. (3.11) and (3.14). For the order parameter $O^0_{a,b}$ in Eq. (3.10a), we list expressions for the two independent bosonic correlators $C_1(x,y) = \langle \psi_{x,1}\psi_{x,2}\psi_{y,1}\psi_{y,2} \rangle$, $C_2(x,y) = \langle \psi_{x,1}\psi_{x,2}\psi_{y,3}\psi_{y,4} \rangle$ and the fermionic correlator $F_1(x,y) = \langle \psi_{x,1}\psi_{y,1} \rangle$. It can be shown that the correlators $C_1(x,y)$ and $F_1(x,y)$ can get non-zero contributions only when $n_{even} = n_{odd}$ and the sites x and y have opposite site-parity i.e. one is odd and the other even. The contribution to these quantities in the configuration C is given by

$$\begin{aligned} C_1(x,y)_C &= U^k (DetA)^4 \ (DetW_1)^2 (DetW_0)^2 / Z \\ F_1(x,y)_C &= \sigma_f \ U^k (DetA)^4 \ (DetW_1)(DetW_0)^3 / Z \end{aligned} \tag{3.25}$$

where W_0 is the propagator matrix connecting every even monomer site to every odd monomer site in the configuration, W_1 is the matrix obtained from W_0 by adding an extra column and row corresponding to the source sites x and y and σ_f is a sign

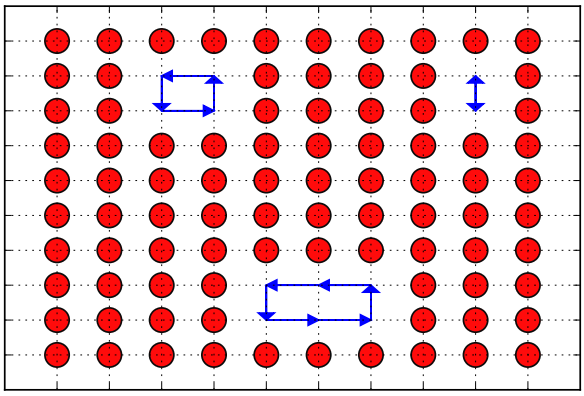

FIGURE 3.2: Fermion bag configurations with the circles indicating the presence of monomers. In the strong coupling picture, when there are very few free sites, observables can be expressed in terms of the staggered matrix elements between free sites. The fermions in a bag of free sites can only hop within the bag.

factor that depends on the ordering of the sites in W_0 and W_1. W_0 has dimensions $n_{odd} \times n_{even}$, while W_1 has dimensions $(n_{odd}+1) \times (n_{even}+1)$. The expression for $C_2(x,y)$ is a bit more complicated and we discuss this in Section 4.7.

3.4.2 Strong coupling approach

In this approach, we perform the Grassmann integral over the monomer terms first. Using the relation in Eq. (3.22), we can express the partition function in Eq. (3.18) in terms of a smaller reduced staggered matrix $\tilde{A}$ as

$$Z(C) = U^k \left(Det\tilde{A}\right)^4, \tag{3.26}$$

where $\tilde{A}$ is the sub-matrix of A obtained by including only the rows and columns corresponding to the free sites. It has dimensions $\frac{(V-k)}{2} \times \frac{(V-k)}{2}$.

For large values of the coupling, configurations with large number of monomers are enhanced due to the presence of the term U^k in Eq. (3.18). Since k is large, computations using Eq. (3.23) are cumbersome. However in this limit, the number of

free sites $(V-k)$ is small and hence the configuration weights are easier to compute using Eq. (3.26). In this picture, the fermions can be thought of as hopping within the set of free sites. Fig. (3.2) shows this limit.

Since the matrix $\tilde{A}$ connects only nearest-neighbors, when the lattice is disconnected into many regions of free sites, then $\tilde{A}$ has a special property. It is block-diagonal with each block corresponding to a set of connected points. This is equivalent to the view point that fermions can hop only within a fermion bag. This property is crucial in arguing for the presence of the PMS phase and we will come back to this later.

To summarize, in the fermion bag approach, the partition function can be expressed as a sum over determinants of fermion matrices that depend on the monomer configurations in two different but equivalent ways. All correlation functions can also be expressed in a similar manner. As we will explain in the next chapter, since it is not practically possible to compute the exact sum, we will use *Monte Carlo methods* to estimate the observables.

3.5 Fermion Bags at strong couplings

The Fermion Bag approach also gives us an intuitive understanding of the PMS phase. It can be argued that all fermionic and bosonic correlators decay exponentially at large U. First, let us consider the fermionic correlator $F_1(x,y)$. In the strong coupling picture, it can be written as

$$\begin{aligned} F_1(x,y) &= \langle \psi_{x,1}\psi_{y,1}\rangle \\ &= \frac{1}{Z}\sum_{[m]} U^k Det(\tilde{A})^4 \tilde{A}^{-1}_{x,y} \end{aligned} \tag{3.27}$$

where $\tilde{A}$ has been defined in Eq. (3.26) and the sum is over all monomer configurations. Since the matrix A is block diagonal as discussed in Section 3.4.2, $\tilde{A}$ is also

block diagonal. Hence, its inverse is also block diagonal. As a result, $\tilde{A}^{-1}_{x,y}$ is zero if x and y belong to different fermion bags. Hence the fermionic correlator gets zero contributions from configurations if the source points are placed in different bags, as shown in Fig. (3.3).

Now, let us understand the behavior of the bosonic correlator $C_1(x,y)$ at strong couplings. Consider a fermion bag configuration with four disconnected fermion bags in the strong coupling approach. The matrix $\tilde{A}$ that links the free even and odd sites, will be block-diagonal with the form shown below.

$$\tilde{A} = \begin{array}{c} \\ bag1 \\ bag2 \\ bag3 \\ bag4 \end{array} \begin{array}{c} \begin{array}{cccc} bag1 & bag2 & bag3 & bag4 \end{array} \\ \left(\begin{array}{c|c|c|c} B_1 & 0 & 0 & 0 \\ \hline 0 & B_2 & 0 & 0 \\ \hline 0 & 0 & B_3 & 0 \\ \hline 0 & 0 & 0 & B_4 \end{array}\right) \end{array} \tag{3.28}$$

The contribution of this configuration to the bosonic correlator $C_1(x,y)$ is given by

$$\begin{aligned} C_1(x,y)_C &= \langle \psi_{x,1}\psi_{x,2}\psi_{y,1}\psi_{y,2}\rangle_C \\ &= \frac{1}{Z}U^k (Det\tilde{A}')^2 \ (Det\tilde{A})^2 \end{aligned} \tag{3.29}$$

where x and y are the source points. These have to be free sites with opposite parity and without loss of generality, we can assume x to be even and y to be odd. The matrix $\tilde{A}'$ is obtained from $\tilde{A}$ by removing one row and one column corresponding to the source points x and y. Since $\tilde{A}$ given in Eq. (3.28) is block diagonal, $\tilde{A}'$ will also be block diagonal. In Eq. (3.29), the fermion flavors 1 and 2 contribute a factor $Det\tilde{A}'$ each, while flavors 3 and 4 contribute a factor $Det\tilde{A}$. The matrix $\tilde{A}'$ can be

written in the form

$$\tilde{A}' = \begin{array}{c} \\ bag1 \\ bag2 \\ bag3 \\ bag4 \end{array} \begin{array}{c} \begin{array}{cccc} bag1 & bag2 & bag3 & bag4 \end{array} \\ \left(\begin{array}{c|c|c|c} B_1^{'} & 0 & 0 & 0 \\ \hline 0 & B_2^{'} & 0 & 0 \\ \hline 0 & 0 & B_3^{'} & 0 \\ \hline 0 & 0 & 0 & B_4^{'} \end{array}\right) \end{array} \tag{3.30}$$

Here, the block matrices $B_i{}'$ are obtained from the matrices B_i in the following way. If the block B_i contains the row corresponding to the even site x, $B_i{}'$ will be obtained from B_i by removing that row. Similarly, if the block B_i contains the column corresponding to the site y, $B_i{}'$ will be obtained from B_i by removing that column. For all blocks B_i that contain neither x nor y, $B_i{}'$ will be the same as B_i. The determinant of both $\tilde{A}$ and $\tilde{A}'$ can be written as

$$Det\tilde{A} = Det(B_1) \times Det(B_2) \times Det(B_3) \times Det(B_4) \tag{3.31}$$

$$Det\tilde{A}' = Det(B_1') \times Det(B_2') \times Det(B_3') \times Det(B_4'). \tag{3.32}$$

Using the Leibniz formula for the determinant of a matrix [45], it can be argued that in a block diagonal matrix, even if a single block is not a square matrix, the determinant of the matrix is zero. Hence, for the right hand side in Eq. (3.29) to be non-zero, each of the blocks B_i and B_i' must be square matrices. It is easy to argue that unless both x and y belong to the same bag, determinant of either A or $\tilde{A}'$ will be zero. A similar argument can be used for the correlator $C_2(x, y)$. Thus, all contributions with the source points x and y in different bags as shown in Fig. (3.3), give zero contributions to correlators $F_1(x, y)$ and $C_1(x, y)$ and $C_2(x, y)$.

Since the bosonic and fermionic correlators get zero contributions from disconnected fermion bags, for a configuration to give a non-zero contribution to the corre-

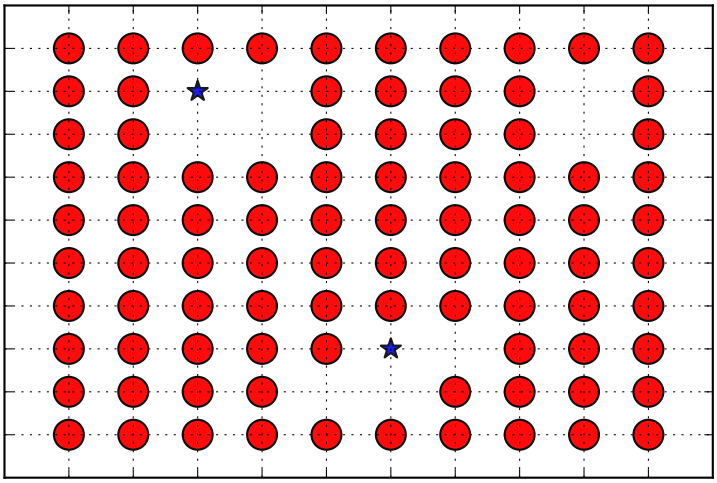

FIGURE 3.3: Fermion bag configuration with the source points (denoted by stars) in disconnected bags. In the strong coupling limit, such monomer configurations give a null contribution.

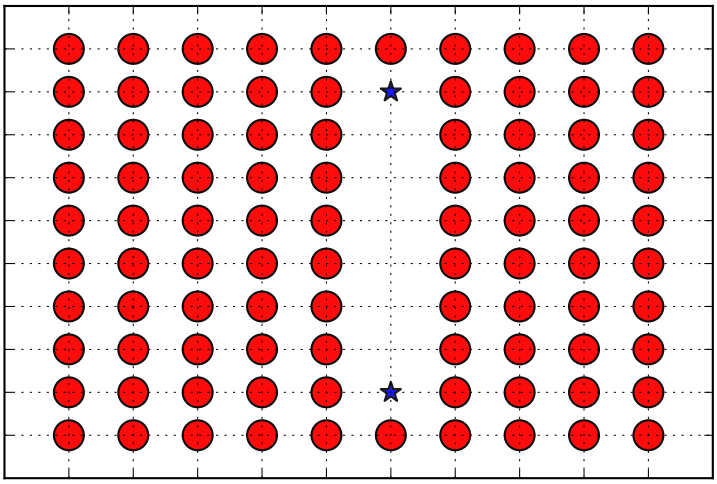

FIGURE 3.4: Fermion bag configuration with both the source points (denoted by stars) in the same fermion bag. In the strong coupling limit, the leading contribution comes from such configurations.

lators, there must be a path of free sites connecting the two source points x and y as shown in Fig. (3.4). In the limit $|x-y| \to \infty$, the contributions of such configurations to the bosonic and fermionic correlators have the form $U^{-(x-y)} = e^{-(x-y)\ln(U)}$. Thus, in the large U limit all correlators will decay exponentially.

We will now argue that all correlators of the form $C(x,y) = \langle O_x O_y \rangle$ defined in Eq. (3.11) have the same behavior. The argument used in the previous paragraph for the order parameter O^0 in Eq. (3.10) can also applied to O^{2A} and O^{2B} . But, the correlators of O^1 and O^3 can get contributions from configurations with source points in two different bags. However, in these cases we can argue that such contributions from fermion bag configurations that are related by symmetry transformations will cancel each other when the fermion bags are far separated.

Thus, all correlators decay exponentially in the limit of large U. Based on the argument in Section 3.3, the exponential decay of the fermionic correlator $F_1(x,y)$ at large U implies the existence of massive fermions. In addition, the exponential decay of all bosonic correlators $C(x,y)$ implies the absence of fermion bilinear condensates. This massive symmetric phase at strong couplings is the PMS phase.

Thus, the phase diagram has a massless PMW phase at weak couplings and a massive PMS phase at strong couplings. This implies that a phase transition from the massless to the massive phase must occur somewhere in between. Our aim is to study this intermediate region to look one or more phase transitions.

4

Monte-Carlo methods

In the previous chapter we explained how the Fermion bag approach helps us express all observables of interest as a classical statistical mechanics problem. The next step is to compute these expressions numerically for finite lattice systems. However, the exact answer involves a sum over an exponentially large number of terms. For example, on a lattice with V sites, the sum involves 2^V terms. Even for a 4^3 lattice, this involves about 10^{19} terms. Since the exact sum cannot be practically computed, one needs alternative ways to perform the sum. Thanks to powerful computers today, such calculations can be done efficiently using Monte Carlo methods [46], by employing the idea of importance sampling [47, 48].

4.1 Importance Sampling

Although the configuration space is exponentially large, in statistical mechanics, only a very small subset of these configurations are important. Importance sampling is a technique to sample such distributions using a simpler distribution. Consider a statistical mechanics system with partition function Z. The general form of the

expectation value of an observable for this system can be written in the form

$$\langle \hat{O} \rangle = \frac{1}{Z} \sum_C O(C) = \frac{\sum_C O(C)}{\sum_C W(C)} \tag{4.1}$$

where both $\hat{O}$ and Z have been expressed as a sum of terms over the configurations C. $W(C)$ is the Boltzmann weight of the configuration C. We can express the numerator in Eq. (4.1) in terms of $W(C)$, to get :

$$\langle \hat{O} \rangle = \frac{\sum_C \tilde{O}(C) W(C)}{\sum_C W(C)} \tag{4.2}$$

where $\tilde{O}(C) = \frac{O(C)}{W(C)}$. If we sample configurations according to the Boltzmann weight $W(C)$ and compute $\tilde{O}(C)$ for that sample, then the resulting average of this sample would be a good estimate of $\langle \hat{O} \rangle$, if the distribution functions of O and Z behave in a similar manner. By increasing the sample size, we can systematically reduce the errors. This is the concept of Importance Sampling. However, if there exist configurations C' for which $O(C')$ is large but $W(C')$ is small, then the sampling method will not be effective. For example, if there exist configurations for which $W(C') = 0$ but $O(C') \neq 0$, then such configurations will never be sampled and the sampled sum will not be correct. Such problems can sometimes be seen as large fluctuations in the value of observables in the sampled configurations.

4.1.1 Sign Problems

It is not always possible to use importance sampling while studying quantum statistical mechanics problems. The barrier comes in the form of negative or complex Boltzmann weights, which is referred to as the *Sign Problem*. In these cases, the concept of probability is not clearly defined and the sampling process cannot be performed. Even if the sampling is performed using the absolute values of the Boltzmann

weights, the negative signs cause large fluctuations rendering the sampling process ineffective. One way to solve sign problems is to find a representation or re-summation of the partition function so that all configuration weights are non-negative. Solving sign problems is an interesting area of research. Some solutions have emerged in the Fermion Bag approach [41, 49] discussed before in Section 3.4 and the Meron cluster method [50, 51, 52]. Other methods that have been tried to solve the sign problem include the Complex Langevin method [53], Lefschetz thimbles [54], Density of states [55] [56], etc. Our model does not suffer from sign problems and the Fermion Bag approach makes this very explicit. As we showed in Eq. (3.23), the configuration weights can be expressed as a fourth-power of the determinant of real matrices and hence they are all positive.

4.2 Update algorithms

For a system without a sign problem, we can generate configurations distributed according to their Boltzmann weights and use them to compute observables. To sample configurations with the correct distribution, we have to design update algorithms. Efficient algorithms enable us to move around in configuration space quickly in what is called *simulation time* τ.

Update algorithms are constructed through a transition probability, that must satisfy two important conditions. Let C be the current configuration and C' be the target configuration. The transition probability $P(C \to C')$ is defined as the probability to move from C to C'. The two conditions the transition probability matrix must satisfy are:

1. Detailed Balance

   If $W(C)$ and $W(C')$ represent the configuration weights of configurations C

and C', then the condition of detailed balance is given by

$$W(C)P(C \to C') = W(C')P(C' \to C) \tag{4.3}$$

2. Ergodicity

   The transition probability matrix is said to be ergodic if it allows one to reach every configuration, starting from any configuration. In other words, the update algorithm must keep the configuration space connected.

   Detailed balance and ergodicity ensure that configurations obtained after sufficiently many steps are sampled appropriately according to the Boltzmann weight of the configurations. Practical Monte-Carlo algorithms often involve multiple algorithms that are implemented in sequence. As long as the condition of detailed balance is obeyed by each algorithm and ergodicity is obtained due to all the algorithms working together, correct sampling can be achieved.

4.3 Autocorrelation and Equilibriation

Since it is difficult to design update algorithms that satisfy detailed balance when configurations change by a large amount, most updates have proposal functions that modify the configurations by small amounts. As a result, successive configurations are highly correlated and hence do not serve as independent samples. On the other hand, the error in an observable can only be reduced when many uncorrelated configurations can be generated. An update algorithm is considered efficient when many independent configurations can be generated quickly. The efficiency of update algorithms can be quantified using the concepts of equilibriation time and autocorrelation time.

Autocorrelation is a measure of the correlation among a sequence of configurations as computed through the values of observables as a function of simulation time.

Consider an observable O that assumes the value O_τ at the simulation time τ. The autocorrelation $A(t)$ between observable values separated by time t is defined as

$$A_t = \frac{\langle (O_{t+\tau} - \mu)\ (O_\tau - \mu) \rangle_\tau}{\langle (O_\tau - \mu)^2 \rangle_\tau} \tag{4.4}$$

where $\mu = \langle O \rangle_\tau = \sum_{\tau=0}^{N-1} \frac{O_\tau}{N}$ is the average of the sample and N is the sample size, which is assumed to be large. Typically, the autocorrelation function decays as $e^{(-t/\tau_{aut})}$ for large times t, where τ_{aut} is defined as the *autocorrelation time*. However, a practical definition of the autocorrelation time is the time taken for the autocorrelation function to approach zero within errors.

The first independent configuration is usually obtained with an update algorithm, by starting from some initial configuration that is not part of the representative sample. During this process, many transient configurations are generated until the system thermalizes. This is known as *Equilibriation*. The time taken to thermalize is called *Equilibriation time*. The configurations obtained before the system thermalizes are not representative of the actual distribution and hence need to be discarded. For example, if we start from a configuration with no monomers and perform a series of updates for a non-zero U, the initial configurations will have very few monomers. These will not be representatives of the actual distribution and hence need to be discarded.

4.4 Standard update algorithms

As mentioned earlier, a complete Monte-Carlo update involves multiple update algorithms that are impelemented in sequence. Although the choice of these updates is dependent on the physical system, there are some standard procedures used to construct them. We describe two of the most popular ones below [57].

The **Metropolis** algorithm is one of the most widely used algorithms. The

transition probability $P(C \rightarrow C')$ in a Metropolis algorithm consists of two parts, a *proposal function*, which is a rule to propose a new configuration and an *acceptance function*, which either accepts the target configuration or retains the original configuration. This can be written as

$$P(C \rightarrow C') = p(C \rightarrow C')\ a(C \rightarrow C') \tag{4.5}$$

where $p(C \rightarrow C')$ and $a(C \rightarrow C')$ represent the proposal and acceptance functions for the move from configurations C to C'. The acceptance function for the Metropolis algorithm is given by :

$$a(C \rightarrow C') = \ \min\ \left(1, \frac{p(C' \rightarrow C)}{p(C \rightarrow C')} \frac{W(C')}{W(C)}\right) \tag{4.6}$$

$$a(C' \rightarrow C) = \ \min\ \left(1, \frac{p(C \rightarrow C')}{p(C' \rightarrow C)} \frac{W(C)}{W(C')}\right) \tag{4.7}$$

where $W(C)$ and $W(C')$ are the configuration weights for configurations C and C' respectively. A careful choice of the proposal function p can help improve the efficiency of the Metropolis algorithm.

Another commonly used algorithm is the **Heat-bath** algorithm. In the heat-bath algorithm, instead of looking at just one target configuration, we look at a small set of target configurations. Let $\{C_1 \ ... \ C_n\}$ be a set of n target configurations. In the heat bath update, the target configuration is chosen from this set according to the transition probability given by

$$P(C_i \rightarrow C_f) = \left(\frac{W(C_f)}{\sum_{t=1}^{n} W(C_t)}\right), \tag{4.8}$$

where C_i and C_f represent the initial and final configurations. Thus a heat-bath update has no memory of the previous configuration, at least within the chosen set.

4.5 Fermion bag updates

In our first paper [35], we performed calculations on lattices up to size 28^3 using three different and independent update algorithms. These updates have been explained in detail in that paper. In order to perform computations on larger lattices, we developed a new set of more efficient algorithms. In this section, we briefly describe these latter update algorithms. In particular we will discuss two different update algorithms that we use.

First, we discuss some notation. As mentioned earlier, lattice sites are defined according to their site-parity as odd ($\epsilon_x = -1$) or even ($\epsilon_x = +1$). Lattice sites are defined according to their filling state as filled when the site contains a monomer ($m_x = 1$) or empty if the site does not contain a monomer ($m_x = 0$). The *nearest-neigbors* of a lattice site are the set of sites at a distance of one lattice unit from the original site. The *next-nearest-neighbors* of a lattice site are the set of sites at a distance of $\sqrt{2}$ lattice units. For example in 3D, each site has 6 nearest-neighbors and 12 next-neighbors. Two sites are defined to be *compatible* if either of the following conditions are met:

a: They have the same site-parity but different filling.

b: They have different site-parities but the same filling.

For example, two even sites are compatible if and only if one is a monomer and the other is a free site.

4.5.1 Worm algorithm with heat-bath

The first update algorithm that we discuss is a worm algorithm with a heat-bath acceptance condition. The worm update starts at a lattice site, moves around the lattice while changing monomers on the sites it visits. Like other worm algorithms

[58, 59], this method is very efficient in propagating a local change around the lattice. We have designed two forms of this algorithm:

A) Complete monomer update

In this update, while the worm moves around, it adds and removes monomers and also moves them around. The steps involved are:

Step 1 Choose a site at random that has at least one compatible neighbor (either nearest or next-nearest) and introduce a worm head on that site. This starts the worm update.

Step 2 With probability P_{quit}, the head on the site is removed and the worm update ends. Otherwise the algorithm moves on to step 3.

Step 3 Pick a neighbor site at random and check if the two points are compatible. If the answer is no, do nothing and go to step 2. Otherwise, propose flipping the filling state of both sites and go to step 4. For two sites with the same filling, this can add or subtract two monomers from both sites. For two sites with different filling, this can move an existing monomer around.

Step 4 Perform a heat bath update with transition probability $P(C_{old} \to C_{new}) = \frac{W_{new}}{W_{new}+W_{old}}$ and $P(C_{old} \to C_{old}) = \frac{W_{old}}{W_{new}+W_{old}}$.

Step 5 If the new configuration is accepted, then move the worm head to the new neighbor. If the older configuration is retained, then keep the worm head at the same point. Now return to step 2.

This algorithm is ergodic and hence it is sufficient to implement the sampling. However, empirical evidence suggests that its efficiency is not as high as the other algorithms we discuss below.

B) Monomer move update

In this update, as the worm moves, only the existing monomers are moved around and the monomer number remains unchanged. The steps involved are:

Step 1 Choose a monomer site at random that has at least one next-nearest free site and use that as the worm head. This starts the worm update.

Step 2 With probability P_{quit}, the head on the site is removed and the worm update ends. Otherwise the algorithm moves on to step 3.

Step 3 Pick a next-neighbor site at random and check if the two points are compatible. If the answer is no, do nothing and return to step 2. Otherwise, propose flipping the filling state of both sites and go to step 4. This becomes a proposal to move an existing monomer.

Step 4 Perform a heat bath update with transition probability $P(C_{old} \rightarrow C_{new}) = \frac{W_{new}}{W_{new}+W_{old}}$ and $P(C_{old} \rightarrow C_{old}) = \frac{W_{old}}{W_{new}+W_{old}}$.

Step 5 If the new configuration is accepted, then move the worm head to the new neighbor. If the older configuration is retained, then keep the worm head at the same point. Now return to step 2.

This algorithm is not ergodic and needs to be combined with another algorithm to sample configurations correctly. However, it is very efficient at making quick global changes to the configurations, without altering the total monomer number.

4.5.2 Enhanced Metropolis update

This update modifies the monomer configurations using a Metropolis update that takes into account the number of allowed sites where the updates can be made. This additional global information helps in enhancing the acceptance probabilities.

Although each update is local, the use of the global information makes it efficient. We designed two forms of this algorithm as given below:

A) Monomer add-remove update

This method creates and destroys monomers on the lattice. The steps involved are:

Step 1 Compute all possible pairs of nearest-neighbor sites that are compatible and store them.

Step 2 With a probability of half, choose to either add or subtract monomers. Accordingly, pick a pair of compatible sites at random and propose a new configuration obtained by flipping the filling of the two sites. This has the effect of adding or removing 2 monomers. For example, if the two sites have monomers initially, they will become free sites after the flip.

Step 3 Use a Metropolis update to accept or reject the new configuration with probability given by

$$P = \frac{N_{initial}}{N_{final}} \frac{W_{final}}{W_{initial}}$$

where $W_{initial}$ is the weight of the initial configuration $C_{initial}$ and $N_{initial}$ is the number of possible compatible sites for adding (removing) monomers from $C_{initial}$, while W_{final} is the weight of the final configuration C_{final} and N_{final} is the number of possible compatible sites for the reverse process of removing (adding) monomers from C_{final}. For example, while adding monomers, $N_{initial}$ is the number of compatible pairs of free sites in $C_{initial}$ while N_{final} is the number of compatible monomer pairs in C_{final}.

Step 4 If the flip is accepted, modify the monomer configuration.

This update is ergodic and is very effective in decreasing the equilibriation

time, due to a large value of the ratio $N_{initial}/N_{final}$ at weak couplings. It is repeated a fixed number of times.

B) Monomer move update

This method moves existing monomers around on the lattice. The steps involved are:

Step 1 Compute all possible pairs of next-nearest-neighbor sites that are compatible and store them.

Step 2 Pick a pair of these at random and propose a new configuration obtained by flipping the filling of the two sites. This has the effect of moving a monomer.

Step 3 Use a Metropolis update to accept or reject the new configuration with probability given by

$$P = \frac{N_{initial}}{N_{final}} \frac{W_{final}}{W_{initial}}$$

where $N_{initial}$ is the number of possible compatible sites and $W_{initial}$ is the configuration weight of the initial configuration $C_{initial}$, while N_{final} and W_{final} are similar quantities for the final configuration C_{final}.

Step 4 If the flip is accepted, modify the monomer configuration.

This algorithm is not ergodic and hence needs to be combined with another algorithm to achieve ergodicity. It is repeated a fixed number of times.

It can be shown that all the algorithms discussed above satisfy detailed balance. In the testing phase, we found that the add-remove monomer part of the Metropolis update had the best acceptance ratio while the monomer move part of the Heat-bath update was the most economical in terms of computational cost since it made fast

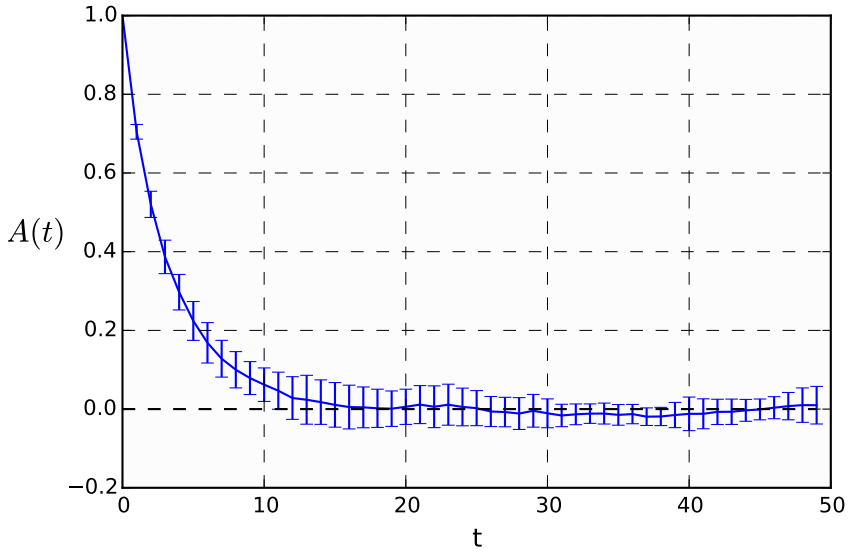

FIGURE 4.1: This figure shows the a plot of the autocorrelation for the observable ρ_m for a lattice of size L=28 at U=0.95. The errors have been obtained using 10 parallel runs, each having 2000 sweeps. The autocorrelation time is seen to be roughly 10 sweeps.

global changes with minimal modifications. Hence, for actual data-runs, we used only these 2 algorithms.

4.6 A Monte-Carlo sweep

A Monte-Carlo *sweep* is defined as a set of updates on the entire lattice such that the configuration obtained after these updates is significantly different from the original configuration. To define a sweep, we divided the lattice into blocks and performed updates within the block. By repeating this process multiple times on many randomly selected blocks, we updated the entire lattice. If B_{vol} is the volume of the block used for update, then we define a *block update* as a set of $B_{vol}/20$ monomer-move heat-bath updates and another $B_{vol}/3$ monomer add-remove Metropolis updates. A sweep is then defined as a set of $\left(\frac{V}{B_{vol}} + 1\right)$ such block updates performed on randomly chosen blocks of the lattice.

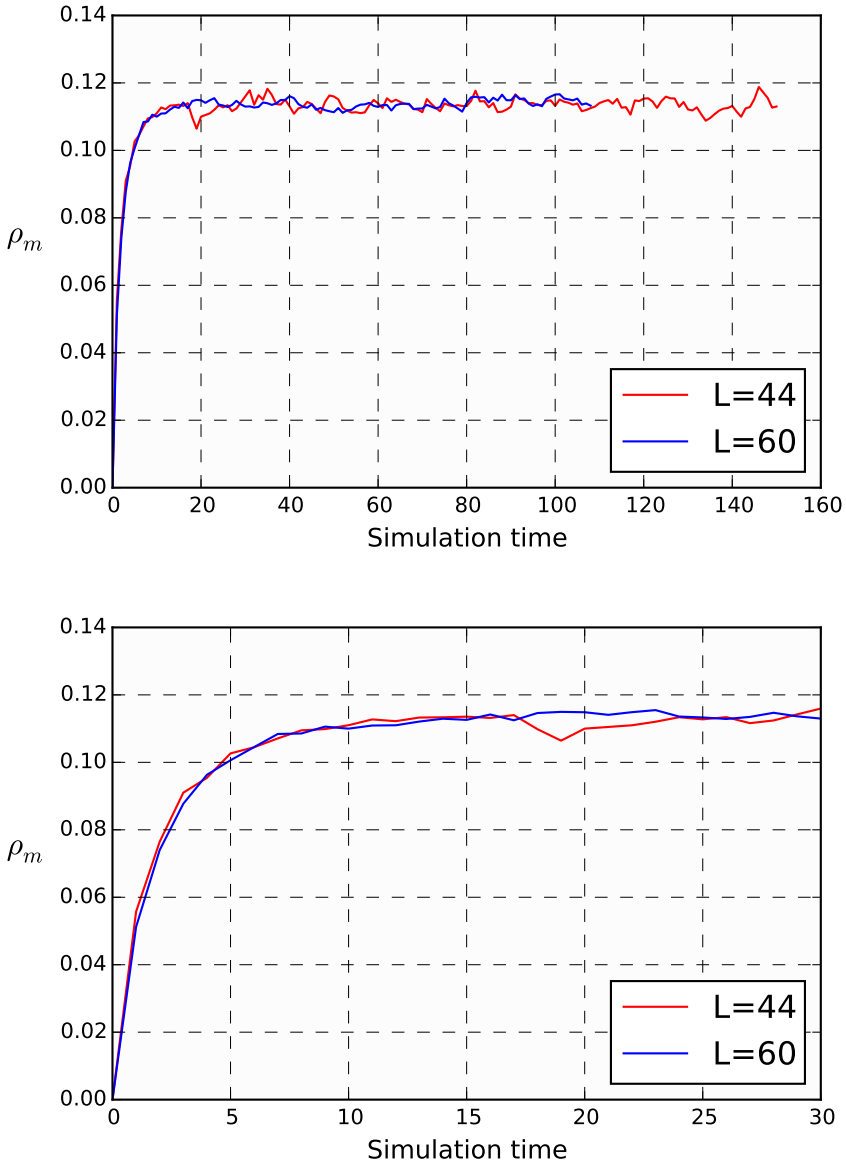

FIGURE 4.2: The two figures show the behavior of the observable ρ_m in simulation time for sequential runs starting with 0 monomers at $U = 0.95$, for the lattice sizes L=44 and L=60. The top figure shows the entire run, while the bottom figure shows the first 30 sweeps. The system seems to thermalize within the first 30 sweeps. But, to be conservative, we take the equilibriation time to be 50 sweeps. Note that the number of sweeps need for equilibriation does not seem to depend on the lattice size.

We have found that the above definition of the sweep gives us an autocorrelation of about 10 sweeps for the monomer density close to the transition. Fig. (4.1) shows the autocorrelation for one sequential run for the observable ρ_m. From the graph, we see that the auto-correlation time is roughly 10 sweeps. Hence, we strive to keep at least 100 sweeps of data before we compute our results from a single sequential run. This ensures at least 10 independent configurations from each sequential run. We also run these simulations in parallel on different computing nodes. With N nodes, we can obtain about $10N$ independent configurations. In our case, N is of the order of 100.

In order to estimate the number of sweeps needed for equilibriating a random configuration, we plot the variation of the observable ρ_m for a coupling $U = 0.95$ for the lattice sizes $L = 44$ and $L = 60$ in Fig. (4.2). It can be seen that, the system seems to thermalize within the first 50 sweeps for both lattices. Typically, we take equilibriation to be at least 50 sweeps.

All our computations were performed using the Open Science Grid (OSG) [60, 61] and the local Duke cluster. We obtained data for a range of couplings and lattice sizes. In 3D, a calculation on a $60 \times 60 \times 60$ lattice at the coupling $U = 0.95$ took about 19700 seconds per sweep and needed a peak memory of about 7GB, while the same for a $40 \times 40 \times 40$ lattice took about 1400 seconds per sweep and needed a peak memory of about 1.2 GB.

4.7 Reducing fluctuations

In this section, we present some technical details of our computation that help in reducing fluctuations in observables. Observables obtained using the importance sampling procedure described in Eq. (4.2) often show large fluctuations in sample values. One way to decrease fluctuations is to compute observables for pairs of configurations and average them to create what are referred to as *Improved Estimators*

that show less fluctuations. In this work, we use such a technique and we describe this procedure below. The expression for the expectation value of an observable $\hat{O}$ given in Eq. (4.1) can also be written as

$$\begin{aligned}\langle\hat{O}\rangle &= \frac{\sum_C O(C)}{\sum_C W(C)} \\ &= \frac{\sum_C \left\{\frac{1}{2}\frac{O(C)+O(C')}{W(C)+W(C')}\right\} W(C)}{\sum_C W(C)}\end{aligned} \tag{4.9}$$

where we assume there is an invertible mapping from C to a unique configuration C' and $W(C)$, $W(C')$ represent configuration weights of these two configurations and $O(C)$ and $O(C')$ represent the values of the observable in them. The sum is over all configurations which includes C and C'. Being an average, the quantity $\tilde{O} = \frac{1}{2}\frac{O(C)+O(C')}{W(C)+W(C')}$ typically has lesser fluctuations. If we estimate the observable through this improved estimator $\tilde{O}$, we should see reduced errors.

We apply this technique to our model and give expressions for the improved estimators of the observables $C_1(x,y)$, $C_2(x,y)$ and $F_1(x,y)$. Consider a configuration C with $2k$ monomers. As explained before, for the configuration to have a non-zero contribution to the partition function, there should be an equal number of even and odd monomers. Let x and y be two free sites such that x is odd and y is even. Let C' be the unique configuration obtained by flipping monomers at x and y. From Eq. (3.23), the configuration weights of C and C' are given by

$$\begin{aligned}W(C) &= Det(A)^4 U^{2k} Det(W_0)^4 \\ W(C') &= Det(A)^4 U^{2k+2} Det(W_1)^4\end{aligned} \tag{4.10}$$

where W_0 is the propagator matrix of size $k \times k$ connecting even and odd monomers of C and W_1 is obtained from W_0 by adding one row and one column corresponding

to the addition of monomers at sites x and y. W_0 and W_1 will have the form:

$$W_0 = \begin{bmatrix} w_{1,1} & w_{1,2} & \cdots & w_{1,k} \\ w_{2,1} & w_{2,2} & \cdots & w_{2,k} \\ \vdots & & \ddots & \vdots \\ w_{k,1} & w_{k,2} & \cdots & w_{k,k} \end{bmatrix} \tag{4.11}$$

$$W_1 = \left[\begin{array}{cccc|c} w_{1,1} & w_{1,2} & \cdots & w_{1,k} & w_{1,y} \\ w_{2,1} & w_{2,2} & \cdots & w_{2,k} & w_{2,y} \\ \vdots & & \ddots & \vdots & \vdots \\ w_{k,1} & w_{k,2} & \cdots & w_{k,k} & w_{k,y} \\ \hline w_{x,1} & w_{x,2} & \cdots & w_{x,k} & w_{x,y} \end{array}\right] \tag{4.12}$$

where $w_{i,j}$ corresponds to the propagator between the i^{th} odd site and the j^{th} even site. First, let us write an expression for the improved estimator of the bosonic correlator $C_1(x,y) = \langle \psi_{x,1}\psi_{x,2}\psi_{y,1}\psi_{y,2} \rangle$. This observable can be obtained from C by inserting the fields ψ_1 and ψ_2 in the integrand of the partition function at the source points x and y. It can also be obtained from C' by removing the fields ψ_3 and ψ_4 from the integrand of the partition function at x and y. Its value in both C and C' is the same and is given by:

$$C_1(x,y)_{(C)} = C_1(x,y)_{(C')} = Det(A)^4 U^{2k} Det(W_0)^2 Det(W_1)^2 \tag{4.13}$$

Substituting this in Eq. (4.9), the improved estimator for $C_1(x,y)$ in configurations C and C' is given by

$$\tilde{C_1}(x,y)_{(C,C')} = \frac{w^2}{1+U^2w^4} \tag{4.14}$$

where $w = \frac{DetW_1}{DetW_0}$. Similarly, for the fermionic correlator $F_1(x,y) = \langle \psi_{x,1}\psi_{y,2} \rangle$, the values in C and C' are given by

$$F_1(x,y)_{(C)} = F_1(x,y)_{(C')} = \sigma_f Det(A)^4 U^{2k} \det(W_0)^3 \det(W_1) \tag{4.15}$$

where σ_f is the sign factor that we encountered in Eq. (3.25). Substituting this in Eq. (4.9), the improved estimator for $F_1(x,y)$ in configurations C and C' is given by

$$\tilde{F}(x,y)_{(C,C')} = \sigma_f \frac{w}{1+U^2w^4} \tag{4.16}$$

The computation of the bosonic correlator $C_2(x,y) = \langle \psi_{x,1}\psi_{x,2}\psi_{y,3}\psi_{y,4}\rangle$ is a bit more subtle. It can get non-zero contributions only when both x and y have the same site-parity i.e., both are odd or both are even. Let configuration C have $2k$ monomers with the site x among them. Let configuration C' also have $2k$ monomers with the monomer at site x being replaced by y. Assuming both x and y are odd, we choose to move the sites x and y to the last row in the computation of the matrix W for each reduced staggered flavor. Then the two matrices W_1 (contaning the ψ field at x) and W_2 (contaning the ψ field at y) are given by

$$W_1 = \left[\begin{array}{ccccc} w_{1,1} & w_{1,2} & \cdots & w_{1,k-1} & w_{1,k} \\ w_{2,1} & w_{2,2} & \cdots & w_{2,k-1} & w_{2,k} \\ \vdots & & \ddots & \vdots & \vdots \\ w_{k-1,1} & w_{k-1,2} & \cdots & w_{k-1,k-1} & w_{k-1,k} \\ \hline w_{x,1} & w_{x,2} & \cdots & w_{x,k-1} & w_{x,k} \end{array}\right] \tag{4.17}$$

$$W_2 = \left[\begin{array}{ccccc} w_{1,1} & w_{1,2} & \cdots & w_{1,k-1} & w_{1,k} \\ w_{2,1} & w_{2,2} & \cdots & w_{2,k-1} & w_{2,k} \\ \vdots & & \ddots & \vdots & \vdots \\ w_{k-1,1} & w_{k-1,2} & \cdots & w_{k-1,k-1} & w_{k-1,k} \\ \hline w_{y,1} & w_{y,2} & \cdots & w_{y,k-1} & w_{y,k} \end{array}\right] \tag{4.18}$$

The configuration weights of C and C' are given by

$$\begin{aligned} W(C) &= Det(A)^4 U^{2k} \det(W_1)^4 \\ W(C') &= Det(A)^4 U^{2k} \det(W_2)^4 \end{aligned} \tag{4.19}$$

The bosonic correlator $C_2(x,y) = \langle \psi_{x,1}\psi_{x,2}\psi_{y,3}\psi_{y,4}\rangle$ can be obtained from C by removing the fields ψ_3 and ψ_4 at x and adding them at the site y in the integrand

of the partition function. It can also be obtained from C' by removing the fields ψ_1 and ψ_2 at y and adding them to the site x in the integrand of the partition function. The value of this observable in both C and C' is given by

$$C_2(x,y)_{(C)} = C_2(x,y)_{(C')} = Det(A)^4 U^{2k-1} \det(W_1)^2 \det(W_2)^2 \tag{4.20}$$

Substituting these in Eq. (4.9), the improved estimator for $C_2(x,y)$ in configuration C is given by

$$\tilde{C}_2(x,y)_{(C,C')} = \frac{w^2}{U\,(1+w^4)} \tag{4.21}$$

where $w = \frac{DetW_1}{DetW_2}$. Note that the bosonic correlators are always positive but the fermionic correlator $F_1(x,y)$ can be negative and hence will contain greater fluctuations.

In addition to decreasing the fluctuations, the improved estimator serves another purpose. Since it is a sum over 2 configurations, the improved estimator will reproduce the actual result only if both configurations are sampled appropriately. If the sampling is not appropriate, the improved estimator will show large deviations from the actual value. This helps us confirm our sampling procedure.

4.8 Fast Updates : The Background Field Method

Configuration weights in the sampling process contain matrix determinants of free propagators connecting monomer sites in the weak coupling fermion bag picture (Eq. (3.23)) and of the free staggered matrix connecting free sites in the strong coupling picture (Eq. (3.26)). Hence, as we move around in configuration space, each proposal of a new configuration involves the computation of ratios of determinants. This ratio can be computed as an inverse of an appropriate matrix, which takes $O(N^2)$ operations for an $N \times N$ matrix. However, this method computes the inverse from the information of the current configuration. It does not have any memory of earlier

configurations, and hence it does not take into account the possibility of retracement of the path in configuration space. In such cases, the same calculation may be repeated several times, resulting in a waste of computing cycles. In our work, we have developed a new technique that is capable of reducing the computing time when there is retracement. The idea is to view every new configuration as a perturbation about an initial background configuration. Using the idea of computing Feynman diagrams in a background field configuration, we can compute the weights of all possible perturbations of the background configuration at the beginning and store them. Using this information, we can compute configuration weights and observables for any perturbation as a determinant of a matrix whose size scales with the size of the perturbation. In particular, when there is a retracement of configurations, the size of the perturbation does not increase. We illustrate this idea below.

Let us consider a background configuration C_0 with equal number of even and odd monomers sites m. A configuration update involves adding and removing some monomers to obtain a new configuration C_1 which should also contain an equal number of odd and even monomers. Let the configuration C_1 be obtained from C_0, by removing the odd and even monomer sites $[a]$ and $[b]$ respectively and adding new monomers at the odd and even free sites $[c]$ and $[d]$. Let the sizes of the sets $[a], [b], [c], [d]$ be a, b, c, d respectively. Let W_0 and W_1 be the propagator matrices connecting odd and even monomer sites corresponding to configurations C_0 and C_1. Hence, W_0 has dimensions $m \times m$ and W_1 has dimensions $(m-a+c) \times (m-b+d)$. Since the configuration weights are functions of determinants of the propagator matrices connecting the monomers in the weak coupling approach as seen in Eq. (3.23), it is clear that the ratio of the configuration weights of C_1 and C_0 is related to the ratio of the determinants of W_0 and W_1. It can be shown that this ratio is given by

$$Det(W_1)/Det(W_0) = Det(W')\sigma \tag{4.22}$$

where σ is a sign factor that cancels in our computations since the determinants appear only as squares. W' is a $(b+c)\times(a+d)$ matrix defined as

$$W' = \begin{array}{c} \\ b \\ \\ c \\ \\ \end{array} \begin{array}{c} \begin{array}{cc} \leftarrow\ a\ \rightarrow & \leftarrow\ d\ \rightarrow \end{array} \\ \left(\begin{array}{c|c} -W_{inv1} & W_{inv2}\ C \\ \hline B\ W_{inv3} & D - B\ W_0^{-1}\ C \end{array}\right) \end{array} \tag{4.23}$$

where W_0^{-1} is the inverse of the matrix W_0 and $W_{inv1}, W_{inv2}, W_{inv3}$ are sub-matrices of W_0^{-1} connecting the removed monomers and added monomers. For example, W_{inv2} has dimensions of $(b \times m)$ and connects the removed b even monomer sites to the original m odd monomer sites. The matrices B, C, D are propagator matrices connecting the newly added monomer sites with the old monomer sites. For example, the matrix B has dimensions $(c \times m)$ and connects the newly added c odd monomer sites with the original m even monomer sites. Refer to Appendix D for a more general discussion.

Thus, the ratio of the configuration weight of any new configuration C_1 to the weight of the background configuration can be obtained by computing the determinant of W'. Now, by allowing $[a]$ and $[b]$ to include all odd and even monomer sites and $[c]$ and $[d]$ to include all odd and even free sites, we can compute the corresponding matrix W' in Eq. (4.23). Let us call this W'_{master}. It is clear that any sub-matrix of W'_{master} corresponds to the matrix W' in Eq. (4.23) for a certain perturbation about the background configuration and the configuration weight ratio can be obtained by computing the determinant of this sub-matrix W'. Thus, W'_{master} contains the information to compute the ratio of configuration weight for all possible new configurations with respect to the background configuration. Thus, starting from a given background configuration C_0, we first need to compute W_0^{-1},

whose computation time scales as $O(N^3)$ [62]. Using this we can compute the matrix W'_{master} and store it. The ratio of the configuration weight of any new configuration to the configuration weight of C_0 can be obtained by computing the determinant of the corresponding sub-matrix W' of W'_{master}. Hence, the time for subsequent updates now scales as $O(n^3)$, where $n = (a + b + c + d)$ is assumed to be small. As we move around in configuration space, n increases. Once it becomes sufficiently large, we can reset the background configuration and recompute the matrix W'_{master} using a method that scales as $O(N^2)$. The real advantage of this method comes from the fact that a retracement of the path in configuration space does not increase n. For example, while a monomer is being moved from one end of the lattice to the other through a series of updates, n is always two. We have empirical proof that this method is very efficient.

In addition to the update, the elements of W'_{master} can also be used to compute the observables through Eqs. (4.14,4.16,4.21). For example, every element in the matrix $D - BW_0^{-1}C$ in the lower right block of W' in Eq. (4.23) gives the weight ratio for an update that involves the addition of an even and an odd monomer, while every element of the matrix $-W_{inv1}$ in the upper left block of W' gives the same for the removal of an even monomer and an odd monomer. Thus, these correspond to the ratio w appearing in Eqs. (4.14,4.16) for the observables C_1 and F_1. Similarly, every element of the matrix $B\ W_{inv3}$ in the lower left block of W' gives the weight ratio for moving an even monomer from an existing site to a new site and every element of $W_{inv2}\ C$ in the upper right block of W' gives the ratio for moving an odd monomer to a new site. These are the elements appearing as w in Eq. (4.21) for the observable C_2. A similar fast computational scheme can be formulated in the strong coupling limit using the free staggered matrix connecting free sites instead of the propagator matrix connecting monomer sites.

One drawback of this method is the large memory required to store the matrix

W'_{master}. For example, for a lattice of size $40 \times 40 \times 40$, this matrix has a size of roughly 32000×32000. Storing such a large matrix requires about 8 gigabytes of memory. To make calculations more amenable, we divide the lattice into sub-blocks of volume roughly 20^3 as discussed at the end of in Section 4.5. Using this technique, we have been able to perform computations on lattices upto size 60^3. Calculations on such large lattices with exactly massless fermions are unprecedented.

5

Results: 3D

In Chapter 3 we introduced a lattice four-fermion model through the action described in Eq. (3.1) and argued that, the model contains a massless fermion (PMW) phase at weak couplings and a massive fermion (PMS) phase at strong couplings. No spontaneous symmetry breaking of any lattice symmetries occurs at strong couplings. In this chapter, we present results in 3D at intermediate couplings obtained using the Monte Carlo methods discussed in Chapter 4 and argue for the presence of a direct second order PMW-PMS phase transition.

5.1 Observables and finite size scaling

In order to explore the physics of our model, we focus on the following observables.

- Average monomer density:

$$\rho_m = \frac{U}{V} \sum_x \langle \psi_{x,1} \psi_{x,2} \psi_{x,3} \psi_{x,4} \rangle \tag{5.1}$$

- Bosonic correlators:

$$C_1(x,y) = \langle \psi_{x,1}\psi_{x,2}\psi_{y,1}\psi_{y,2}\rangle \tag{5.2}$$

$$C_2(x,y) = \langle \psi_{x,1}\psi_{x,2}\psi_{y,3}\psi_{y,4}\rangle \tag{5.3}$$

- Bosonic Susceptibilites:

$$\chi_1 = \frac{1}{2}\sum_x \langle \psi_{0,1}\psi_{0,2}\psi_{x,1}\psi_{x,2}\rangle \tag{5.4}$$

$$\chi_2 = \frac{1}{2}\sum_x \langle \psi_{0,1}\psi_{0,2}\psi_{x,3}\psi_{x,4}\rangle \tag{5.5}$$

Below, we discuss the expected finite size scaling of these observables in different phases.

5.1.1 Scaling in free theory

First we consider the expected scaling of the observables in the free theory. Here we can obtain the results using simple dimensional analysis. Generalizing the continuum free fermionic action given in Eq. (2.8) to d dimensions, it is clear that the fermion field ψ has a mass dimensions $(d-1)/2$. Hence, the long distance correlation functions $C_1(0, L/2-1)$ and $C_2(0, L/2)$ that contain 4 fermion fields should have mass dimensions $2(d-1)$. Assuming that the only scale in the problem is the length of the box L, one expects

$$C_a \sim L^{-2(d-1)} \tag{5.6}$$

for $a = 1, 2$. The susceptibilities are obtained by integrating the correlation functions over the space-time volume. However in 3D and 4D, since the correlations decay sufficiently rapidly at large distances, the susceptibilities χ_1 and χ_2 will be independent of L. The corresponding observables in the lattice theory obtained upon discretizing this continuum theory should behave similarly. The average monomer

density vanishes in the free theory since the Boltzmann weights of a single monomer configuration is zero.

5.1.2 Critical scaling

Assuming our model has a second order critical point at U_c, it would be useful to understand the finite size scaling in the critical region. As we argued in Section 2.3, the form of an observable O with length dimension p near a critical point is given by

$$O \sim L^p \; g\left((U - U_C)L^{\frac{1}{\nu}}\right) \tag{5.7}$$

where U is the coupling, $g(x)$ is an analytic function near $x = 0$ and ν is one of the critical exponents.

However, in this critical region, the dimension p of the observable is not the same as that in the free theory. In principle, every field in the theory gets a new scaling dimension. Usually, in a four-fermion theory, an on site fermion bilinear term like $\overline{\psi}\psi$ is thought of as a bosonic field whose scaling mass dimension is defined as $(d-2+\eta)/2$, where the exponent η quantifies the anomalous dimension with respect to the free scaling dimension. In our model, due to the $SU(4)$ symmetry, we expect $\psi_{x,1}\psi_{x,2}$ and $\psi_{x,3}\psi_{x,4}$ to have the same scaling dimension. This means that in the critical region, the correlators should scale as

$$C_a = L^{-(d-2+\eta)} g_a\left((U - U_C)L^{\frac{1}{\nu}}\right) \tag{5.8}$$

Assuming η is smaller than 2, we also obtain

$$\chi_a = L^{2-\eta} f_a\left((U - U_C)L^{\frac{1}{\nu}}\right) \tag{5.9}$$

where f_a, g_a for $a = 1, 2$ are universal functions that are in general, different. In contrast to the correlation functions, the leading behavior of the average monomer density ρ_m is expected to be a smooth function at U_c, since it behaves like a density and is insensitive to long range correlations.

5.1.3 *Scaling in the PMS phase*

In the PMS phase, one expects massive fermions without any fermion bilinear condensates. This is signalled by exponentially decaying correlation functions. Hence, the correlators and susceptibilities should scale as

$$C_a \quad \sim e^{-m(U)L} \tag{5.10}$$

$$\chi_a \quad \sim \text{Constant} \tag{5.11}$$

where $a = 1, 2$ and $m(U)$ is the mass of a bosonic particle that depends on U. In the critical region, as one approaches the critical point U_c from PMS phase, the correlation lengths diverge as discussed in Eq. (2.22). Since the mass is the inverse of the correlation length, it should scale as

$$m \sim (U - U_c)^{\nu} \tag{5.12}$$

For large couplings in the PMS phase, since configurations with more monomers are enhanced, the average monomer density ρ_m should smoothly approach the value 1.

5.2 General behavior of Observables

The goal of this study is to look for one or more phase transitions between the PMW and PMS phases. The presence of an intermediate phase will mean at least two transitions. However, in case there is just a single transition, we wish to find if it is second order by exploring if the observables show critical scaling. We have performed large scale computations to calculate observables for a range of values of the coupling U. The average monomer density ρ_m and susceptibilities χ_1 and χ_2 were calculated in our first study [35] on lattice sizes up to $L = 28$. In our second study [63], we measured ρ_m, C_1 and C_2 on much larger lattices up to $L = 60$, using a more efficient technique discussed in Section 4.8. We first present the general behavior of our observables as a function of the bare coupling U and lattice size L.

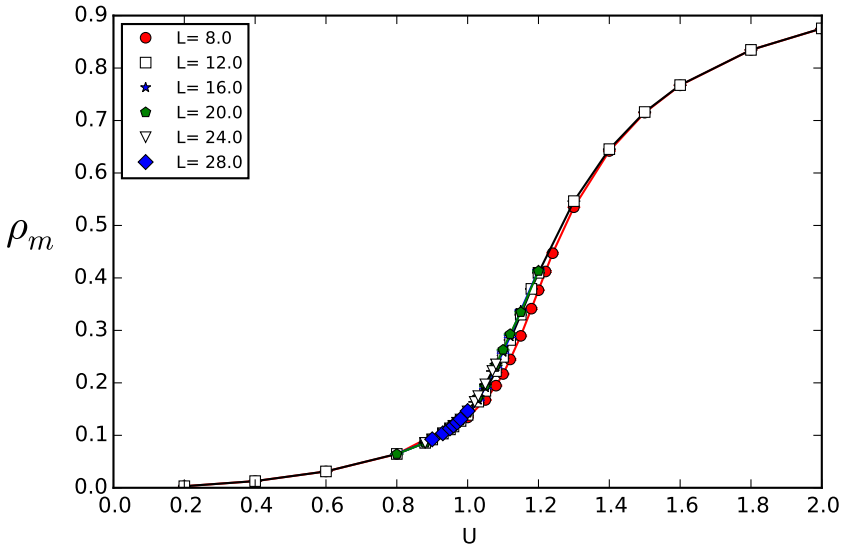

FIGURE 5.1: Figure showing the variation of the average monomer density ρ_m with coupling U for various lattice sizes. ρ_m does not show any discontinuity but increases sharply near $U \sim 1$.

We first plot the variation of the average monomer density ρ_m as a function of the coupling U in Fig. (5.1). It increases smoothly with U as expected, showing a rapid increase around $U \sim 1$. Although it does not vanish in either phase, we believe ρ_m acts as a pseudo order parameter, in the sense that it is small in the PMW phase and large in the PMS phase. Curves for different values of L fall on top of each other for larger lattices, indicating that finite size effects are negligible for lattices beyond size $L = 16$ for this observable.

To understand the physics of the model in more detail, we plot the variation of the bosonic susceptibilities χ_1 and χ_2 with coupling U in Fig. (5.2) for various lattice sizes. Note that for a fixed value of L, the susceptibilities increase as a function of U, reaching a maximum somewhere near $U \sim 1$ and then decrease again at large couplings. The value of the peak susceptibility (χ_{peak}) increases while the location of the peak (U_{peak}) decreases with L. In order to qualitatively understand the scaling of these susceptibilities with L, we plot these susceptibilities as a function of lattice size

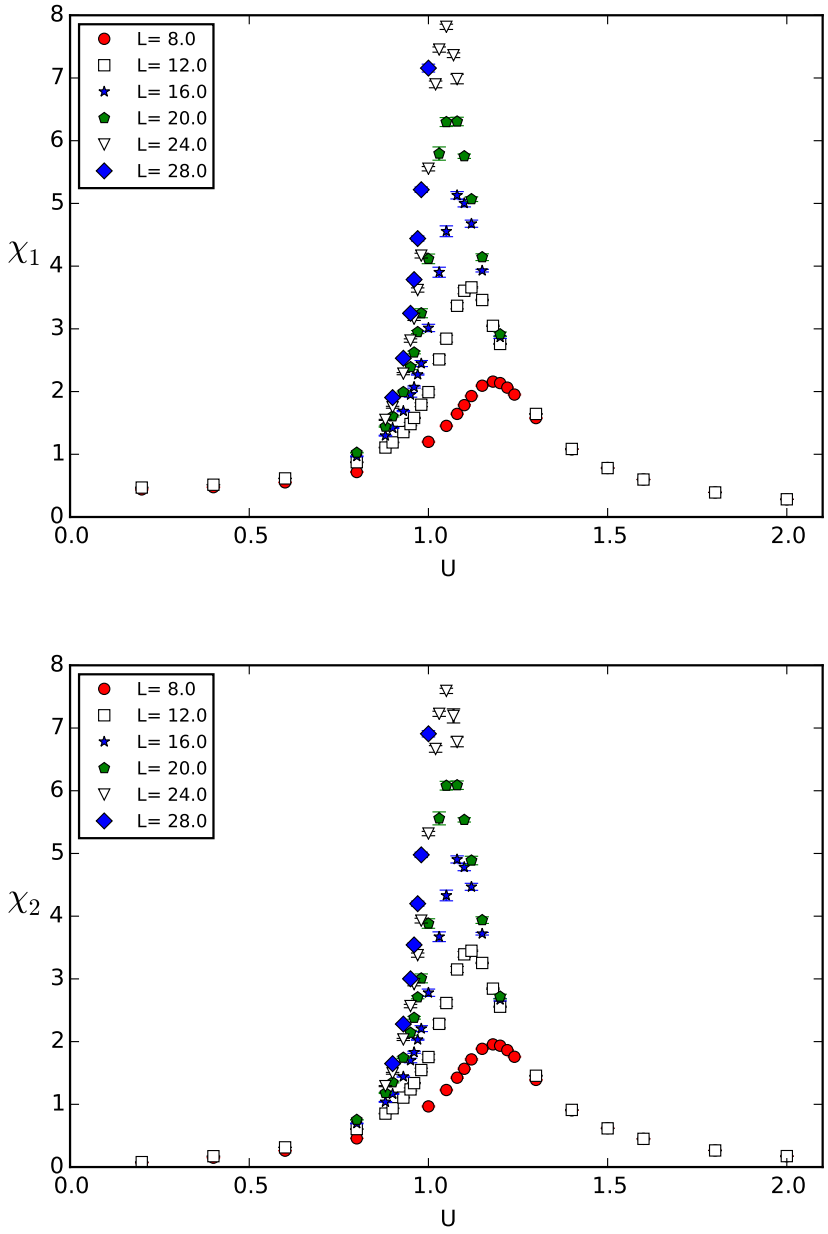

FIGURE 5.2: Plot of the susceptibilities χ_1 and χ_2 as a function of U. The susceptibilities increase sharply near $U \sim 1$ to reach a maximum and then decrease in the strong coupling limit.

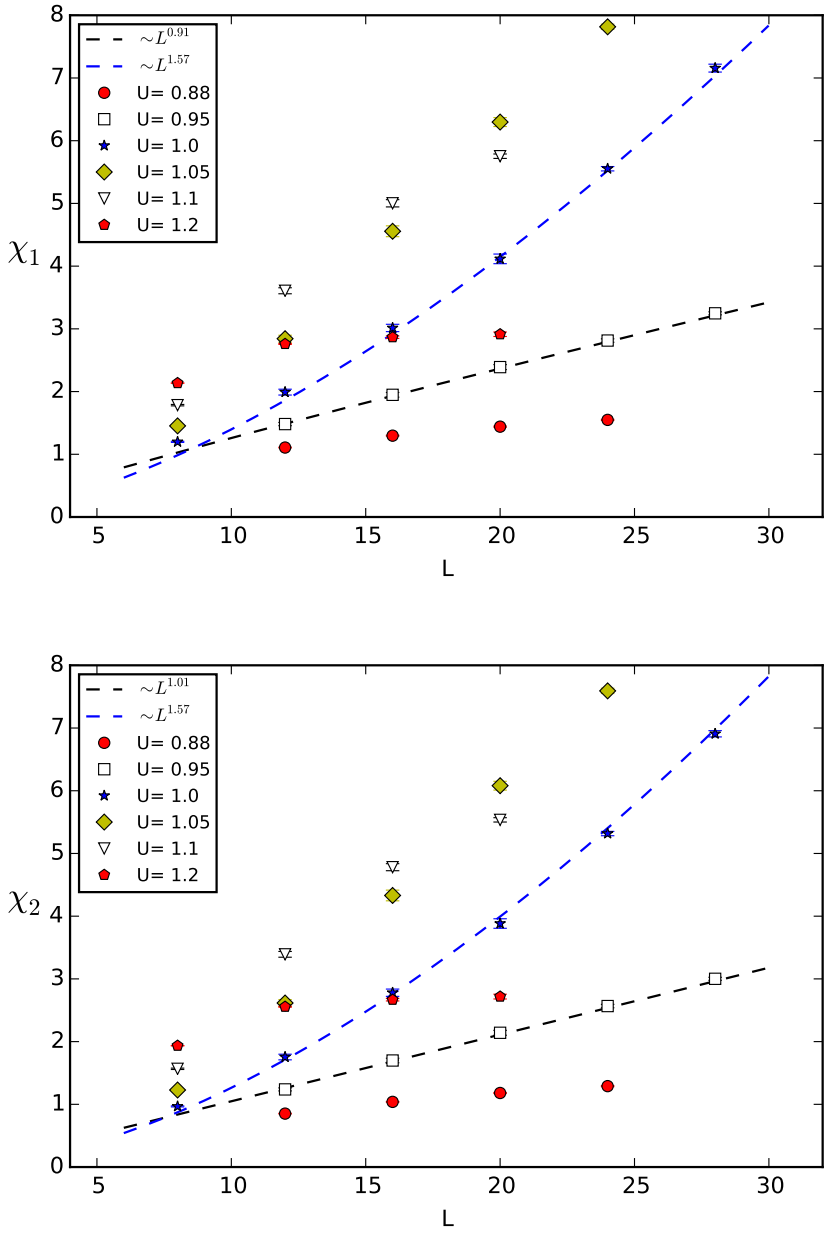

FIGURE 5.3: Plot of the susceptibilities χ_1 and χ_2 as a function of L. The susceptibilities saturate for small (U=0.88) and large (U=1.2) couplings. The steepest growth of χ_1 and χ_2 in the intermediate region is at U=1.0, where they grow as $\sim L^{1.6}$. The absence of an L^3 growth of the susceptibilities in the coupling space points to the absence of SSB.

L in Fig. (5.3). For small couplings ($U = 0.88$), the susceptibilities saturate with an increase in the lattice size, as expected in the PMW phase. For couplings close to $U = 0.95$, both susceptibilities grow linearly with the lattice size. For large couplings ($U = 1.2$), the susceptibilities again saturate, as expected in the PMS phase. The steepest growth of the susceptibilities is near U = 1.0, where they grow as $L^{1.6}$. As indicated in Eq. (3.13), if a fermion bilinear condensate forms (i.e. $\langle \psi_{x,1} \psi_{x,2} \rangle \neq 0$), we expect $\chi_1 \sim L^3$. Thus, based on Fig. (5.3), it is quite clear that there is no coupling where fermion bilinear condensates form. Thus, data from our first study with $L \leqslant 28$ points to a single phase transition between the PMW and PMS phases.

To explore this phase transition further, we looked at the behavior of the correlators on much larger lattices. The long distance behavior of the correlators $C_1(x, y)$ and $C_2(x, y)$ can be studied using the correlator ratios defined as

$$\begin{aligned} R_1 &= \frac{C_1\left(0, \frac{L}{2} - 1\right)}{C_1(0, 1)} \\ R_2 &= \frac{C_2\left(0, \frac{L}{2}\right)}{C_2(0, 0)} \end{aligned} \tag{5.13}$$

These correlator ratios scale like the correlation functions.

Fig. (5.4) shows the behavior of these correlator ratios as a function of coupling U for various lattice sizes. Like the susceptibilities, these ratios show a maximum for an intermediate value of U. However, the correlator ratios decrease with lattice size L as opposed to the susceptibilities which increase with lattice size. Fig. (5.5) shows the behavior of the correlator ratios R_1 and R_2 as a function of lattice size L for various couplings in a log-linear plot. The correlators decay as a power-law for small ($U = 0.85$) and intermediate couplings ($U = 0.95$). At large couplings close to $U = 1.03$, the decay becomes exponential as $e^{0.07L}$ and this indicates the onset of the massive phase at large U. At $U = 1.0$ (not shown in the figure), where the susceptibilities showed the steepest rise, we find that the correlator ratios decay as a

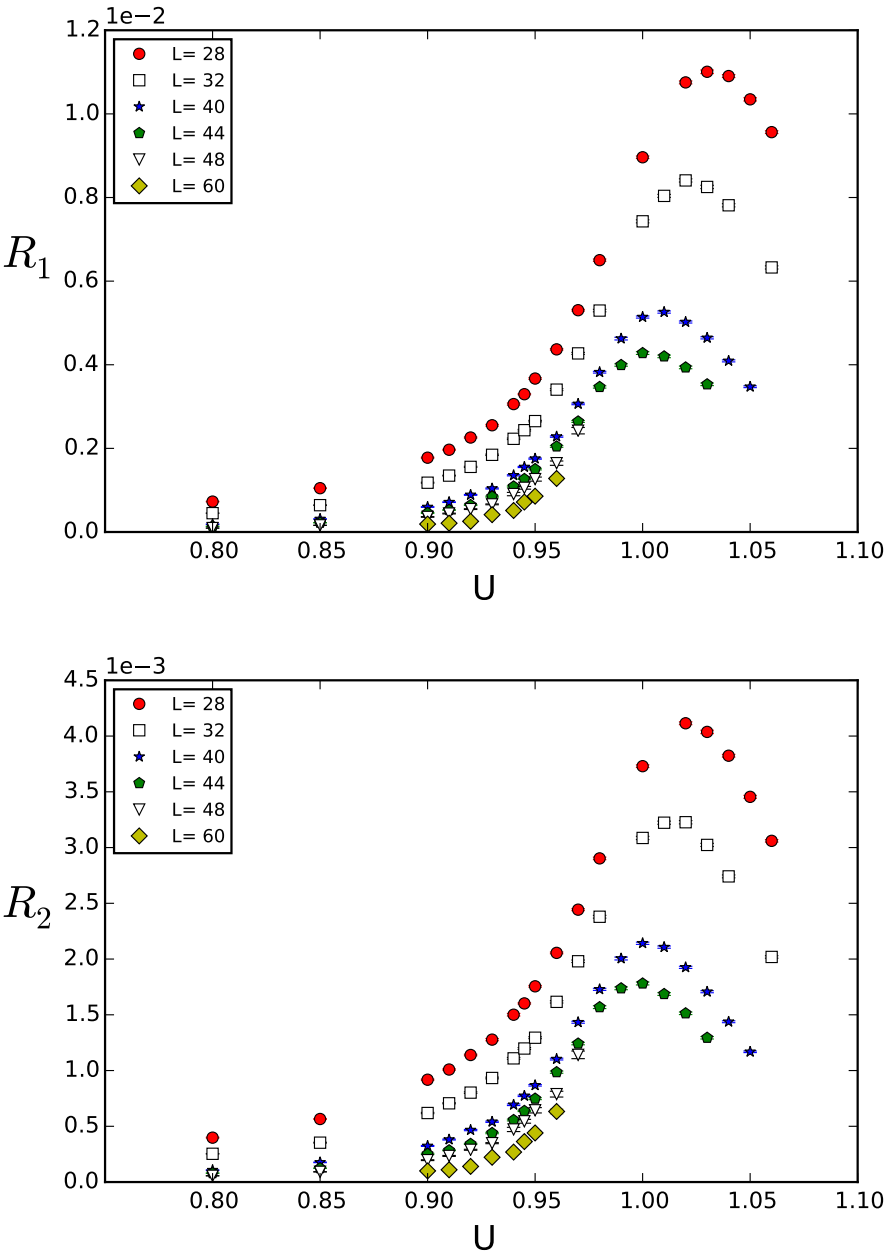

FIGURE 5.4: Plot of the correlator ratios R_1 and R_2 as a function of U. The correlator ratios show a peak for intermediate values of the coupling U before decaying exponentially to zero at large couplings.

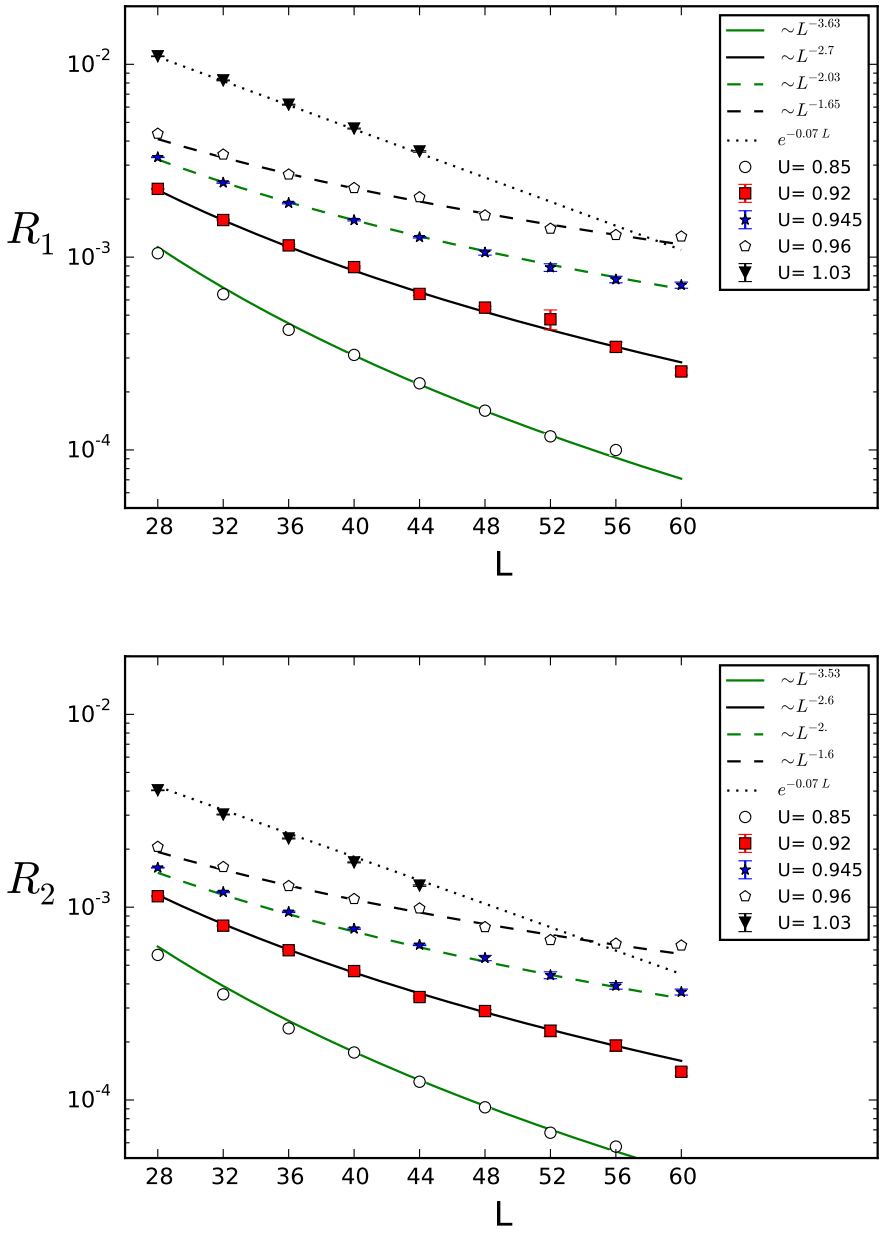

FIGURE 5.5: Log-linear plot of the correlator ratios R_1 and R_2 as a function of L. For small couplings ($U = 0.85$), the correlator ratios decay roughly as $L^{-3.6}$, which is close to the free theory behavior of L^{-4}. Near $U = 0.945$, the decay is a power-law given by $\sim L^{-2}$. For large couplings ($U = 1.03$), the decay is exponential, thereby indicating the onset of the massive phase.

power-law and the decay gets steeper as we include data for larger lattices. All this implies the absence of any condensates and hence an intermediate FM phase. Thus, the large lattice data confirms the earlier prediction that the PMW and PMS phases in this model are separated by a single phase transition, without the presence of any intermediate phase. Our entire 3D data has been tabulated in Appendix E.

5.3 Analysis

The qualitative behavior of the correlator ratios R_1 and R_2 clearly indicate the presence of a single phase transition between the PMW and PMS phases at a point U_c. We now wish to perform an analysis to see if the data is consistent with a single second order transition. Our approach is to try fitting the data to the expected forms given in Eq. (5.8) for a second-order phase transition. For a first order phase transition, this procedure will fail since correlation lengths do not diverge.

At the critical point, it is clear from Eq. (5.8) that the correlators must decay as a power-law and such a fit should enable the extraction of critical exponents. However, even with high precision data on large lattices up to size $L = 60$, we found it difficult to extract the critical quantities by performing a simple power-law fit. Hence, we had to carry out a more sophisticated analysis to understand the nature of the phase transition and compute the critical exponents and we describe this below. This analysis has been published as part of the supplementary material to [63].

5.3.1 Critical finite size scaling

From Eq. (5.8) we expect the correlation ratios R_1 and R_2 to scale according to the form

$$R_a(U, L) \;=\; \frac{1}{L^{(1+\eta)}}\; g_a\left((U - U_c)\; L^{\frac{1}{\nu}}\right) \tag{5.14}$$

where $g_a(x),\ a = 1, 2$ are universal functions of the variable $x = (U - U_c)\, L^{\frac{1}{\nu}}$. Usually, by expanding $g_a(x)$ in a power series and fitting the data to Eq. (5.14), the unknown coefficients and critical quantities $(U_c,\ \nu,\ \eta)$ can be extracted. However, such fits with unknown powers are known to be unstable. Hence we use a more elaborate analysis. We first note that when $U = U_c$ we expect

$$R_a(U_c, L) = \frac{f_a}{L^{1+\eta}} \tag{5.15}$$

where f_a is a constant and the critical exponent η is the same for both R_1 and R_2.

Since neither the location of the critical point nor the value of η at that point are known, it is difficult to compute U_c and η together using the above relation. This is typical for all second order critical points and one usually finds that many couplings near the critical point obey power law scaling with slightly different values of η. A combined fit of both correlation ratios to the form given in Eq. (5.15) for the couplings in the range $0.85 \leqslant U \leqslant 0.96$ and lattice sizes $L \geqslant 32$, yields the results shown in Table 5.1.

The low χ^2 values of the fits imply that the critical point could be at any value of U in the range $0.93 < U_c < 0.95$. Note that the fit is poor for $U = 0.96$, indicating perhaps that we have reached the massive phase. The behavior of η as a function of U is shown in Fig. (5.6). While this figure gives us a relation between U_c and η, it does not constrain them. Hence, we have used an independent analysis to constrain them and this is dicussed below.

5.3.2 Scaling of Pseudo-Critical Points

While critical points are defined only in the thermodynamic limit, there exists a notion of pseudo-critical points even in a finite system. Interestingly, quantities close to the pseudo-critical points also obey critical scaling and thus can help in the extraction of critical quantities independently. Consider for example the variation of

Table 5.1: The critical exponent η as a function of the critical coupling U_c from the powerlaw fits ignoring corrections to scaling.

U_c	f_1	f_2	η	χ^2
0.85	68(10)	38(5)	2.34(4)	2.2
0.92	15(3)	8(1)	1.64(5)	4.1
0.93	9(1)	4.5(5)	1.44(3)	1.9
0.94	4.8(4)	2.4(2)	1.22(2)	1.0
0.945	2.5(2)	1.2(1)	1.00(2)	0.7
0.95	1.2(1)	0.59(5)	0.77(2)	1.1
0.96	1.0(2)	0.46(8)	0.63(5)	6.4

correlation ratios R_1 and R_2 with coupling U for different lattice sizes shown in Fig. (5.7). It is clear from the figure that the ratios display a maximum for certain value of the coupling (which we refer to as $U_{a,p}$). These define one set of pseudo-critical couplings. At the peak, the value of the ratio itself is given by $R_{a,p}$. From the scaling relation in Eq. (5.14), we note that the peak occurs when the function $g_a(x)$ reaches a maximum. Assuming this occurs at $x = d_a$, it can be shown that:

$$R_{a,p} = \frac{b_a}{L^{1+\eta}} \tag{5.16}$$

$$U_{a,p} = U_c + d_a/L^{\frac{1}{\nu}}. \tag{5.17}$$

Thus, if we can compute $R_{a,p}$ as a function of L, we would have an independent way to estimate η using Eq. (5.16). We can then use the η vs U_c plot of Fig. (5.6) to estimate U_c. Using this value of U_c in Eq. (5.17) we can compute ν.

In order to extract $U_{a,p}$ and $R_{a,p}$, we approximate the behavior of the correlation ratios around the peak as a quadratic. Table 5.2 shows the results of such fits. The errors in the fits include systematic errors associated with choosing a quadratic form near the peak instead of say a cubic or quartic form.

Using the data for $R_{1,p}$ and $R_{2,p}$ from Table 5.2, we have performed a combined fit of the form expected in Eq. (5.16). Including the entire data from above ($24 \leqslant L \leqslant$

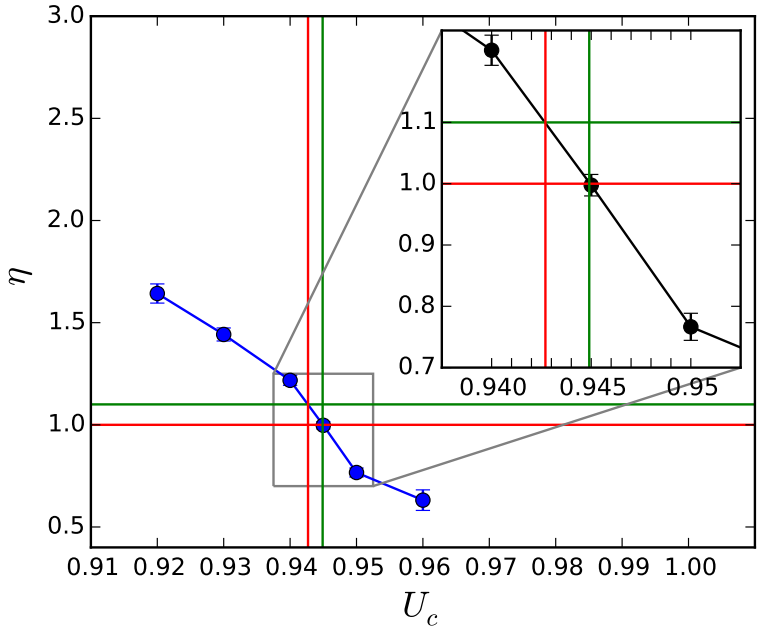

FIGURE 5.6: Plot of η as a function of U_c using the fits in Table 5.1. We have used the power-law fits to obtain the η values assuming the location of the critical point.

44) gives us $b_1 = 6.3(9)$, $b_2 = 2.4(4)$, $\eta = 0.91(4)$, $\chi^2 = 94.9$. A closer examination shows that while $R_{1,p}$ fits well to a single power law in the entire region giving $b_1 = 11.2(2)$, $\eta = 1.08(1)$ with a $\chi^2/d.o.f = 1$, $R_{2,p}$ is not consistent with a single power law. Table 5.3 shows the results of fitting $R_{2,p}$ individually and dropping the lower lattice sizes systematically.

We interpret the drift of η to larger values as a sign that $R_{2,p}$ contains pronounced corrections to scaling. If we only keep the lattice sizes of $L = 40, 44$ in the $R_{2,p}$ data and perform a combined fit of both $R_{1,p}$ and $R_{2,p}$ we obtain $b_1 = 11.1(2)$, $b_2 = 4.6(1)$, $\eta = 1.08(1)$, $\chi^2 = 0.77$. The goodness of the fit is shown in the top plot of Fig. (5.8).

In order to confirm that the drift of η is consistent with the presence of corrections to scaling, we added a correction term for $R_{2,p}$ and performed a combined fit of the

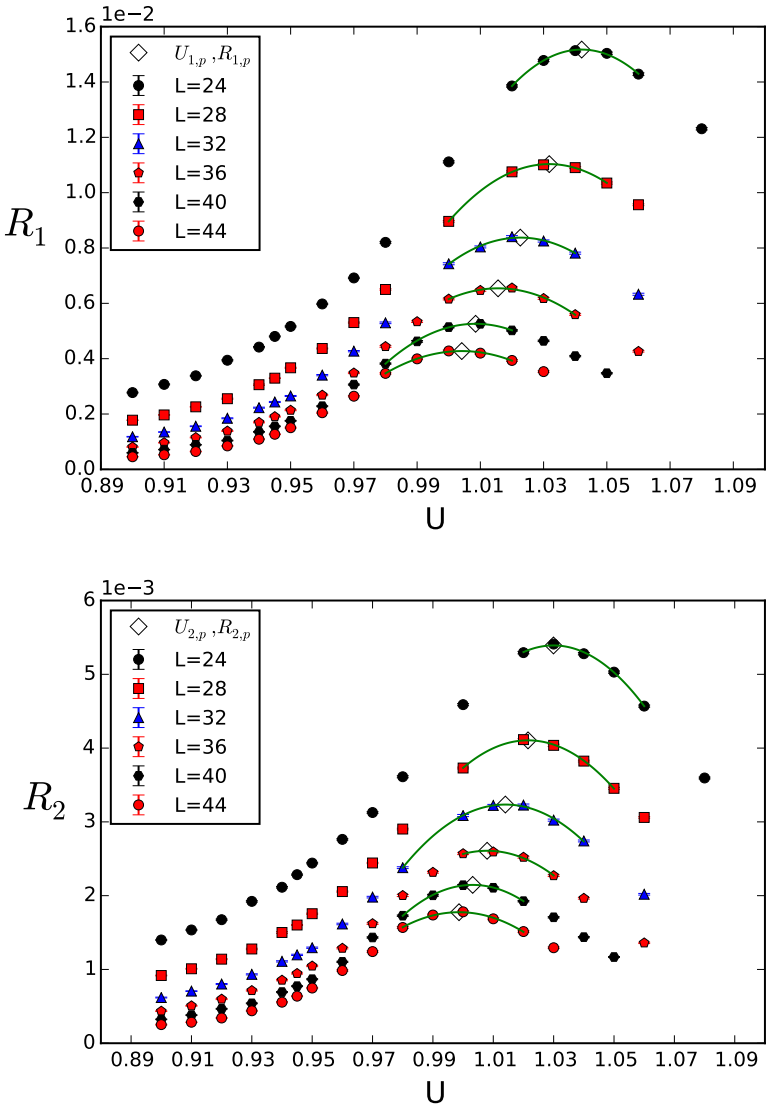

FIGURE 5.7: Plot of correlation ratios $R_a, a = 1, 2$ as a function of coupling U. These ratios display a maximum at $(U_{a,p}, R_{a,p})$. We use these peak values to estimate the critical exponents.

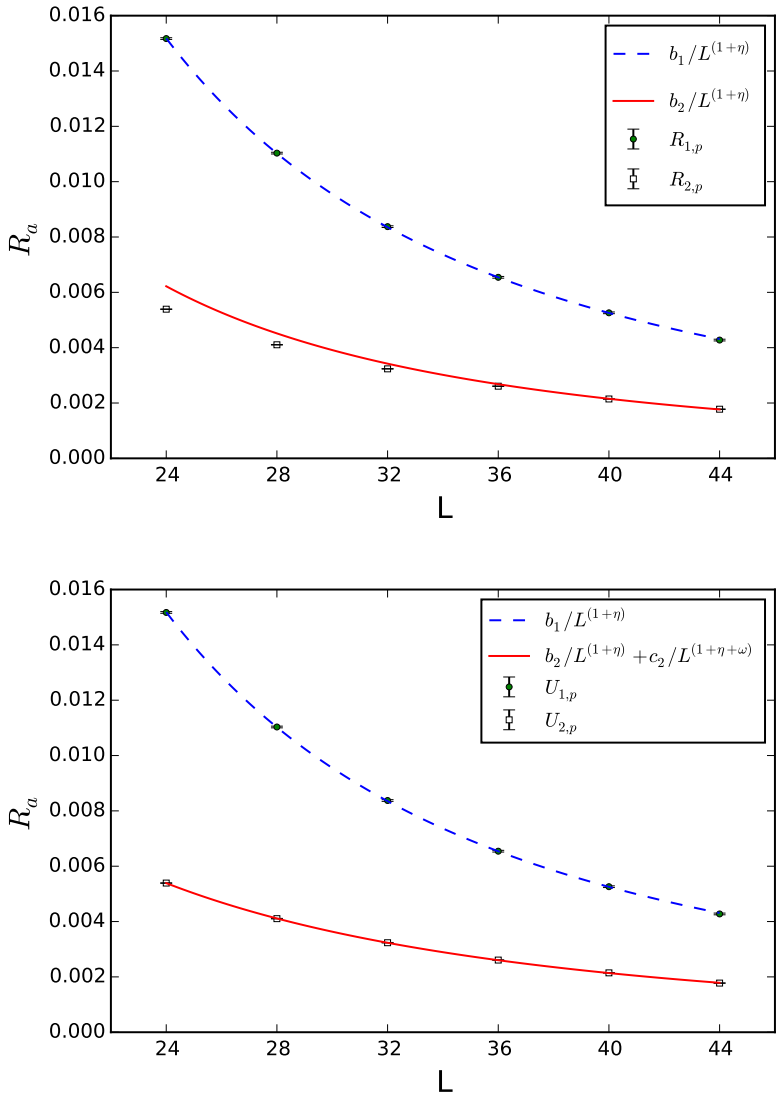

FIGURE 5.8: Plots of $R_{1,p}$ and $R_{2,p}$ as a function of L. In the top plot, the solid and dashed lines show fits to the form Eq. (5.16), while in the bottom plot these lines show fits to the form in Eqs. (5.18) and (5.19) that include corrections to scaling. To achieve a good fit, in the top figure it was necessary to drop the data for $R_{2,p}$ in the region $L \leqslant 36$, while in the bottom figure we could fit the entire data by assuming the correction to the scaling exponent $\omega = 1$.

Table 5.2: Results for the value of $R_{1,p}$, $U_{1,p}$, $R_{2,p}$ and $U_{2,p}$ obtained from a quadratic fit of the data near the peak.

L	$U_{1,p}$	$R_{1,p}$	χ^2	$U_{2,p}$	$R_{2,p}$	χ^2
24.0	1.0420(8)	$1.517(3) \times 10^{-02}$	0.473	1.0299(8)	$5.391(9) \times 10^{-03}$	1.734
28.0	1.0318(8)	$1.103(3) \times 10^{-02}$	0.1622	1.0215(8)	$4.105(9) \times 10^{-03}$	0.8016
32.0	1.0226(8)	$8.38(3) \times 10^{-03}$	1.519	1.0140(8)	$3.235(9) \times 10^{-03}$	1.407
36.0	1.0156(8)	$6.54(3) \times 10^{-03}$	1.752	1.0080(8)	$2.608(9) \times 10^{-03}$	2.004
40.0	1.0085(8)	$5.26(3) \times 10^{-03}$	0.4788	1.0032(8)	$2.146(9) \times 10^{-03}$	0.21
44.0	1.0041(8)	$4.28(3) \times 10^{-03}$	0.7981	0.9986(8)	$1.776(9) \times 10^{-03}$	0.9341

Table 5.3: Fits of $R_{2,p}$ as a function of L to the expected scaling form for different ranges of lattice sizes. Importantly η drifts upwards.

L-Range	b_2	η	χ^2
24-44	1.68(3)	0.81(1)	6.3
28-44	1.84(5)	0.83(1)	3.9
32-44	2.10(11)	0.86(2)	2.3
36-44	2.38(25)	0.90(3)	2.2
40-44	3.25(76)	0.99(6)	0.0

entire data to the form:

$$R_{1,p} = \frac{b_1}{L^{1+\eta}} \tag{5.18}$$

$$R_{2,p} = \frac{b_2}{L^{1+\eta}} + \frac{c_2}{L^{1+\eta+\omega}} \tag{5.19}$$

Now including the entire data set in Table 5.2, we find a good fit as shown in the bottom plot of Fig. (5.8), giving us $b_1 = 11.2(2)$, $b_2 = 5.6(4)$, $c_2 = -25(12)$, $\eta = 1.08(1)$, $\omega = 0.9(2)$, $\chi^2 = 0.752$. This gives some credence to our belief that $R_{2,p}$ data contains corrections to scaling.

However, there is a bias in the above analysis since it is likely that the presence of smaller lattice data in $R_{1,p}$ affects the fitting. Hence we roughly estimate the systematic errors in η due to the the range of lattice sizes we use in the fit. Keeping

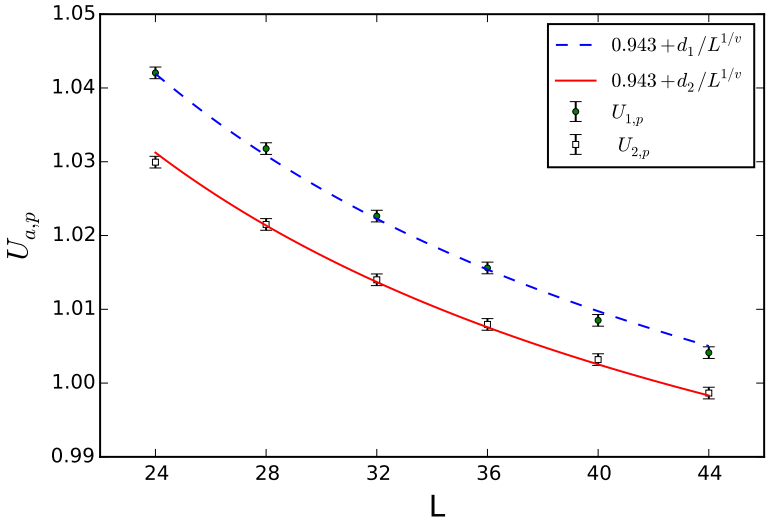

FIGURE 5.9: Plots of $U_{1,p}$ and $U_{2,p}$ as a function of L. The solid and dashed lines are fits to Eq. (5.17) assuming $U_c = 0.943$. We obtain $d_1 = 1.14(6)$ and $d_2 = 1.02(5)$ and the $\chi^2/\text{dof} = 1.0$.

only $L = 40, 44$ data for both $R_{1,p}$ and $R_{2,p}$ and ignoring corrections to scaling we obtained $\eta \approx 1.05$ but with a $\chi^2/dof = 2.5$ which is rather large. But by keeping $L = 36$ and dropping $L = 44$ instead, we get a good fit but with $\eta \approx 1.02$. Thus, a conservative estimate would be $\eta = 1.05(5)$.

Using $\eta = 1.05(5)$ we can again conservatively estimate U_c from Fig. (5.6) to be $U_c = 0.943(2)$. We can then use Eq. (5.17) to estimate ν. Again assuming no corrections to scaling we find that a combined fit of both the data $U_{1,p}$ and $U_{2,p}$ fits well to single power law. Performing two fits by fixing $U_c = 0.945$ and $U_c = 0.941$ we obtain $\nu = 1.30(7)$. The goodness of the fits, assuming $U_c = 0.943$, are shown in Fig. (5.9). For this value of U_c we obtain $d_1 = 1.14(6)$ and $d_2 = 1.02(5)$ with $\chi^2/\text{dof} = 1.0$.

5.4 Corrections to Scaling

Since we have ignored corrections to scaling in the analysis above, one might wonder if introducing corrections to scaling can change the results. Experience tells us that usually once we include corrections to scaling the fits become unstable unless we can constrain at least some of the exponents by other arguments. This is difficult in our context due to the exotic nature of the phase transition. Here we use corrections to scaling to check if our data is consistent with the exponents from large N predictions in a typical Gross Neveu model, i.e. $\eta = 1$ and $\nu = 1$.

Assuming no corrections to scaling, but fixing $\eta = 1$ and removing data for $L = 24, 28, 32, 36$ for $R_{2,p}$ which gave a good fit above yields $b_1 = 8.5(1)$, $b_2 = 3.4(1)$, with a $\chi^2/\text{dof}= 21$. The fit is shown on the top plot of Fig. (5.10). We note that the fit does seems to roughly pass through all the points although the the χ^2/dof is large. The reason for this is that our data is quite precise and we are sensitive to corrections to scaling assuming they are present. Indeed, if we introduce corrections to scaling and assume

$$R_{a,p} = \frac{b_a}{L^{1+\eta}} + \frac{c_a}{L^{1+\eta+\omega}} \tag{5.20}$$

and fix for example $\omega = 1$ then one can fit the entire data set ($24 \leqslant L \leqslant 44$) for both correlation ratios very well. We obtain $b_1 = 7.92(8)$, $c_1 = 20(2)$, $b_2 = 3.91(2)$, $c_2 = -19.2(6)$, with a $\chi^2/\text{dof} = 1.1$. The goodness of the fit is shown in the bottom plot of Fig. (5.10).

From Table 5.1, we note that $\eta = 1$ gives $U_c = 0.945$ assuming corrections to scaling are small at the critical point. Fixing $\nu = 1$ and $U_c = 0.945$, a combined fit of $U_{1,p}$ and $U_{2,p}$ data to the form Eq. (5.17) gives $d_1 = 2.45(5)$, $d_2 = 2.18(5)$ with a $\chi^2/\text{dof} = 20$. This is clearly a bad fit as shown in the top plot of Fig. (5.11). On

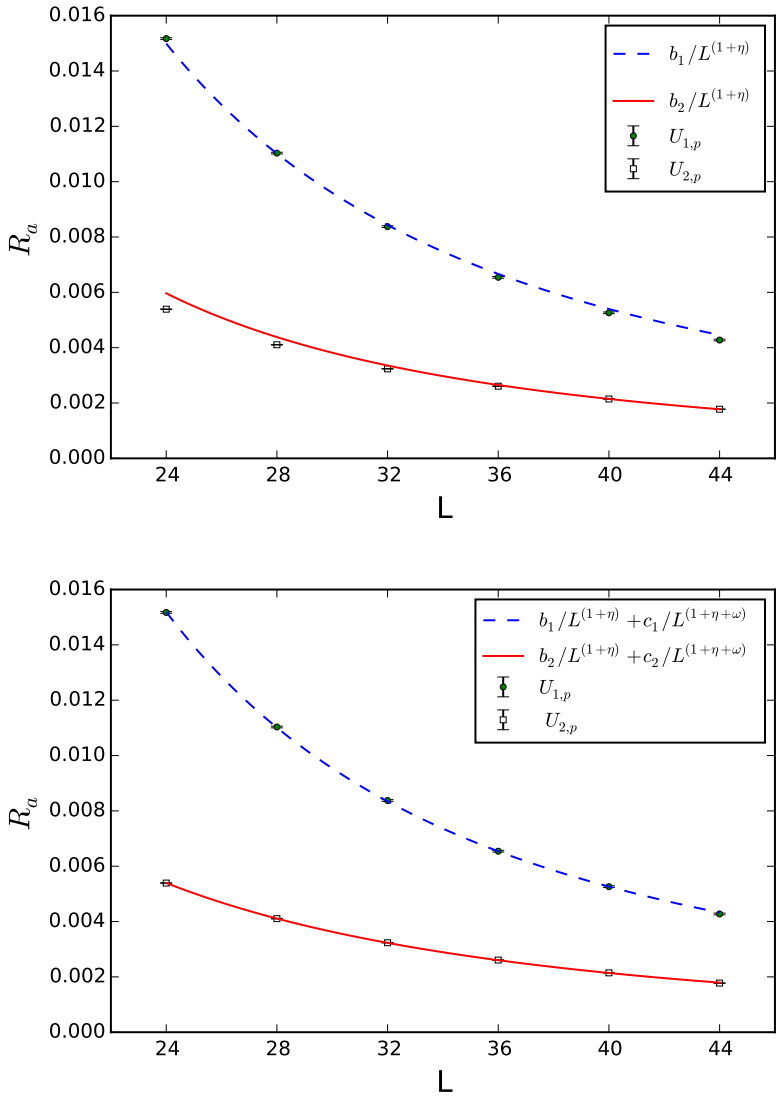

FIGURE 5.10: Plots of $R_{1,p}$, $R_{2,p}$ as a function of L showing fits to large N exponents with (bottom) and without (top) corrections to scaling. In the fits we fix $\eta = 1$ and $\omega = 1$. The χ^2/dof for the fits are 21 when the corrections to scaling are omitted and 1.1 when they are included.

the other hand if we introduce corrections to scaling and assume

$$U_{a,p} = U_c + \frac{d_a}{L^{\frac{1}{\nu}}} + \frac{h_a}{L^{\left(\frac{1}{\nu}+\omega\right)}}, \tag{5.21}$$

with $U_c = 0.945$, $\nu = 1$ and $\omega = 1$ as before, we obtain a good fit as shown in the bottom plot of Fig (5.11). The fit yields $d_1 = 2.91(2)$, $h_2 = -13.9(7)$, $d_2 = 2.74(2)$, $h_2 = -16.9(7)$ which a $\chi^2/\text{dof} = 0.2$. If we do not fix U_c while ignoring the corrections to scaling, again we obtain a good fit with $U_c = 0.960(1)$, $d_1 = 1.98(4)$, $d_2 = 1.70(4)$, and $\chi^2/\text{dof} = 1.18$. However, this value of U_c cannot be consistent with our data in Table 5.1, again suggesting the presence of large corrections to scaling.

Thus, we believe that including scaling corrections will enable us to fit the data to large N exponents of $\eta = 1$ and $\nu = 1$. However, if we take this view point one has to argue that there are significant corrections to scaling even up to $L = 44$. On the other hand since we were able to fit the data without corrections to scaling to a different set of exponents, we believe that our original analysis should be correct.

5.5 Universal Function

A good way to further test if the PMW-PMS transition is second order is to look at the behavior of the universal functions g_a in Eq. (5.14). It is clear from Eq. (5.14) that a plot $R_a L^{1+\eta}$ as a function of $(U - U_c)L^{\frac{1}{\nu}}$ should be a smooth function for a second order transition. Fig. (5.12) shows such a plot assuming $U_c = 0.943$, $\eta = 1.05$ and $\nu = 1.30$ obtained from our analysis. We also plot the universal functions obtained using the large N exponents $\eta = 1$ and $\nu = 1$, with $U_c = 0.945$. This is shown in Fig. (5.13). All these plots look reassuring and seem to indicate that the transition is indeed second order.

Based on the above analysis we can conclude that either we have a new set of exponents with $\eta = 1.05(5)$ and $\nu = 1.30(7)$, or there are large corrections to scaling

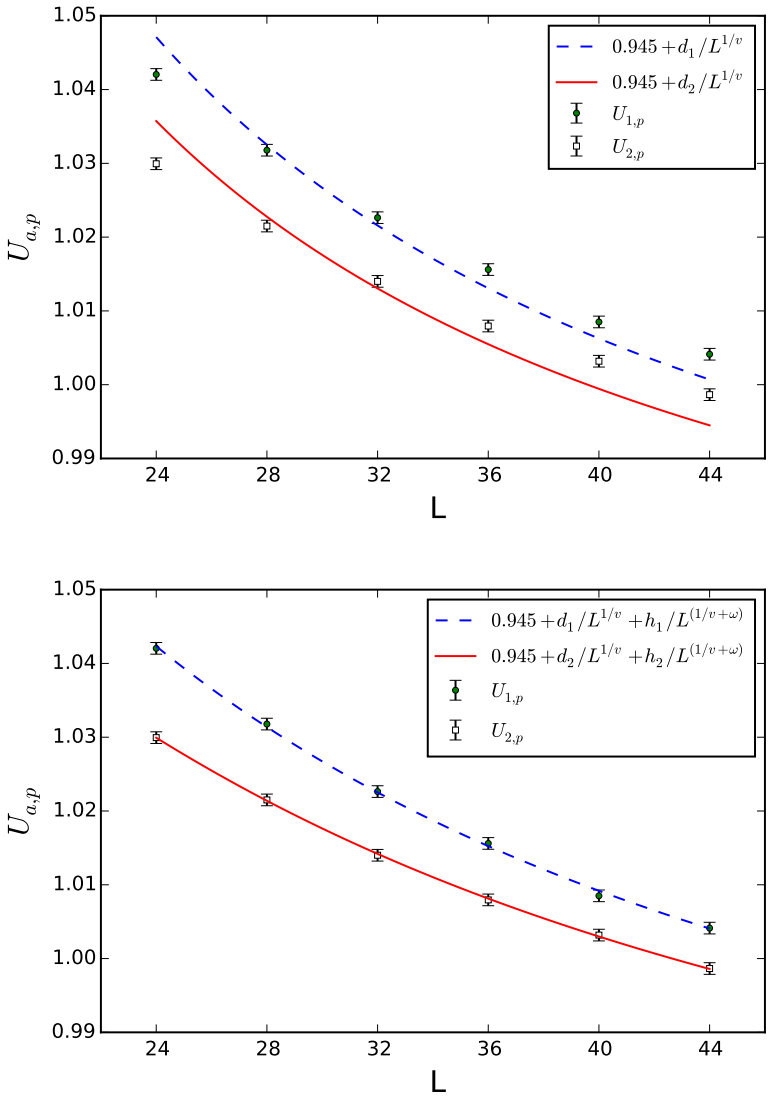

FIGURE 5.11: Plots of $U_{1,p}$, $U_{2,p}$ as a function of L showing fits to large N exponents with (bottom) and without (top) corrections to scaling. In the fits we fix $U_c = 0.945$, $\nu = 1$ and $\omega = 1$. The χ^2/dof for the fits are 20 when the corrections to scaling are omitted and 0.2 when they are included.

up to lattice sizes of the order of $L = 44$ and the exponents are very close to the large N values. While calculations at larger lattices may be useful to get better estimates of the critical exponents, given the difficulty in performing large scale Monte Carlo calculations, it will be useful to explore new techniques of analysis that reduces the

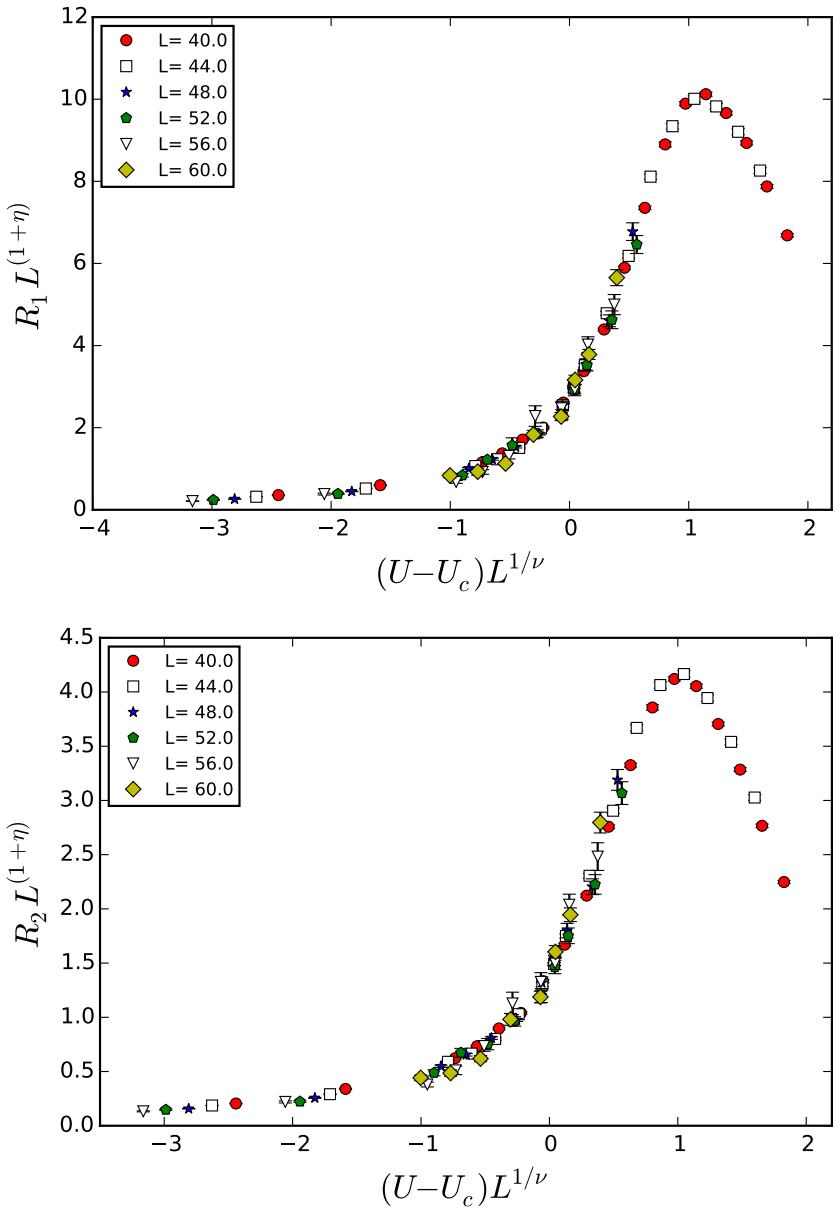

FIGURE 5.12: Plots of the universal functions $g_1(x)$ (top) and $g_2(x)$ (bottom) assuming $U_c = 0.943$, $\nu = 1.30$, and $\eta = 1.05$. A smooth curve confirms that the transition is second order.

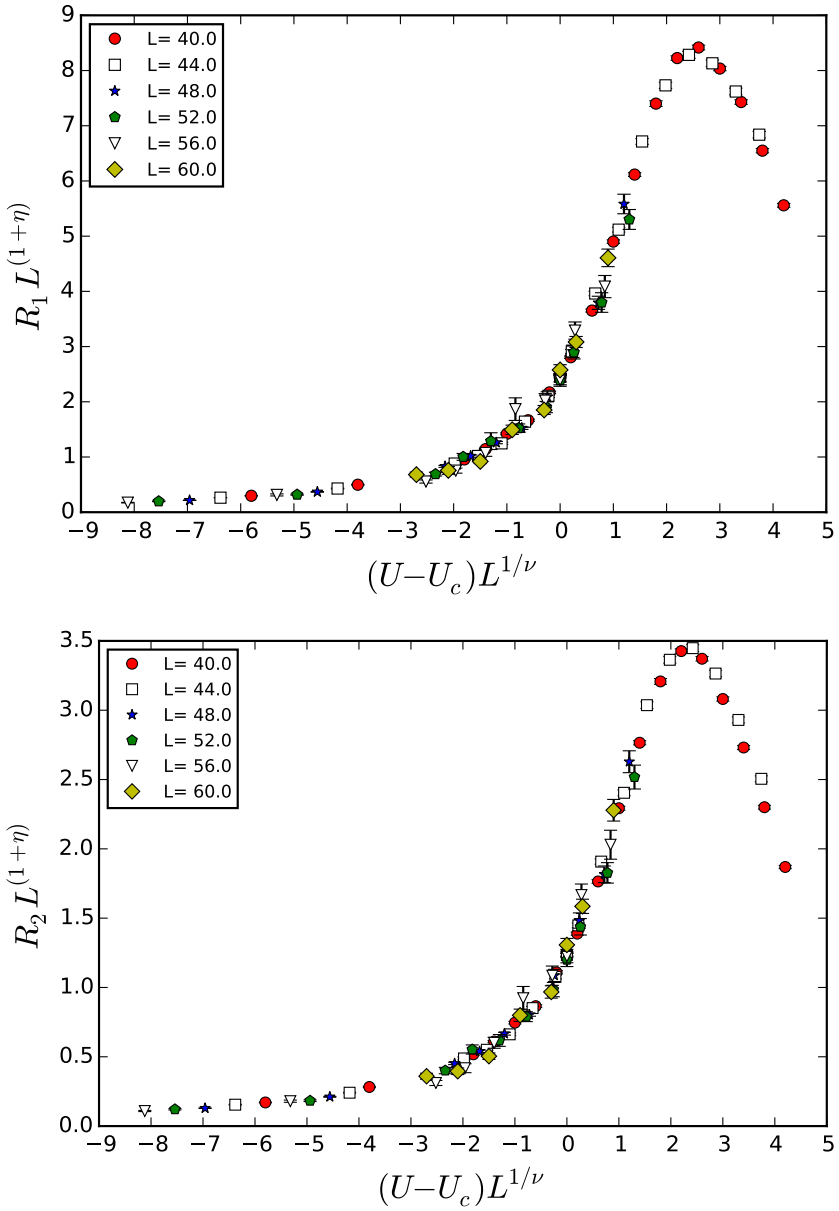

FIGURE 5.13: Plots of the universal functions $g_1(x)$ (top) and $g_2(x)$ (bottom) assuming $U_c = 0.945$, $\nu = 1$, and $\eta = 1$. Again we find a smooth curve. Hence, we cannot rule out the large N exponents $\nu = 1,\ \eta = 1$.

systematic errors due to corrections to scaling.

5.6 Summary of results

To summarize, our analysis of the Monte Carlo data up to lattices $L = 60$ provides strong evidence that the lattice model studied in our work has a single phase transition between the PMW and the PMS phase, without any intermediate FM phase. Our analysis shows that this transition is second order. We estimate $U_c = 0.943(2)$, $\eta = 1.05(5)$ and $\nu = 1.30(7)$. However, we cannot rule out the large N exponents $\eta = 1,\ \nu = 1$ with $U_c = 0.945$ if we allow for large corrections to scaling in our data.

6

Results: 4D

In the previous chapter, we discussed the results in 3 Euclidean dimensions. We have also performed calculations using the same model in 4 Euclidean dimensions. Unfortunately, the extra dimension increases both the time of computation and also the memory requirements. As a result, we could only explore lattices as large as 14^4. In 4D, the goal is either to confirm earlier findings of a wide spontaneously broken intermediate phase [10] or find some evidence of a direct second order transition like in 3D. We will argue below that in contrast to 3D, we do find a narrow intermediate phase which spontaneously breaks the $SU(4)$ symmetry.

6.1 General Behavior of Observables

We first look at the general behavior of the observables as a function of the bare coupling U and lattice size L. Fig. (6.1) shows the variation of the average monomer density ρ_m as a function of the coupling U for various values of L. As in the 3D case, the average monomer density increases smoothly with U, but shows a rapid increase around $U \sim 1.75$. Finite size effects seem to be negligible for lattices larger than $L = 12$.

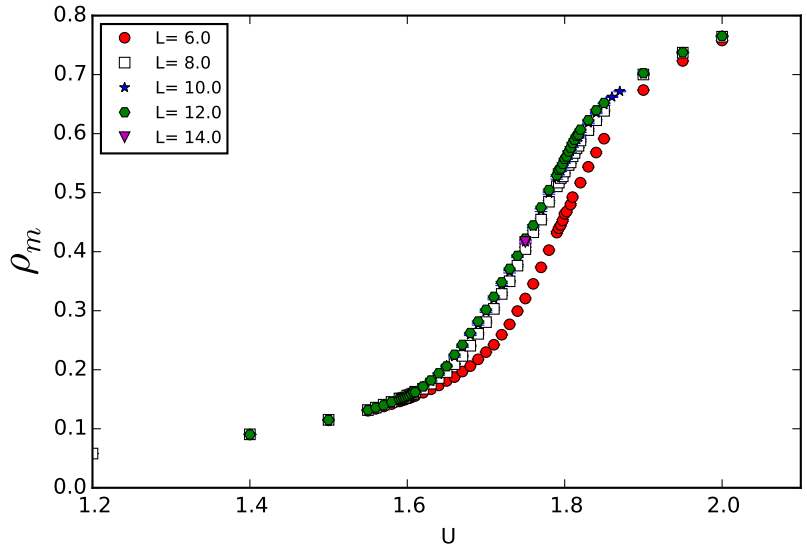

FIGURE 6.1: Plot of the variation of the average monomer density ρ_m with coupling U. The average monomer density rises sharply in the region close to $U = 1.75$.

The qualitative behavior of the susceptibilities is also similar to 3D. As seen in Fig. (6.2), the bosonic susceptibilities χ_1 and χ_2 increase with the coupling to reach a maximum and then decrease again at large couplings. Deviations from the 3D case begin to emerge when we start looking at the variation of the susceptibilities with lattice size L. This is shown as a log-log plot in Fig. (6.3). For small ($U = 1.4$) and large ($U = 1.9$) couplings, the susceptibilities seem to saturate as the lattice size increases. These correspond to the PMW and PMS phases respectively, where bilinear condensates vanish. However, for intermediate couplings close to $U = 1.75$, both susceptibilities seem to grow rapidly. As indicated in Eq. (3.13), if a fermion bilinear condensate forms (i.e. $\langle \psi_{x,1} \psi_{x,2} \rangle \neq 0$), we expect $\chi_{1,2} \sim L^4$. To investigate the presence of such a condensate at intermediate couplings, we plot the variation of χ_1/L^4 and χ_2/L^4 as a function of lattice size L in Fig. (6.4). The curves seem to saturate with lattice size, thereby indicating the presence of fermion bilinear condensates in a range of intermediate couplings. Thus the behavior of both

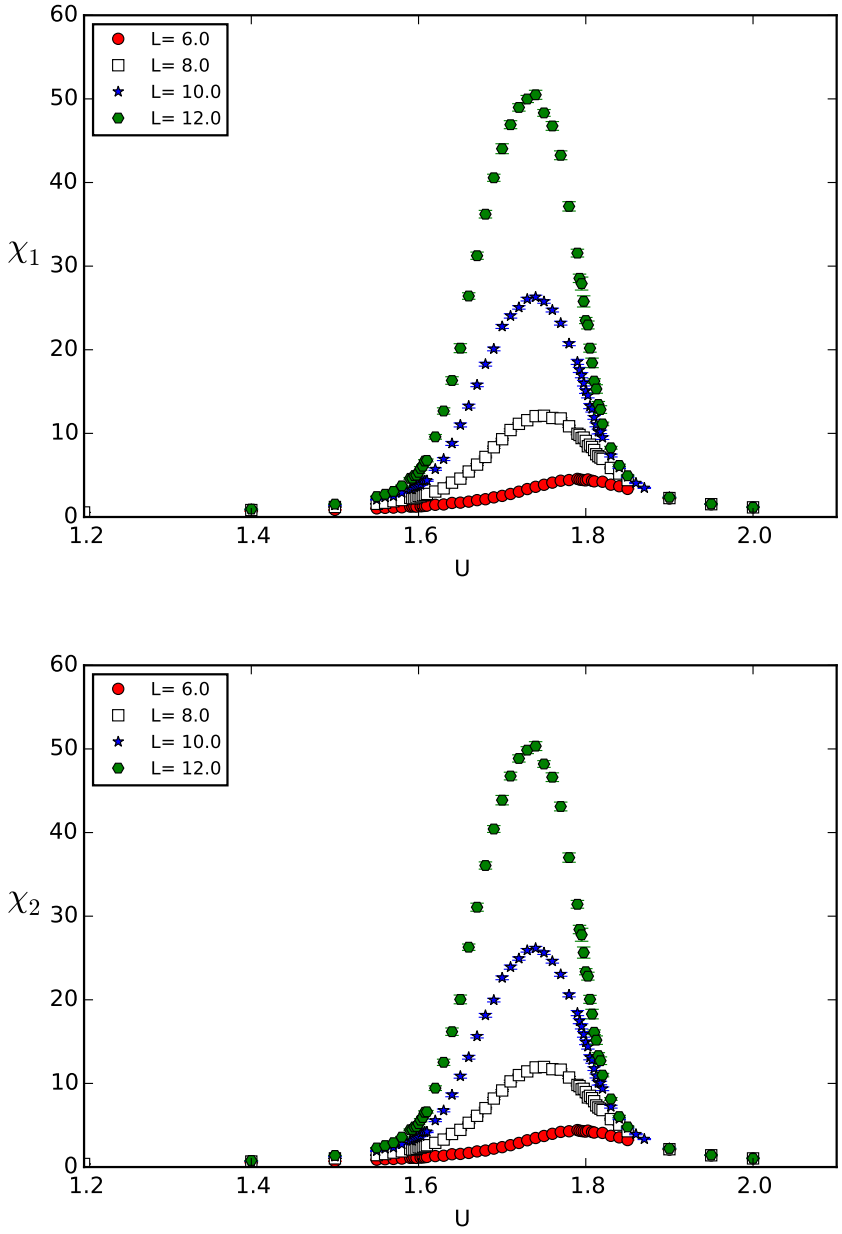

FIGURE 6.2: Plot of the susceptibilities χ_1 and χ_2 as a function of U. As in the 3D case, the susceptibilities rise sharply at intermediate couplings to show a peak and then decay at large couplings.

susceptibilities points to a three phase structure with a spontaneously broken FM phase separating the PMW and PMS phases. We present our entire data for 4D in Appendix F.

6.2 Analysis

6.2.1 Critical points

The behavior of the susceptibilities χ_1 and χ_2 suggests the existence of two phase transitions. It is clear from Eq. (5.9) that the susceptibilities near a second-order critical point must scale as $\chi_a = L^{2-\eta} g_a \left((U - U_C) L^{\frac{1}{\nu}} \right)$. Hence, a plot of $\chi_a \, / L^{2-\eta}$ as a function of the coupling U should intersect at the critical points where $U = U_c$. Making an ansatz that the two critical points are second order with the mean field critical exponents $\eta = 0$ and $\nu = 0.5$, we plot $\chi_{1,2} \, / L^{2-\eta}$ as a function of the coupling U in Fig. (6.5). It is clear that both the curves intersect quite well at two different couplings. Thus our data is consistent with two second order transitions with mean field exponents separating the three phases. The approximate locations of the critical points are $U_{c1} = 1.60$ and $U_{c2} = 1.81$. Thus the FM phase is quite narrow as compared to previous results [8].

6.2.2 Presence of condensates in the FM phase

As discussed in the previous section, the susceptibilities seem to grow as L^4 in the intermediate phase, thereby indicating the presence of fermion bilinear condensates. To understand this in more detail, we fit the susceptibilities to the form

$$\chi_a \;=\; \frac{1}{4} \Phi_a^2 L^4 + b_a L^2 \tag{6.1}$$

for $a = 1, 2$. Here, Φ_a denotes the fermion bilinear condensate. Due to the $SU(4)$ symmetry, we expect Φ_1 and Φ_2 to be the same. Given the small range of lattice sizes available to us and the possibility that we may have underestimated the errors

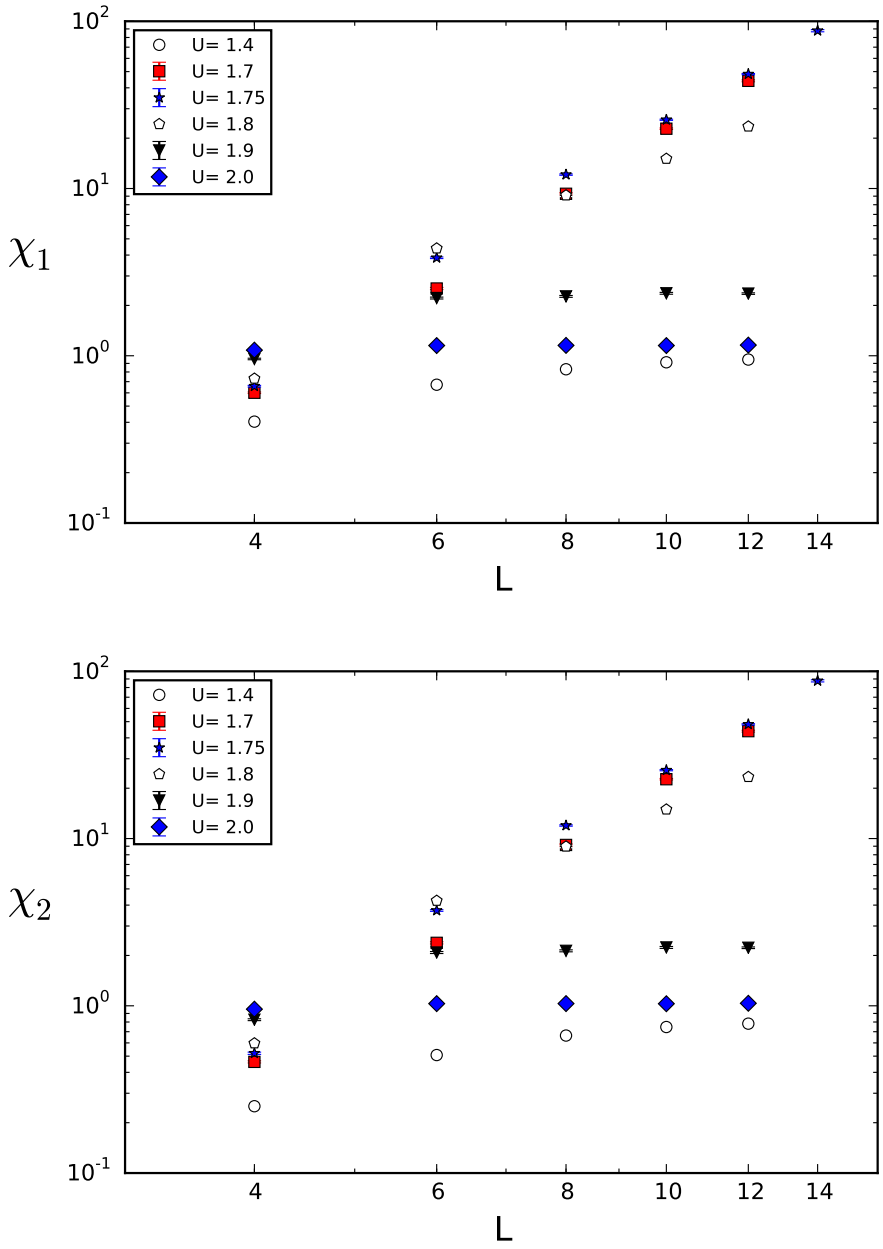

FIGURE 6.3: Log-log plot of the susceptibilities χ_1 and χ_2 as a function of L for various couplings. The susceptibilities saturate at weak (U=1.4) and strong (U=1.9) couplings. In the intermediate region, they grow quite rapidly.

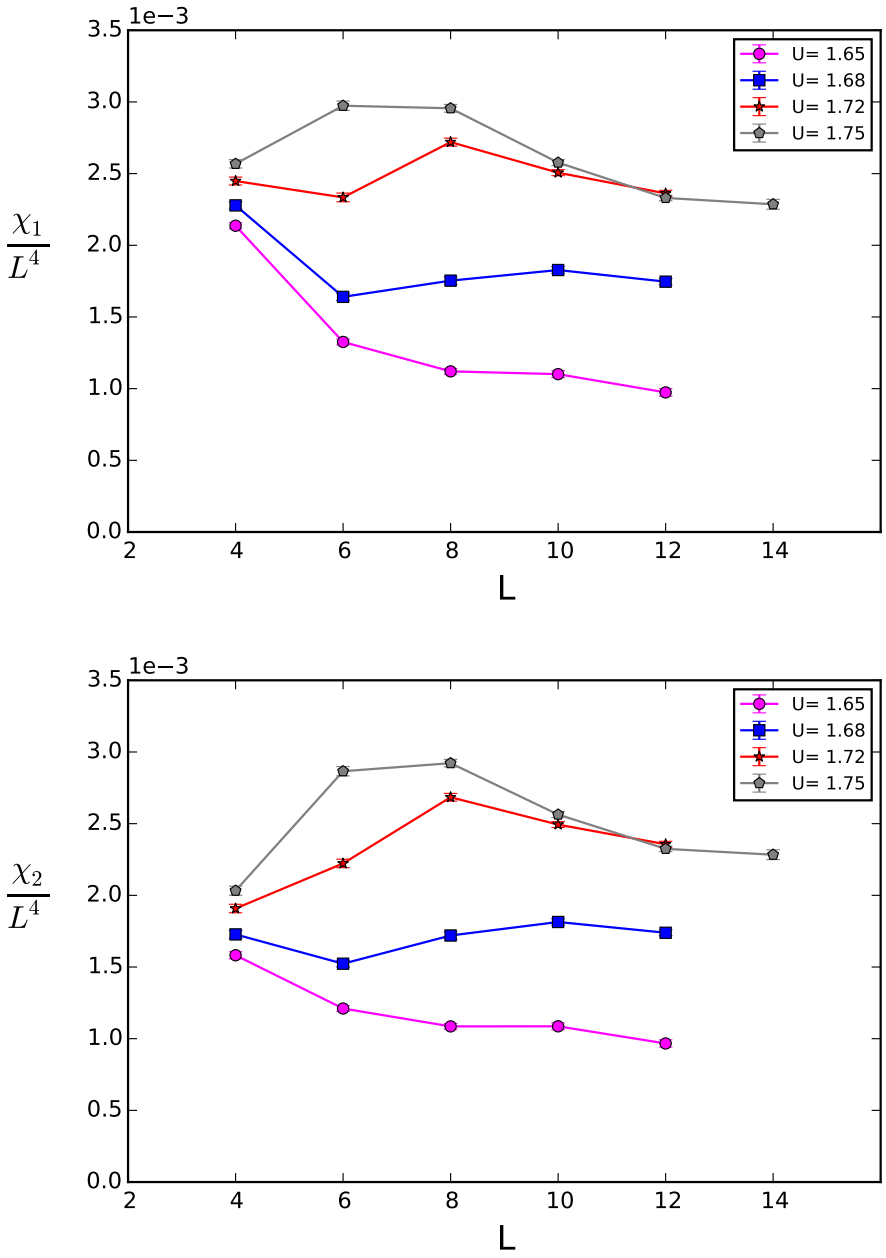

FIGURE 6.4: Plot of χ_1/L^4 and χ_2/L^4 as a function of L for some couplings between $U = 1.4$ and $U = 1.81$. Since the curves seem to saturate with lattice size, one expects the formation of fermion bilinear condensates.

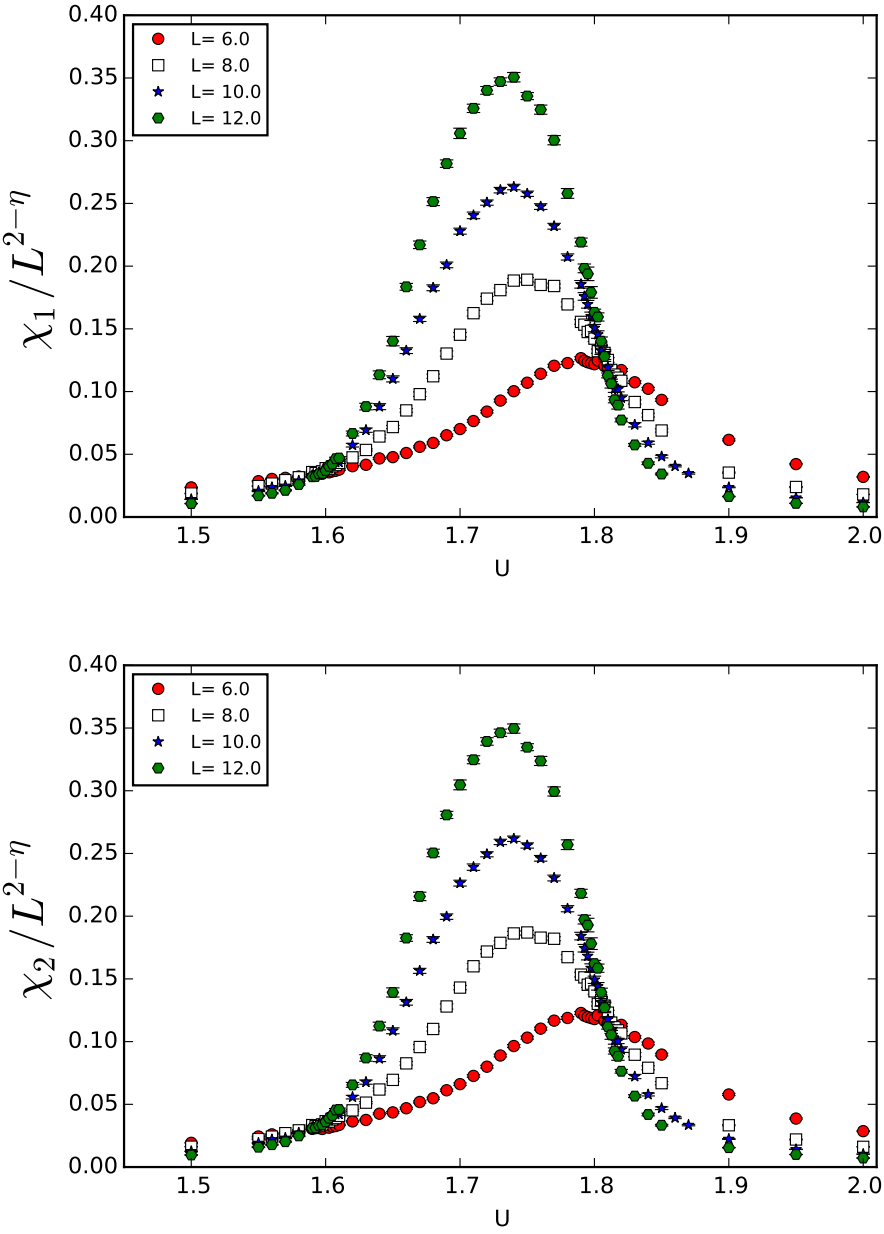

FIGURE 6.5: Plot of $\chi / L^{2-\eta}$ as a function of U for the susceptibilities χ_1 (top figure) and χ_2 (bottom figure) using the large N critical exponents $\eta = 0$ and $\nu = 0.5$. It is clear that the curves intersect at two critical points located roughly at 1.60 and 1.81, which we believe is the region of the intermediate FM phase.

Table 6.1: Table containing the fit parameters obtained by fitting χ_1 and χ_2 to the form given in Eq. (6.1).

	χ_1			χ_2		
U	Φ_1	b_1	χ^2	Φ_2	b_2	χ^2
1.61	$13(3) \times 10^{-3}$	$40(2) \times 10^{-3}$	0.3	$16(2) \times 10^{-3}$	$37(1) \times 10^{-3}$	0.2
1.62	$31(1) \times 10^{-3}$	$32(1) \times 10^{-3}$	0.1	$32(1) \times 10^{-3}$	$29(2) \times 10^{-3}$	0.2
1.63	$417(2) \times 10^{-4}$	$257(3) \times 10^{-4}$	0.0	$423(2) \times 10^{-4}$	$227(4) \times 10^{-4}$	0.0
1.64	$499(9) \times 10^{-4}$	$24(2) \times 10^{-3}$	0.1	$507(10) \times 10^{-4}$	$21(2) \times 10^{-3}$	0.1
1.65	$60(4) \times 10^{-3}$	$14(9) \times 10^{-3}$	1.6	$61(4) \times 10^{-3}$	$11(9) \times 10^{-3}$	1.7
1.66	$71(1) \times 10^{-3}$	$6(4) \times 10^{-3}$	0.4	$71(1) \times 10^{-3}$	$2(5) \times 10^{-3}$	0.5
1.67	$78(3) \times 10^{-3}$	$3(10) \times 10^{-3}$	1.5	$78(3) \times 10^{-3}$	$0(1) \times 10^{-2}$	1.5
1.68	$84(3) \times 10^{-3}$	$0(1) \times 10^{-2}$	1.8	$85(3) \times 10^{-3}$	$0(1) \times 10^{-2}$	2.1
1.69	$871(9) \times 10^{-4}$	$10(4) \times 10^{-3}$	0.2	$88(1) \times 10^{-3}$	$6(5) \times 10^{-3}$	0.3
1.7	$91(4) \times 10^{-3}$	$1(1) \times 10^{-2}$	2.6	$92(4) \times 10^{-3}$	$1(1) \times 10^{-2}$	3.0
1.71	$91(2) \times 10^{-3}$	$32(7) \times 10^{-3}$	0.5	$91(2) \times 10^{-3}$	$29(7) \times 10^{-3}$	0.6
1.72	$913(6) \times 10^{-4}$	$41(3) \times 10^{-3}$	0.1	$917(8) \times 10^{-4}$	$38(3) \times 10^{-3}$	0.2
1.73	$92(2) \times 10^{-3}$	$48(7) \times 10^{-3}$	0.8	$92(2) \times 10^{-3}$	$44(7) \times 10^{-3}$	0.9
1.74	$903(6) \times 10^{-4}$	$58(2) \times 10^{-3}$	0.1	$907(7) \times 10^{-4}$	$55(3) \times 10^{-3}$	0.1
1.75	$858(9) \times 10^{-4}$	$72(4) \times 10^{-3}$	0.3	$86(1) \times 10^{-3}$	$69(4) \times 10^{-3}$	0.3
1.76	$835(2) \times 10^{-4}$	$734(6) \times 10^{-4}$	0.0	$8391(5) \times 10^{-5}$	$702(2) \times 10^{-4}$	0.0
1.77	$75(2) \times 10^{-3}$	$92(6) \times 10^{-3}$	0.6	$76(2) \times 10^{-3}$	$89(6) \times 10^{-3}$	0.6
1.78	$662(10) \times 10^{-4}$	$99(3) \times 10^{-3}$	0.1	$667(8) \times 10^{-4}$	$96(3) \times 10^{-3}$	0.1
1.79	$565(6) \times 10^{-4}$	$105(2) \times 10^{-3}$	0.0	$571(7) \times 10^{-4}$	$102(2) \times 10^{-3}$	0.0
1.8	$324(8) \times 10^{-4}$	$125(1) \times 10^{-3}$	0.0	$333(6) \times 10^{-4}$	$122(1) \times 10^{-3}$	0.0

due to our Monte Carlo runs being short, we multiply the Monte Carlo errors by a factor of two before performing these fits. Table 6.1 shows the results of these fits for χ_1 and χ_2. It is clear that the fits work well at most couplings. Fig. (6.6) shows the variation of the condensates as a function of the coupling U. The condensate value increases smoothly in the FM phase to reach a maximum and then decreases to zero at the phase boundary. As expected, both susceptibilities give the same condensate. Although the results have been obtained using data on small lattices, the evidence for a narrow intermediate FM phase is striking.

To summarize, our results in 4D show the presence of a spontaneously broken FM

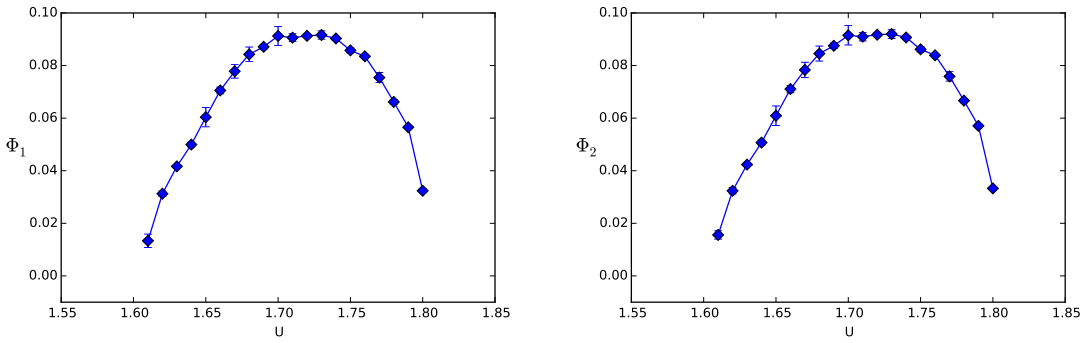

FIGURE 6.6: Plot of the condensates extracted from the susceptibilities χ_1 (left figure) and χ_2 (right figure) as a function of the coupling U in the intermediate region. Both susceptibilities give the same condensate as expected.

phase at intermediate couplings separating the PMW and PMS phases. Both the PMS-FM and the FM-PMS transitions seem second order with mean field critical exponents $\eta = 0$ and $\nu = 0.5$. The intermediate FM phase seems rather narrow, extending from about $U_{c1} = 1.60$ to $U_{c2} = 1.81$. These results are summarized in [37].

7

Conclusions

Our study of a lattice field theory model with four flavors of reduced staggered fermions and interacting via a local four fermion interaction in 3D has revealed the existence of a two phase (PMW-PMS) system. Interestingly, the transition from the massless PMW phase to the massive PMS phase seems to be second-order. There are no fermion bilinear condensates in either of the two phases and there is no spontaneous symmetry breaking of any lattice symmetries in both the phases. As mentioned in the Introduction, the existence of such a mechanism has been independently reported by other studies [16, 17, 18, 19]. Although we study a lattice model, the physics close to the second order transition must be describable by a continuum quantum field theory. Computation of the critical exponents has proved quite challenging due the absence of bilinear condensates. Still, using large scale calculations, we estimate the critical exponents as $\eta = 1.05(5)$, $\nu = 1.30(7)$ and $U_c = 0.943(2)$, assuming the absence of corrections to scaling in our data at large values of L. However, we cannot rule out the large N exponents $\nu = 1$ and $\eta = 1$, if we allow corrections to scaling.

In contrast to 3D, the phase diagram in 4D looks different. Data from small

lattices points to the more conventional three phase system (PMW-FM-PMS) with an intermediate spontaneously broken FM phase at intermediate couplings separating the PMW and PMS phases. While this was already found much earlier [10], our work shows that the FM phase is much narrower. The fermions in the FM phase seem to acquire a mass via the conventional mechanism of SSB. Both the PMW-FM and the FM-PMS phase transitions seem second order. Our data is consistent with the mean field critical exponents $\eta = 0$ and $\nu = 0.5$, as expected. Given the narrow FM phase, we wonder if an extension of the model could reveal the existence of a direct second order PMW-PMS phase transition.

It would be very interesting to understand how the fermions acquire a mass in the PMS phase. One possibility is that non-perturbative dynamics creates a fermion bound state containing three fundamental fermions [64, 65]. This composite fermion could couple to a fundamental fermion and such a mass term would appear like a four-fermion condensate in the microscopic theory.

Computing the particle spectrum in the PMS phase close to the critical point in 3D is an interesting direction for future research. Boson and fermion masses can be estimated by computing the correlators discussed in Chapter 3, on asymmetric lattices. The ratio of fermionic mass to bosonic mass as we approach the critical point is an interesting quantity and should be universal. The fermionic correlators show large fluctuations due to presence of the sign factors. This makes them difficult to compute. We are currently exploring ways to reduce these fluctuations.

Appendix A

Symmetry Order Parameters

Spontaneous symmetry breaking is signalled by the non-zero expectation value of a symmetry order parameter. For an operator to serve as a symmetry order parameter, it must vanish in the symmetric phase without vanishing in the spontaneously broken phase. Consider a theory that is invariant under some symmetry group G. Assume that this symmetry is broken down to a subgroup H by the vacuum. If $|\Omega\rangle$ is the vacuum of the theory, P is an element of H and Q is an element of G but not H, then SSB implies

$$\begin{aligned} P|\Omega\rangle &= |\Omega\rangle \\ Q|\Omega\rangle &= |\Omega'\rangle \end{aligned} \tag{A.1}$$

where $|\Omega\rangle \neq |\Omega'\rangle$. Our aim is to choose an operator O, such that its vacuum expectation value $\langle\Omega|O|\Omega\rangle$ becomes non-zero only under SSB.

All operators O constructed with the fundamental fields of the theory transform under some representation of the group G and hence also H. This means the operator $O' = POP^\dagger$ can be represented as $\sum_\beta V_{\alpha,\beta}O_\beta$, where O_β represent a set of basis operators that mix under the action of H and V is the transformation matrix. Then,

for any O_α we can write

$$\langle\Omega|O_\alpha|\Omega\rangle = \langle\Omega|P^\dagger P O_\alpha P^\dagger P|\Omega\rangle$$

$$\langle\Omega|\sum_\beta \delta_{\alpha,\beta} O_\beta|\Omega\rangle = \langle\Omega|\sum_\beta V_{\alpha,\beta} O_\beta|\Omega\rangle$$

This implies that

$$\sum_\beta (\delta_{\alpha,\beta} - V_{\alpha,\beta})\ \langle\Omega|O_\beta|\Omega\rangle = 0 \tag{A.2}$$

Since the above equation must be valid for all elements of P that belong to H, it can be shown that the only solution is

$$\langle\Omega|O_\beta|\Omega\rangle = 0 \tag{A.3}$$

unless $V_{\alpha,\beta} = \delta_{\alpha,\beta}$ (i.e. O is invariant under P). In other words, the symmetry P protects every operator O from getting an expectation value. Hence, to serve as a suitable order parameter, we choose the operator O to be symmetric under the preserved symmetries P i.e. $P^\dagger O P = O$.

Since we want $\langle\Omega|O|\Omega\rangle \neq 0$ if G is broken to H, we choose $Q^\dagger O Q \neq O$. Then, if SSB does not occur, $\langle O\rangle = 0$ using the same argument as above for Q instead of P. But, if SSB occurs, then the argument no longer holds and $\langle O\rangle$ can be nonzero.

Appendix B

Extracting particle masses from lattice field theory

Continuum QFTs are defined by symmetries of the ground state and the particle spectrum of low energy excitations. The goal of a lattice field theory is to be able to extract these properties non-perturbatively, starting from a lattice regulated theory.

One such quantity is the mass of a physical particle with specific quantum numbers. In perturbation theory, particle mass is defined as the pole of the corresponding propagator. The non-perturbative definition of mass suitable for a lattice calculation is the minimum energy of the particle. To compute it, one starts with a lattice theory defined in a finite box with the Euclidean time dimension β being much larger than the space dimensions L. If H represents the lattice Hamiltonian, the partition function is given by $Z = \text{Tr}\,[e^{-\beta H}]$. If $O^\dagger$ is an operator with the right quantum numbers that can create the particle from the vacuum, then the two point correlation function

$$G(t,0) = \frac{\text{Tr}\left[e^{-(\beta-t)H} O e^{(-tH)} O^\dagger\right]}{Z} \tag{B.1}$$

can be used to compute the mass of the particle. Inserting the complete set of energy eigenstates, we get

$$\begin{aligned} G(t,0) &= \frac{\sum_{n,n'}\langle n|e^{-(\beta-t)H}O|n'\rangle\langle n'|e^{(-tH)}O^\dagger|n\rangle}{Z} \\ &= \frac{\sum_{n,n'} e^{-\beta E_n}e^{-t(E_{n'}-E_n)}\langle n|O|n'\rangle\langle n'|O^\dagger|n\rangle}{\sum_n e^{-\beta E_n}} \end{aligned} \tag{B.2}$$

In the limit of large β, we get

$$G(t,0) = \sum_{n'} \frac{e^{(-\beta E_0)}C_{0n'}e^{-t(E_{n'}-E_0)}}{e^{-\beta E_0}} \tag{B.3}$$

where $C_{0n'} = |\langle n'|O|0\rangle^2$. Taking the limit $t \to \infty$ we can neglect all but the lowest energy level $E_{n'} = E_1$ to obtain

$$G(t,0) = C_{01}e^{-t\Delta E(L)} \tag{B.4}$$

where $\Delta E(L) = E_1 - E_0$ is the lowest energy of the particle in a finite spatial box of size L.

To extract the mass, one performs a series of calculations on larger and larger lattices and fits $\Delta E(L)$ to the form $m + a/L^2$. In contrast, for a massless particle one expects $\Delta E(L)$ to scale as $1/L$ for large L.

Appendix C

Zero weight configurations.

Here we prove why fermion bag configurations with unequal number of odd and even monomer sites do not contribute to the partition function.

If n_{even} and n_{odd} represent the number of even and odd monomer sites in a configuration C, its contribution to the partition function is given by Eq. (3.18). We can perform the Grassmann integral over the monomer sites in Eq. (3.18) to obtain

$$Z(C) = U^k \prod_{i=1}^{4} \int [d\psi_i] e^{-\frac{1}{2}\sum_{x,y} \psi_{x,i} \tilde{M}_{x,y} \psi_{y,i}}. \tag{C.1}$$

where the Grassmann integral is only defined over the free sites and $\tilde{M}$ is a sub-matrix of M obtained by removing the monomer sites. Let us consider the integral for one of the four flavors

$$I = \int [d\psi_i] e^{-\frac{1}{2}\sum_{x,y} \psi_{x,i} \tilde{M}_{x,y} \psi_{y,i}} \tag{C.2}$$

Since M has the form given in Eq. (3.19), $\tilde{M}$ also has the same form and hence can

be written as

$$\tilde{M} = \begin{array}{c} \\ even \\ odd \end{array} \begin{array}{c} \begin{array}{cc} even & odd \end{array} \\ \left[\begin{array}{c|c} 0 & \tilde{A} \\ \hline -\tilde{A}^T & 0 \end{array}\right] \end{array} \tag{C.3}$$

where $\tilde{A}$ has dimensions $(V/2 - n_{even}) \times (V/2 - n_{odd})$ on a lattice with V sites. Using the above form of $\tilde{M}$ and the rules for Grassmann algebra, it can be shown that the I in Eq. (C.2) vanishes unless the matrix $\tilde{A}$ is a square-matrix. This can happen only if $n_{even} = n_{odd}$.

Appendix D

Relating matrix determinants in terms of the inverse

Here, we discuss Eq. (4.23) for a more general case. Consider two square matrices W_0 and W_1 such that W_1 is obtained from W_0 by removing the rows $[a]$ and columns $[b]$ and adding some new rows $[c]$ and columns $[d]$. Let the sizes of the sets $[a], [b], [c], [d]$ be a, b, c, d respectively. Let W_0 have dimensions $m \times m$. Hence W_1 will have dimensions $(m - a + c) \times (m - b + d)$ with the condition

$$a + d = b + c \tag{D.1}$$

Consider a matrix W_{full} obtained by adding the $[c]$ rows and $[d]$ columns to W_0. It can be written in the form

$$W_{full} = \begin{array}{c} \\ \uparrow \\ m \\ \downarrow \\ \uparrow \\ c \\ \downarrow \end{array} \begin{array}{c} \begin{array}{cc} \leftarrow \; m \; \rightarrow & \leftarrow \quad d \quad \rightarrow \end{array} \\ \left(\begin{array}{c|c} W_0 & C \\ \hline B & D \end{array} \right) \end{array} \tag{D.2}$$

where the matrices B, C and D connect the old rows and columns with the newly added rows and columns as described below. B has dimensions $c \times m$ and connects the newly added c rows to the original m columns in the matrix W_0. C has dimensions $m \times d$ and connects the original m rows in the matrix W_0 to the newly added d columns. D has dimensions $c \times d$ and connects the newly added c rows to the newly added d columns.

The matrix W_1 is a sub-matrix of W_{full}, obtained by removing the a rows and b columns. Its determinant can be expressed as

$$Det(W_1)/Det(W_0) = Det(W')\sigma \tag{D.3}$$

where σ is a sign factor and W' is a matrix of the form

$$W' = \begin{array}{c} \\ \uparrow \\ b \\ \downarrow \\ \uparrow \\ c \\ \downarrow \end{array} \begin{array}{c} \begin{array}{cc} \leftarrow \quad a \quad \rightarrow & \leftarrow \quad d \quad \rightarrow \end{array} \\ \left(\begin{array}{c|c} -W_{inv1} & W_{inv2}\ C \\ \hline B\ W_{inv3} & D - B\ W_0^{-1}\ C \end{array} \right) \end{array} \tag{D.4}$$

where W_0^{-1} is the inverse of the matrix W_0 and $W_{inv1}, W_{inv2}, W_{inv3}$ are sub-matrices of W_0^{-1}. W_{inv1} has dimensions of $(b \times a)$ and connects the removed b columns and a rows. W_{inv2} has dimensions of $(b \times m)$ and connects the removed b columns and the original m rows. W_{inv3} has dimensions of $(m \times a)$ and connects the original m columns and the removed a rows.

Appendix E

Complete 3D Data

For completeness, we present all our 3D data for ρ_m, R_1 and R_2 in Table E.1.

Table E.1: Results from Monte Carlo calculations in 3D for ρ_m, R_1 and R_2 various values of coupling U and lattice size L.

U	L	ρ_m	R_1	R_2
0.8	28	$6438(5) \times 10^{-5}$	$727(7) \times 10^{-6}$	$398(4) \times 10^{-6}$
0.8	32	$6446(3) \times 10^{-5}$	$450(4) \times 10^{-6}$	$253(2) \times 10^{-6}$
0.8	36	$6441(3) \times 10^{-5}$	$285(4) \times 10^{-6}$	$161(2) \times 10^{-6}$
0.8	40	$6446(3) \times 10^{-5}$	$186(2) \times 10^{-6}$	$106(1) \times 10^{-6}$
0.8	44	$6443(3) \times 10^{-5}$	$136(2) \times 10^{-6}$	$80(1) \times 10^{-6}$
0.8	48	$6448(2) \times 10^{-5}$	$94(1) \times 10^{-6}$	$561(9) \times 10^{-7}$
0.8	52	$6452(5) \times 10^{-5}$	$73(2) \times 10^{-6}$	$45(2) \times 10^{-6}$
0.8	56	$6447(4) \times 10^{-5}$	$55(2) \times 10^{-6}$	$35(1) \times 10^{-6}$
0.85	28	$7689(4) \times 10^{-5}$	$1048(7) \times 10^{-6}$	$565(4) \times 10^{-6}$
0.85	32	$7682(5) \times 10^{-5}$	$642(7) \times 10^{-6}$	$353(4) \times 10^{-6}$
0.85	36	$7693(4) \times 10^{-5}$	$420(5) \times 10^{-6}$	$235(3) \times 10^{-6}$
0.85	40	$7697(4) \times 10^{-5}$	$311(5) \times 10^{-6}$	$176(3) \times 10^{-6}$
0.85	44	$7692(3) \times 10^{-5}$	$222(4) \times 10^{-6}$	$124(2) \times 10^{-6}$
0.85	48	$7695(3) \times 10^{-5}$	$160(3) \times 10^{-6}$	$92(1) \times 10^{-6}$
0.85	52	$7692(5) \times 10^{-5}$	$118(4) \times 10^{-6}$	$68(2) \times 10^{-6}$
0.85	56	$7705(5) \times 10^{-5}$	$100(6) \times 10^{-6}$	$57(3) \times 10^{-6}$
0.9	16	$9245(6) \times 10^{-5}$	$1012(2) \times 10^{-5}$	$449(1) \times 10^{-5}$

Continued on next page

Table E.1 – *Continued from previous page*

U	L	ρ_m	R_1	R_2
0.9	20	$9238(7) \times 10^{-5}$	$486(2) \times 10^{-5}$	$233(1) \times 10^{-5}$
0.9	24	$9253(7) \times 10^{-5}$	$277(2) \times 10^{-5}$	$1399(7) \times 10^{-6}$
0.9	28	$9250(6) \times 10^{-5}$	$178(1) \times 10^{-5}$	$918(5) \times 10^{-6}$
0.9	32	$9247(7) \times 10^{-5}$	$118(1) \times 10^{-5}$	$619(6) \times 10^{-6}$
0.9	36	$9240(6) \times 10^{-5}$	$808(10) \times 10^{-6}$	$435(5) \times 10^{-6}$
0.9	40	$9248(5) \times 10^{-5}$	$598(8) \times 10^{-6}$	$324(4) \times 10^{-6}$
0.9	44	$9251(7) \times 10^{-5}$	$455(10) \times 10^{-6}$	$252(5) \times 10^{-6}$
0.9	48	$9253(6) \times 10^{-5}$	$360(8) \times 10^{-6}$	$196(4) \times 10^{-6}$
0.9	52	$927(1) \times 10^{-4}$	$26(1) \times 10^{-5}$	$148(8) \times 10^{-6}$
0.9	56	$927(2) \times 10^{-4}$	$177(9) \times 10^{-6}$	$99(6) \times 10^{-6}$
0.9	60	$9260(9) \times 10^{-5}$	$19(1) \times 10^{-5}$	$100(6) \times 10^{-6}$
0.91	24	$9606(7) \times 10^{-5}$	$307(2) \times 10^{-5}$	$1535(8) \times 10^{-6}$
0.91	28	$9602(6) \times 10^{-5}$	$197(1) \times 10^{-5}$	$1009(6) \times 10^{-6}$
0.91	32	$9609(5) \times 10^{-5}$	$1349(9) \times 10^{-6}$	$706(5) \times 10^{-6}$
0.91	36	$9606(6) \times 10^{-5}$	$96(1) \times 10^{-5}$	$507(5) \times 10^{-6}$
0.91	40	$9610(5) \times 10^{-5}$	$714(8) \times 10^{-6}$	$381(4) \times 10^{-6}$
0.91	44	$9615(5) \times 10^{-5}$	$526(6) \times 10^{-6}$	$284(3) \times 10^{-6}$
0.91	48	$9618(8) \times 10^{-5}$	$441(9) \times 10^{-6}$	$234(4) \times 10^{-6}$
0.91	52	$962(2) \times 10^{-4}$	$37(2) \times 10^{-5}$	$20(1) \times 10^{-5}$
0.91	56	$963(2) \times 10^{-4}$	$24(1) \times 10^{-5}$	$13(1) \times 10^{-5}$
0.91	60	$961(1) \times 10^{-4}$	$21(2) \times 10^{-5}$	$110(7) \times 10^{-6}$
0.92	20	$9997(7) \times 10^{-5}$	$580(2) \times 10^{-5}$	$274(1) \times 10^{-5}$
0.92	24	$9993(8) \times 10^{-5}$	$338(2) \times 10^{-5}$	$1674(9) \times 10^{-6}$
0.92	28	$9984(7) \times 10^{-5}$	$226(1) \times 10^{-5}$	$1139(7) \times 10^{-6}$
0.92	32	$9994(8) \times 10^{-5}$	$156(1) \times 10^{-5}$	$802(7) \times 10^{-6}$
0.92	36	$10004(8) \times 10^{-5}$	$115(1) \times 10^{-5}$	$598(7) \times 10^{-6}$
0.92	40	$10001(7) \times 10^{-5}$	$89(1) \times 10^{-5}$	$466(6) \times 10^{-6}$
0.92	44	$10007(7) \times 10^{-5}$	$64(1) \times 10^{-5}$	$342(5) \times 10^{-6}$
0.92	48	$10006(7) \times 10^{-5}$	$547(9) \times 10^{-6}$	$289(4) \times 10^{-6}$
0.92	52	$1004(2) \times 10^{-4}$	$48(6) \times 10^{-5}$	$23(2) \times 10^{-5}$
0.92	56	$1001(1) \times 10^{-4}$	$34(2) \times 10^{-5}$	$19(1) \times 10^{-5}$
0.92	60	$1000(1) \times 10^{-4}$	$26(1) \times 10^{-5}$	$140(7) \times 10^{-6}$
0.93	20	$10402(9) \times 10^{-5}$	$639(3) \times 10^{-5}$	$299(1) \times 10^{-5}$
0.93	24	$10420(9) \times 10^{-5}$	$394(2) \times 10^{-5}$	$1923(10) \times 10^{-6}$
0.93	28	$10399(10) \times 10^{-5}$	$255(2) \times 10^{-5}$	$128(1) \times 10^{-5}$
0.93	32	$10410(8) \times 10^{-5}$	$185(2) \times 10^{-5}$	$933(8) \times 10^{-6}$
0.93	36	$10404(8) \times 10^{-5}$	$139(1) \times 10^{-5}$	$714(7) \times 10^{-6}$
0.93	40	$10410(7) \times 10^{-5}$	$104(1) \times 10^{-5}$	$541(6) \times 10^{-6}$
0.93	44	$10418(8) \times 10^{-5}$	$85(1) \times 10^{-5}$	$440(6) \times 10^{-6}$
0.93	48	$10418(7) \times 10^{-5}$	$66(1) \times 10^{-5}$	$349(5) \times 10^{-6}$

Continued on next page

Table E.1 – *Continued from previous page*

U	L	ρ_m	R_1	R_2
0.93	52	$1045(2) \times 10^{-4}$	$56(3) \times 10^{-5}$	$29(1) \times 10^{-5}$
0.93	56	$1043(3) \times 10^{-4}$	$60(7) \times 10^{-5}$	$29(3) \times 10^{-5}$
0.93	60	$1045(1) \times 10^{-4}$	$41(2) \times 10^{-5}$	$22(1) \times 10^{-5}$
0.94	20	$10846(9) \times 10^{-5}$	$713(3) \times 10^{-5}$	$329(1) \times 10^{-5}$
0.94	24	$10841(9) \times 10^{-5}$	$442(2) \times 10^{-5}$	$211(1) \times 10^{-5}$
0.94	28	$1085(1) \times 10^{-4}$	$306(2) \times 10^{-5}$	$150(1) \times 10^{-5}$
0.94	32	$10852(9) \times 10^{-5}$	$223(2) \times 10^{-5}$	$1109(9) \times 10^{-6}$
0.94	36	$10857(9) \times 10^{-5}$	$170(2) \times 10^{-5}$	$855(9) \times 10^{-6}$
0.94	40	$10855(7) \times 10^{-5}$	$136(1) \times 10^{-5}$	$693(7) \times 10^{-6}$
0.94	44	$10861(8) \times 10^{-5}$	$109(2) \times 10^{-5}$	$556(7) \times 10^{-6}$
0.94	48	$1089(3) \times 10^{-4}$	$91(4) \times 10^{-5}$	$47(2) \times 10^{-5}$
0.94	52	$1088(3) \times 10^{-4}$	$70(4) \times 10^{-5}$	$36(2) \times 10^{-5}$
0.94	56	$1090(3) \times 10^{-4}$	$64(4) \times 10^{-5}$	$35(2) \times 10^{-5}$
0.94	60	$1087(2) \times 10^{-4}$	$51(2) \times 10^{-5}$	$27(1) \times 10^{-5}$
0.945	20	$11066(7) \times 10^{-5}$	$744(2) \times 10^{-5}$	$3404(9) \times 10^{-6}$
0.945	24	$11075(7) \times 10^{-5}$	$480(2) \times 10^{-5}$	$2285(8) \times 10^{-6}$
0.945	28	$11082(6) \times 10^{-5}$	$330(1) \times 10^{-5}$	$1602(6) \times 10^{-6}$
0.945	32	$11088(9) \times 10^{-5}$	$243(2) \times 10^{-5}$	$1198(9) \times 10^{-6}$
0.945	36	$11104(8) \times 10^{-5}$	$191(2) \times 10^{-5}$	$945(8) \times 10^{-6}$
0.945	40	$11099(7) \times 10^{-5}$	$155(1) \times 10^{-5}$	$773(6) \times 10^{-6}$
0.945	44	$11104(6) \times 10^{-5}$	$127(1) \times 10^{-5}$	$638(6) \times 10^{-6}$
0.945	48	$1107(2) \times 10^{-4}$	$106(3) \times 10^{-5}$	$54(2) \times 10^{-5}$
0.945	52	$1114(3) \times 10^{-4}$	$88(4) \times 10^{-5}$	$44(2) \times 10^{-5}$
0.945	56	$1110(2) \times 10^{-4}$	$77(3) \times 10^{-5}$	$39(2) \times 10^{-5}$
0.945	60	$1111(2) \times 10^{-4}$	$72(3) \times 10^{-5}$	$36(1) \times 10^{-5}$
0.95	20	$11306(8) \times 10^{-5}$	$789(3) \times 10^{-5}$	$359(1) \times 10^{-5}$
0.95	24	$11322(9) \times 10^{-5}$	$517(2) \times 10^{-5}$	$2441(10) \times 10^{-6}$
0.95	28	$11335(7) \times 10^{-5}$	$367(2) \times 10^{-5}$	$1755(8) \times 10^{-6}$
0.95	32	$11326(9) \times 10^{-5}$	$265(2) \times 10^{-5}$	$1294(9) \times 10^{-6}$
0.95	36	$11355(8) \times 10^{-5}$	$214(2) \times 10^{-5}$	$1047(8) \times 10^{-6}$
0.95	40	$11343(8) \times 10^{-5}$	$175(1) \times 10^{-5}$	$868(7) \times 10^{-6}$
0.95	44	$1136(1) \times 10^{-4}$	$150(2) \times 10^{-5}$	$748(9) \times 10^{-6}$
0.95	48	$1141(3) \times 10^{-4}$	$127(5) \times 10^{-5}$	$64(2) \times 10^{-5}$
0.95	52	$1137(3) \times 10^{-4}$	$107(4) \times 10^{-5}$	$53(2) \times 10^{-5}$
0.95	56	$1138(4) \times 10^{-4}$	$105(5) \times 10^{-5}$	$53(3) \times 10^{-5}$
0.95	60	$1138(1) \times 10^{-4}$	$86(3) \times 10^{-5}$	$44(1) \times 10^{-5}$
0.96	20	$11809(7) \times 10^{-5}$	$880(2) \times 10^{-5}$	$3940(9) \times 10^{-6}$
0.96	24	$11849(10) \times 10^{-5}$	$598(2) \times 10^{-5}$	$2763(10) \times 10^{-6}$
0.96	28	$11862(8) \times 10^{-5}$	$437(2) \times 10^{-5}$	$2055(8) \times 10^{-6}$
0.96	32	$1189(1) \times 10^{-4}$	$340(2) \times 10^{-5}$	$162(1) \times 10^{-5}$

Continued on next page

Table E.1 – *Continued from previous page*

U	L	ρ_m	R_1	R_2
0.96	36	$1189(1) \times 10^{-4}$	$268(2) \times 10^{-5}$	$1288(9) \times 10^{-6}$
0.96	40	$11893(8) \times 10^{-5}$	$228(2) \times 10^{-5}$	$1103(8) \times 10^{-6}$
0.96	44	$1191(1) \times 10^{-4}$	$205(2) \times 10^{-5}$	$986(10) \times 10^{-6}$
0.96	48	$1192(4) \times 10^{-4}$	$165(5) \times 10^{-5}$	$79(3) \times 10^{-5}$
0.96	52	$1187(3) \times 10^{-4}$	$140(7) \times 10^{-5}$	$68(3) \times 10^{-5}$
0.96	56	$1189(7) \times 10^{-4}$	$130(6) \times 10^{-5}$	$65(3) \times 10^{-5}$
0.96	60	$1195(2) \times 10^{-4}$	$128(4) \times 10^{-5}$	$63(2) \times 10^{-5}$
0.97	20	$1238(1) \times 10^{-4}$	$1006(3) \times 10^{-5}$	$442(1) \times 10^{-5}$
0.97	24	$1241(1) \times 10^{-4}$	$692(2) \times 10^{-5}$	$313(1) \times 10^{-5}$
0.97	28	$12441(9) \times 10^{-5}$	$530(2) \times 10^{-5}$	$2443(9) \times 10^{-6}$
0.97	32	$1247(1) \times 10^{-4}$	$427(2) \times 10^{-5}$	$198(1) \times 10^{-5}$
0.97	36	$1249(1) \times 10^{-4}$	$348(2) \times 10^{-5}$	$162(1) \times 10^{-5}$
0.97	40	$12514(9) \times 10^{-5}$	$306(2) \times 10^{-5}$	$1433(9) \times 10^{-6}$
0.97	44	$1251(1) \times 10^{-4}$	$264(2) \times 10^{-5}$	$124(1) \times 10^{-5}$
0.97	48	$1252(5) \times 10^{-4}$	$242(8) \times 10^{-5}$	$114(3) \times 10^{-5}$
0.97	52	$1250(3) \times 10^{-4}$	$196(7) \times 10^{-5}$	$93(3) \times 10^{-5}$
0.98	24	$1305(1) \times 10^{-4}$	$820(3) \times 10^{-5}$	$361(1) \times 10^{-5}$
0.98	28	$1311(1) \times 10^{-4}$	$650(3) \times 10^{-5}$	$290(1) \times 10^{-5}$
0.98	32	$1316(1) \times 10^{-4}$	$530(3) \times 10^{-5}$	$238(1) \times 10^{-5}$
0.98	36	$1318(2) \times 10^{-4}$	$444(3) \times 10^{-5}$	$200(1) \times 10^{-5}$
0.98	40	$1320(1) \times 10^{-4}$	$382(2) \times 10^{-5}$	$1728(9) \times 10^{-6}$
0.98	44	$1324(2) \times 10^{-4}$	$347(3) \times 10^{-5}$	$157(1) \times 10^{-5}$
0.99	36	$1393(2) \times 10^{-4}$	$534(3) \times 10^{-5}$	$232(1) \times 10^{-5}$
0.99	40	$1397(2) \times 10^{-4}$	$463(3) \times 10^{-5}$	$200(1) \times 10^{-5}$
0.99	44	$1400(2) \times 10^{-4}$	$399(3) \times 10^{-5}$	$174(1) \times 10^{-5}$
1.0	20	$1446(2) \times 10^{-4}$	$1472(5) \times 10^{-5}$	$597(2) \times 10^{-5}$
1.0	24	$1458(2) \times 10^{-4}$	$1111(4) \times 10^{-5}$	$459(1) \times 10^{-5}$
1.0	28	$1467(2) \times 10^{-4}$	$896(3) \times 10^{-5}$	$373(1) \times 10^{-5}$
1.0	32	$1475(2) \times 10^{-4}$	$743(4) \times 10^{-5}$	$309(1) \times 10^{-5}$
1.0	36	$1478(2) \times 10^{-4}$	$616(3) \times 10^{-5}$	$257(1) \times 10^{-5}$
1.0	40	$1482(1) \times 10^{-4}$	$514(3) \times 10^{-5}$	$214(1) \times 10^{-5}$
1.0	44	$1485(1) \times 10^{-4}$	$428(3) \times 10^{-5}$	$178(1) \times 10^{-5}$
1.01	32	$1562(2) \times 10^{-4}$	$804(4) \times 10^{-5}$	$322(1) \times 10^{-5}$
1.01	36	$1569(2) \times 10^{-4}$	$647(3) \times 10^{-5}$	$259(1) \times 10^{-5}$
1.01	40	$1572(1) \times 10^{-4}$	$526(3) \times 10^{-5}$	$211(1) \times 10^{-5}$
1.01	44	$1575(2) \times 10^{-4}$	$420(3) \times 10^{-5}$	$169(1) \times 10^{-5}$
1.02	20	$1624(2) \times 10^{-4}$	$1837(5) \times 10^{-5}$	$695(2) \times 10^{-5}$
1.02	24	$1642(2) \times 10^{-4}$	$1386(4) \times 10^{-5}$	$529(2) \times 10^{-5}$
1.02	28	$1656(2) \times 10^{-4}$	$1075(4) \times 10^{-5}$	$411(1) \times 10^{-5}$
1.02	32	$1661(2) \times 10^{-4}$	$841(4) \times 10^{-5}$	$323(1) \times 10^{-5}$

Continued on next page

Table E.1 – *Continued from previous page*

U	L	ρ_m	R_1	R_2
1.02	36	$1667(2) \times 10^{-4}$	$656(3) \times 10^{-5}$	$252(1) \times 10^{-5}$
1.02	40	$1671(1) \times 10^{-4}$	$502(2) \times 10^{-5}$	$1926(10) \times 10^{-6}$
1.02	44	$1671(2) \times 10^{-4}$	$394(3) \times 10^{-5}$	$151(1) \times 10^{-5}$
1.03	24	$1751(2) \times 10^{-4}$	$1478(4) \times 10^{-5}$	$541(2) \times 10^{-5}$
1.03	28	$1758(2) \times 10^{-4}$	$1101(4) \times 10^{-5}$	$404(2) \times 10^{-5}$
1.03	32	$1765(2) \times 10^{-4}$	$825(4) \times 10^{-5}$	$302(1) \times 10^{-5}$
1.03	36	$1771(2) \times 10^{-4}$	$618(3) \times 10^{-5}$	$227(1) \times 10^{-5}$
1.03	40	$1773(2) \times 10^{-4}$	$464(3) \times 10^{-5}$	$1707(9) \times 10^{-6}$
1.03	44	$1774(2) \times 10^{-4}$	$353(3) \times 10^{-5}$	$129(1) \times 10^{-5}$
1.04	16	$1802(4) \times 10^{-4}$	$3079(8) \times 10^{-5}$	$1052(3) \times 10^{-5}$
1.04	20	$1844(3) \times 10^{-4}$	$2117(6) \times 10^{-5}$	$737(2) \times 10^{-5}$
1.04	24	$1863(3) \times 10^{-4}$	$1513(5) \times 10^{-5}$	$528(2) \times 10^{-5}$
1.04	28	$1872(2) \times 10^{-4}$	$1090(4) \times 10^{-5}$	$382(1) \times 10^{-5}$
1.04	32	$1878(2) \times 10^{-4}$	$781(4) \times 10^{-5}$	$274(1) \times 10^{-5}$
1.04	36	$1879(2) \times 10^{-4}$	$559(3) \times 10^{-5}$	$196(1) \times 10^{-5}$
1.04	40	$1881(2) \times 10^{-4}$	$409(2) \times 10^{-5}$	$1438(9) \times 10^{-6}$
1.05	16	$1917(4) \times 10^{-4}$	$3270(9) \times 10^{-5}$	$1074(3) \times 10^{-5}$
1.05	20	$1960(3) \times 10^{-4}$	$2191(6) \times 10^{-5}$	$730(2) \times 10^{-5}$
1.05	24	$1979(3) \times 10^{-4}$	$1504(5) \times 10^{-5}$	$503(2) \times 10^{-5}$
1.05	28	$1993(3) \times 10^{-4}$	$1035(4) \times 10^{-5}$	$345(1) \times 10^{-5}$
1.05	40	$1997(2) \times 10^{-4}$	$347(2) \times 10^{-5}$	$1168(7) \times 10^{-6}$
1.06	16	$2041(4) \times 10^{-4}$	$3396(9) \times 10^{-5}$	$1070(3) \times 10^{-5}$
1.06	20	$2080(3) \times 10^{-4}$	$2200(5) \times 10^{-5}$	$702(2) \times 10^{-5}$
1.06	24	$2104(3) \times 10^{-4}$	$1428(5) \times 10^{-5}$	$457(1) \times 10^{-5}$
1.06	28	$2110(2) \times 10^{-4}$	$956(3) \times 10^{-5}$	$306(1) \times 10^{-5}$
1.06	32	$2120(3) \times 10^{-4}$	$633(4) \times 10^{-5}$	$202(1) \times 10^{-5}$
1.06	36	$2119(2) \times 10^{-4}$	$426(3) \times 10^{-5}$	$1360(9) \times 10^{-6}$
1.07	12	$2073(4) \times 10^{-4}$	$6110(8) \times 10^{-5}$	$1762(3) \times 10^{-5}$
1.07	16	$2181(5) \times 10^{-4}$	$345(1) \times 10^{-4}$	$1039(3) \times 10^{-5}$
1.07	20	$2210(3) \times 10^{-4}$	$2150(6) \times 10^{-5}$	$656(2) \times 10^{-5}$
1.08	12	$2201(4) \times 10^{-4}$	$6273(8) \times 10^{-5}$	$1745(2) \times 10^{-5}$
1.08	16	$2310(5) \times 10^{-4}$	$3469(9) \times 10^{-5}$	$1002(3) \times 10^{-5}$
1.08	20	$2348(3) \times 10^{-4}$	$2055(6) \times 10^{-5}$	$599(2) \times 10^{-5}$
1.08	24	$2369(3) \times 10^{-4}$	$1231(4) \times 10^{-5}$	$359(1) \times 10^{-5}$
1.09	12	$2351(5) \times 10^{-4}$	$6425(8) \times 10^{-5}$	$1715(3) \times 10^{-5}$
1.09	16	$2457(5) \times 10^{-4}$	$3418(9) \times 10^{-5}$	$942(3) \times 10^{-5}$
1.1	12	$2499(5) \times 10^{-4}$	$6514(9) \times 10^{-5}$	$1668(2) \times 10^{-5}$
1.1	16	$2598(5) \times 10^{-4}$	$3314(9) \times 10^{-5}$	$876(2) \times 10^{-5}$
1.1	20	$2634(3) \times 10^{-4}$	$1770(5) \times 10^{-5}$	$471(1) \times 10^{-5}$
1.11	12	$2661(5) \times 10^{-4}$	$6523(8) \times 10^{-5}$	$1597(3) \times 10^{-5}$

Continued on next page

Table E.1 – *Continued from previous page*

U	L	ρ_m	R_1	R_2
1.12	12	$2818(5) \times 10^{-4}$	$6456(8) \times 10^{-5}$	$1516(2) \times 10^{-5}$
1.13	12	$2984(5) \times 10^{-4}$	$6270(9) \times 10^{-5}$	$1409(2) \times 10^{-5}$

Appendix F

Complete 4D data

For completeness, we present all our 4D data for for ρ_m, χ_1 and χ_2 in Table F.1.

Table F.1: Results from Monte Carlo calculations in 4D for ρ_m, χ_1 and χ_2 for various values of coupling U and lattice size L.

U	L	ρ_m	χ_1	χ_2
1.4	4	$852(3) \times 10^{-4}$	$404(3) \times 10^{-3}$	$251(4) \times 10^{-3}$
1.5	4	$1058(4) \times 10^{-4}$	$455(4) \times 10^{-3}$	$308(5) \times 10^{-3}$
1.55	4	$1170(2) \times 10^{-4}$	$482(5) \times 10^{-3}$	$335(6) \times 10^{-3}$
1.56	4	$1194(2) \times 10^{-4}$	$487(5) \times 10^{-3}$	$341(5) \times 10^{-3}$
1.57	4	$1221(2) \times 10^{-4}$	$488(5) \times 10^{-3}$	$342(6) \times 10^{-3}$
1.58	4	$1249(2) \times 10^{-4}$	$486(5) \times 10^{-3}$	$340(5) \times 10^{-3}$
1.59	4	$1276(2) \times 10^{-4}$	$500(5) \times 10^{-3}$	$354(6) \times 10^{-3}$
1.5925	4	$1285(2) \times 10^{-4}$	$506(5) \times 10^{-3}$	$362(6) \times 10^{-3}$
1.595	4	$1292(2) \times 10^{-4}$	$512(5) \times 10^{-3}$	$368(6) \times 10^{-3}$
1.5975	4	$1299(2) \times 10^{-4}$	$507(5) \times 10^{-3}$	$364(6) \times 10^{-3}$
1.6	4	$1309(2) \times 10^{-4}$	$527(5) \times 10^{-3}$	$386(6) \times 10^{-3}$
1.6025	4	$1311(2) \times 10^{-4}$	$517(5) \times 10^{-3}$	$375(6) \times 10^{-3}$
1.605	4	$1318(2) \times 10^{-4}$	$514(5) \times 10^{-3}$	$369(6) \times 10^{-3}$
1.6075	4	$1329(2) \times 10^{-4}$	$519(5) \times 10^{-3}$	$378(6) \times 10^{-3}$
1.61	4	$1336(2) \times 10^{-4}$	$516(5) \times 10^{-3}$	$371(6) \times 10^{-3}$
1.62	4	$1368(2) \times 10^{-4}$	$528(5) \times 10^{-3}$	$386(6) \times 10^{-3}$
1.63	4	$1397(2) \times 10^{-4}$	$535(5) \times 10^{-3}$	$393(6) \times 10^{-3}$

Continued on next page

Table F.1 – *Continued from previous page*

U	L	ρ_m	χ_1	χ_2
1.64	4	$1431(2) \times 10^{-4}$	$554(6) \times 10^{-3}$	$413(6) \times 10^{-3}$
1.65	4	$1468(2) \times 10^{-4}$	$547(5) \times 10^{-3}$	$405(6) \times 10^{-3}$
1.66	4	$1507(3) \times 10^{-4}$	$565(6) \times 10^{-3}$	$424(6) \times 10^{-3}$
1.67	4	$1537(3) \times 10^{-4}$	$578(6) \times 10^{-3}$	$437(7) \times 10^{-3}$
1.68	4	$1574(3) \times 10^{-4}$	$583(6) \times 10^{-3}$	$442(7) \times 10^{-3}$
1.69	4	$1612(3) \times 10^{-4}$	$590(6) \times 10^{-3}$	$449(7) \times 10^{-3}$
1.7	4	$1653(3) \times 10^{-4}$	$601(6) \times 10^{-3}$	$462(7) \times 10^{-3}$
1.71	4	$1697(3) \times 10^{-4}$	$609(6) \times 10^{-3}$	$469(7) \times 10^{-3}$
1.72	4	$1746(3) \times 10^{-4}$	$627(7) \times 10^{-3}$	$488(8) \times 10^{-3}$
1.73	4	$1790(4) \times 10^{-4}$	$634(7) \times 10^{-3}$	$496(8) \times 10^{-3}$
1.74	4	$1836(4) \times 10^{-4}$	$643(7) \times 10^{-3}$	$507(8) \times 10^{-3}$
1.75	4	$1892(4) \times 10^{-4}$	$657(7) \times 10^{-3}$	$520(8) \times 10^{-3}$
1.76	4	$1944(4) \times 10^{-4}$	$679(7) \times 10^{-3}$	$544(8) \times 10^{-3}$
1.77	4	$1995(4) \times 10^{-4}$	$700(8) \times 10^{-3}$	$565(9) \times 10^{-3}$
1.78	4	$2054(4) \times 10^{-4}$	$712(8) \times 10^{-3}$	$575(9) \times 10^{-3}$
1.79	4	$2118(5) \times 10^{-4}$	$726(9) \times 10^{-3}$	$589(10) \times 10^{-3}$
1.7925	4	$2142(5) \times 10^{-4}$	$736(9) \times 10^{-3}$	$602(9) \times 10^{-3}$
1.795	4	$2148(5) \times 10^{-4}$	$740(8) \times 10^{-3}$	$606(8) \times 10^{-3}$
1.7975	4	$2171(5) \times 10^{-4}$	$739(8) \times 10^{-3}$	$605(9) \times 10^{-3}$
1.8	4	$2189(5) \times 10^{-4}$	$730(8) \times 10^{-3}$	$597(9) \times 10^{-3}$
1.8025	4	$2204(6) \times 10^{-4}$	$741(8) \times 10^{-3}$	$607(9) \times 10^{-3}$
1.8075	4	$2241(6) \times 10^{-4}$	$755(8) \times 10^{-3}$	$621(9) \times 10^{-3}$
1.81	4	$2252(5) \times 10^{-4}$	$738(9) \times 10^{-3}$	$600(9) \times 10^{-3}$
1.82	4	$2334(6) \times 10^{-4}$	$762(9) \times 10^{-3}$	$628(9) \times 10^{-3}$
1.83	4	$2409(6) \times 10^{-4}$	$791(10) \times 10^{-3}$	$66(1) \times 10^{-2}$
1.84	4	$2491(7) \times 10^{-4}$	$809(9) \times 10^{-3}$	$675(10) \times 10^{-3}$
1.85	4	$2590(7) \times 10^{-4}$	$854(10) \times 10^{-3}$	$72(1) \times 10^{-2}$
1.9	4	$313(1) \times 10^{-3}$	$96(1) \times 10^{-2}$	$83(1) \times 10^{-2}$
1.95	4	$397(2) \times 10^{-3}$	$104(1) \times 10^{-2}$	$91(1) \times 10^{-2}$
2.0	4	$502(2) \times 10^{-3}$	$1081(10) \times 10^{-3}$	$95(1) \times 10^{-2}$
1.4	6	$902(2) \times 10^{-4}$	$671(6) \times 10^{-3}$	$508(6) \times 10^{-3}$
1.5	6	$1143(2) \times 10^{-4}$	$849(9) \times 10^{-3}$	$694(9) \times 10^{-3}$
1.55	6	$1305(2) \times 10^{-4}$	$103(1) \times 10^{-2}$	$88(1) \times 10^{-2}$
1.56	6	$1338(2) \times 10^{-4}$	$109(1) \times 10^{-2}$	$94(1) \times 10^{-2}$
1.57	6	$1377(2) \times 10^{-4}$	$112(2) \times 10^{-2}$	$97(2) \times 10^{-2}$
1.58	6	$1418(2) \times 10^{-4}$	$116(2) \times 10^{-2}$	$101(2) \times 10^{-2}$
1.59	6	$1462(2) \times 10^{-4}$	$125(2) \times 10^{-2}$	$110(2) \times 10^{-2}$
1.5925	6	$1475(2) \times 10^{-4}$	$127(2) \times 10^{-2}$	$112(2) \times 10^{-2}$
1.595	6	$1488(2) \times 10^{-4}$	$127(2) \times 10^{-2}$	$112(2) \times 10^{-2}$
1.5975	6	$1496(2) \times 10^{-4}$	$124(2) \times 10^{-2}$	$109(2) \times 10^{-2}$

Continued on next page

Table F.1 – *Continued from previous page*

U	L	ρ_m	χ_1	χ_2
1.6025	6	$1518(2) \times 10^{-4}$	$128(2) \times 10^{-2}$	$113(2) \times 10^{-2}$
1.605	6	$1532(2) \times 10^{-4}$	$131(2) \times 10^{-2}$	$116(2) \times 10^{-2}$
1.6075	6	$1549(3) \times 10^{-4}$	$133(2) \times 10^{-2}$	$118(2) \times 10^{-2}$
1.61	6	$1556(3) \times 10^{-4}$	$136(2) \times 10^{-2}$	$121(2) \times 10^{-2}$
1.62	6	$1610(3) \times 10^{-4}$	$146(2) \times 10^{-2}$	$131(2) \times 10^{-2}$
1.63	6	$1669(3) \times 10^{-4}$	$150(2) \times 10^{-2}$	$135(2) \times 10^{-2}$
1.64	6	$1734(3) \times 10^{-4}$	$168(3) \times 10^{-2}$	$153(3) \times 10^{-2}$
1.65	6	$1811(4) \times 10^{-4}$	$172(3) \times 10^{-2}$	$157(3) \times 10^{-2}$
1.66	6	$1875(4) \times 10^{-4}$	$184(3) \times 10^{-2}$	$169(3) \times 10^{-2}$
1.67	6	$1969(5) \times 10^{-4}$	$201(3) \times 10^{-2}$	$187(3) \times 10^{-2}$
1.68	6	$2061(5) \times 10^{-4}$	$213(3) \times 10^{-2}$	$197(3) \times 10^{-2}$
1.69	6	$2176(6) \times 10^{-4}$	$235(3) \times 10^{-2}$	$220(3) \times 10^{-2}$
1.7	6	$2298(7) \times 10^{-4}$	$252(4) \times 10^{-2}$	$238(4) \times 10^{-2}$
1.71	6	$2423(7) \times 10^{-4}$	$275(4) \times 10^{-2}$	$261(4) \times 10^{-2}$
1.72	6	$2593(8) \times 10^{-4}$	$302(4) \times 10^{-2}$	$288(4) \times 10^{-2}$
1.73	6	$277(1) \times 10^{-3}$	$334(4) \times 10^{-2}$	$320(4) \times 10^{-2}$
1.74	6	$299(1) \times 10^{-3}$	$361(4) \times 10^{-2}$	$347(4) \times 10^{-2}$
1.75	6	$321(1) \times 10^{-3}$	$385(4) \times 10^{-2}$	$371(4) \times 10^{-2}$
1.76	6	$345(1) \times 10^{-3}$	$411(4) \times 10^{-2}$	$397(4) \times 10^{-2}$
1.77	6	$373(1) \times 10^{-3}$	$434(4) \times 10^{-2}$	$420(4) \times 10^{-2}$
1.78	6	$403(1) \times 10^{-3}$	$442(4) \times 10^{-2}$	$428(4) \times 10^{-2}$
1.79	6	$432(2) \times 10^{-3}$	$456(4) \times 10^{-2}$	$442(4) \times 10^{-2}$
1.7925	6	$440(2) \times 10^{-3}$	$448(4) \times 10^{-2}$	$435(4) \times 10^{-2}$
1.795	6	$445(2) \times 10^{-3}$	$444(4) \times 10^{-2}$	$431(4) \times 10^{-2}$
1.7975	6	$453(2) \times 10^{-3}$	$441(4) \times 10^{-2}$	$428(4) \times 10^{-2}$
1.8	6	$464(1) \times 10^{-3}$	$438(4) \times 10^{-2}$	$425(4) \times 10^{-2}$
1.8025	6	$468(1) \times 10^{-3}$	$449(4) \times 10^{-2}$	$435(4) \times 10^{-2}$
1.8075	6	$480(1) \times 10^{-3}$	$433(4) \times 10^{-2}$	$420(4) \times 10^{-2}$
1.81	6	$492(1) \times 10^{-3}$	$426(4) \times 10^{-2}$	$413(4) \times 10^{-2}$
1.82	6	$517(1) \times 10^{-3}$	$422(4) \times 10^{-2}$	$408(4) \times 10^{-2}$
1.83	6	$544(1) \times 10^{-3}$	$387(4) \times 10^{-2}$	$373(4) \times 10^{-2}$
1.84	6	$568(1) \times 10^{-3}$	$368(4) \times 10^{-2}$	$355(4) \times 10^{-2}$
1.85	6	$591(1) \times 10^{-3}$	$336(4) \times 10^{-2}$	$323(4) \times 10^{-2}$
1.9	6	$6738(7) \times 10^{-4}$	$221(3) \times 10^{-2}$	$208(3) \times 10^{-2}$
1.95	6	$7232(4) \times 10^{-4}$	$152(2) \times 10^{-2}$	$139(2) \times 10^{-2}$
2.0	6	$7578(3) \times 10^{-4}$	$115(1) \times 10^{-2}$	$103(1) \times 10^{-2}$
0.8	8	$223(2) \times 10^{-4}$	$373(3) \times 10^{-3}$	$171(4) \times 10^{-3}$
1.2	8	$580(2) \times 10^{-4}$	$546(7) \times 10^{-3}$	$367(7) \times 10^{-3}$
1.4	8	$9057(10) \times 10^{-5}$	$830(10) \times 10^{-3}$	$664(8) \times 10^{-3}$
1.5	8	$1151(2) \times 10^{-4}$	$120(1) \times 10^{-2}$	$104(1) \times 10^{-2}$

Continued on next page

Table F.1 – *Continued from previous page*

U	L	ρ_m	χ_1	χ_2
1.55	8	$1317(3) \times 10^{-4}$	$158(2) \times 10^{-2}$	$142(2) \times 10^{-2}$
1.56	8	$1358(3) \times 10^{-4}$	$171(3) \times 10^{-2}$	$155(2) \times 10^{-2}$
1.57	8	$1408(4) \times 10^{-4}$	$188(3) \times 10^{-2}$	$173(3) \times 10^{-2}$
1.58	8	$1454(4) \times 10^{-4}$	$203(3) \times 10^{-2}$	$187(3) \times 10^{-2}$
1.59	8	$1513(5) \times 10^{-4}$	$229(4) \times 10^{-2}$	$214(4) \times 10^{-2}$
1.5925	8	$1510(5) \times 10^{-4}$	$224(4) \times 10^{-2}$	$208(4) \times 10^{-2}$
1.595	8	$1519(6) \times 10^{-4}$	$224(4) \times 10^{-2}$	$209(4) \times 10^{-2}$
1.5975	8	$1528(5) \times 10^{-4}$	$233(4) \times 10^{-2}$	$218(4) \times 10^{-2}$
1.6	8	$1562(5) \times 10^{-4}$	$249(4) \times 10^{-2}$	$234(4) \times 10^{-2}$
1.6025	8	$1568(5) \times 10^{-4}$	$247(4) \times 10^{-2}$	$232(4) \times 10^{-2}$
1.605	8	$1583(6) \times 10^{-4}$	$258(5) \times 10^{-2}$	$243(5) \times 10^{-2}$
1.6075	8	$1596(6) \times 10^{-4}$	$265(5) \times 10^{-2}$	$250(4) \times 10^{-2}$
1.61	8	$1628(6) \times 10^{-4}$	$276(4) \times 10^{-2}$	$261(4) \times 10^{-2}$
1.62	8	$1677(5) \times 10^{-4}$	$304(5) \times 10^{-2}$	$289(5) \times 10^{-2}$
1.63	8	$1764(7) \times 10^{-4}$	$342(6) \times 10^{-2}$	$329(6) \times 10^{-2}$
1.64	8	$186(1) \times 10^{-3}$	$411(8) \times 10^{-2}$	$396(8) \times 10^{-2}$
1.65	8	$1960(9) \times 10^{-4}$	$459(8) \times 10^{-2}$	$445(8) \times 10^{-2}$
1.66	8	$2095(9) \times 10^{-4}$	$544(9) \times 10^{-2}$	$529(9) \times 10^{-2}$
1.67	8	$223(1) \times 10^{-3}$	$63(1) \times 10^{-1}$	$61(1) \times 10^{-1}$
1.68	8	$241(1) \times 10^{-3}$	$72(1) \times 10^{-1}$	$70(1) \times 10^{-1}$
1.69	8	$261(2) \times 10^{-3}$	$83(1) \times 10^{-1}$	$82(1) \times 10^{-1}$
1.7	8	$281(2) \times 10^{-3}$	$93(1) \times 10^{-1}$	$92(1) \times 10^{-1}$
1.71	8	$303(2) \times 10^{-3}$	$104(1) \times 10^{-1}$	$102(1) \times 10^{-1}$
1.72	8	$328(2) \times 10^{-3}$	$111(1) \times 10^{-1}$	$110(1) \times 10^{-1}$
1.73	8	$350(1) \times 10^{-3}$	$116(1) \times 10^{-1}$	$114(1) \times 10^{-1}$
1.74	8	$376(2) \times 10^{-3}$	$121(1) \times 10^{-1}$	$119(1) \times 10^{-1}$
1.75	8	$404(3) \times 10^{-3}$	$121(1) \times 10^{-1}$	$120(1) \times 10^{-1}$
1.76	8	$433(3) \times 10^{-3}$	$118(1) \times 10^{-1}$	$117(1) \times 10^{-1}$
1.77	8	$454(2) \times 10^{-3}$	$118(1) \times 10^{-1}$	$116(1) \times 10^{-1}$
1.78	8	$485(2) \times 10^{-3}$	$108(1) \times 10^{-1}$	$107(1) \times 10^{-1}$
1.79	8	$511(2) \times 10^{-3}$	$100(1) \times 10^{-1}$	$98(1) \times 10^{-1}$
1.7925	8	$517(3) \times 10^{-3}$	$98(1) \times 10^{-1}$	$97(1) \times 10^{-1}$
1.795	8	$525(3) \times 10^{-3}$	$94(1) \times 10^{-1}$	$93(1) \times 10^{-1}$
1.7975	8	$528(3) \times 10^{-3}$	$95(1) \times 10^{-1}$	$94(1) \times 10^{-1}$
1.8	8	$536(3) \times 10^{-3}$	$91(1) \times 10^{-1}$	$90(1) \times 10^{-1}$
1.8025	8	$548(2) \times 10^{-3}$	$85(1) \times 10^{-1}$	$83(1) \times 10^{-1}$
1.805	8	$547(3) \times 10^{-3}$	$87(1) \times 10^{-1}$	$85(1) \times 10^{-1}$
1.8075	8	$551(2) \times 10^{-3}$	$84(1) \times 10^{-1}$	$82(1) \times 10^{-1}$
1.81	8	$562(2) \times 10^{-3}$	$80(1) \times 10^{-1}$	$79(1) \times 10^{-1}$
1.8125	8	$567(2) \times 10^{-3}$	$75(1) \times 10^{-1}$	$74(1) \times 10^{-1}$

Continued on next page

Table F.1 – *Continued from previous page*

U	L	ρ_m	χ_1	χ_2
1.815	8	$576(2) \times 10^{-3}$	$73(1) \times 10^{-1}$	$71(1) \times 10^{-1}$
1.8175	8	$579(3) \times 10^{-3}$	$71(1) \times 10^{-1}$	$70(1) \times 10^{-1}$
1.82	8	$588(2) \times 10^{-3}$	$69(1) \times 10^{-1}$	$68(1) \times 10^{-1}$
1.83	8	$606(2) \times 10^{-3}$	$59(1) \times 10^{-1}$	$57(1) \times 10^{-1}$
1.84	8	$623(2) \times 10^{-3}$	$520(10) \times 10^{-2}$	$506(10) \times 10^{-2}$
1.85	8	$639(2) \times 10^{-3}$	$441(8) \times 10^{-2}$	$428(8) \times 10^{-2}$
1.9	8	$7002(10) \times 10^{-4}$	$226(3) \times 10^{-2}$	$213(3) \times 10^{-2}$
1.95	8	$7371(7) \times 10^{-4}$	$153(2) \times 10^{-2}$	$140(2) \times 10^{-2}$
2.0	8	$7642(6) \times 10^{-4}$	$1153(9) \times 10^{-3}$	$1031(9) \times 10^{-3}$
1.4	10	$903(1) \times 10^{-4}$	$914(9) \times 10^{-3}$	$747(9) \times 10^{-3}$
1.5	10	$1150(2) \times 10^{-4}$	$141(2) \times 10^{-2}$	$125(2) \times 10^{-2}$
1.55	10	$1317(3) \times 10^{-4}$	$207(3) \times 10^{-2}$	$192(3) \times 10^{-2}$
1.56	10	$1358(3) \times 10^{-4}$	$237(5) \times 10^{-2}$	$220(5) \times 10^{-2}$
1.57	10	$1395(4) \times 10^{-4}$	$248(4) \times 10^{-2}$	$232(4) \times 10^{-2}$
1.58	10	$1447(4) \times 10^{-4}$	$289(5) \times 10^{-2}$	$273(5) \times 10^{-2}$
1.59	10	$1510(5) \times 10^{-4}$	$332(8) \times 10^{-2}$	$317(8) \times 10^{-2}$
1.5925	10	$1510(4) \times 10^{-4}$	$330(7) \times 10^{-2}$	$315(7) \times 10^{-2}$
1.595	10	$1523(4) \times 10^{-4}$	$355(6) \times 10^{-2}$	$340(6) \times 10^{-2}$
1.5975	10	$1546(5) \times 10^{-4}$	$365(7) \times 10^{-2}$	$350(7) \times 10^{-2}$
1.6	10	$1558(4) \times 10^{-4}$	$372(7) \times 10^{-2}$	$356(7) \times 10^{-2}$
1.6025	10	$1575(5) \times 10^{-4}$	$386(9) \times 10^{-2}$	$372(8) \times 10^{-2}$
1.605	10	$1604(7) \times 10^{-4}$	$435(10) \times 10^{-2}$	$420(9) \times 10^{-2}$
1.6075	10	$1605(6) \times 10^{-4}$	$435(10) \times 10^{-2}$	$420(10) \times 10^{-2}$
1.61	10	$1617(6) \times 10^{-4}$	$437(10) \times 10^{-2}$	$422(10) \times 10^{-2}$
1.62	10	$1716(7) \times 10^{-4}$	$57(1) \times 10^{-1}$	$56(1) \times 10^{-1}$
1.63	10	$1801(10) \times 10^{-4}$	$69(2) \times 10^{-1}$	$68(2) \times 10^{-1}$
1.64	10	$192(1) \times 10^{-3}$	$88(2) \times 10^{-1}$	$86(2) \times 10^{-1}$
1.65	10	$207(1) \times 10^{-3}$	$110(2) \times 10^{-1}$	$109(2) \times 10^{-1}$
1.66	10	$222(1) \times 10^{-3}$	$133(2) \times 10^{-1}$	$131(2) \times 10^{-1}$
1.67	10	$239(1) \times 10^{-3}$	$158(2) \times 10^{-1}$	$156(2) \times 10^{-1}$
1.68	10	$259(1) \times 10^{-3}$	$183(2) \times 10^{-1}$	$181(2) \times 10^{-1}$
1.69	10	$277(2) \times 10^{-3}$	$201(2) \times 10^{-1}$	$200(2) \times 10^{-1}$
1.7	10	$299(1) \times 10^{-3}$	$228(2) \times 10^{-1}$	$226(2) \times 10^{-1}$
1.71	10	$320(2) \times 10^{-3}$	$240(3) \times 10^{-1}$	$239(3) \times 10^{-1}$
1.72	10	$344(2) \times 10^{-3}$	$251(2) \times 10^{-1}$	$249(2) \times 10^{-1}$
1.73	10	$366(2) \times 10^{-3}$	$261(2) \times 10^{-1}$	$259(2) \times 10^{-1}$
1.74	10	$392(2) \times 10^{-3}$	$263(2) \times 10^{-1}$	$262(2) \times 10^{-1}$
1.75	10	$417(2) \times 10^{-3}$	$258(2) \times 10^{-1}$	$256(2) \times 10^{-1}$
1.76	10	$443(3) \times 10^{-3}$	$247(2) \times 10^{-1}$	$246(2) \times 10^{-1}$
1.77	10	$470(2) \times 10^{-3}$	$232(2) \times 10^{-1}$	$230(2) \times 10^{-1}$

Continued on next page

Table F.1 – *Continued from previous page*

U	L	ρ_m	χ_1	χ_2
1.78	10	$499(2) \times 10^{-3}$	$207(2) \times 10^{-1}$	$206(2) \times 10^{-1}$
1.79	10	$525(2) \times 10^{-3}$	$185(3) \times 10^{-1}$	$184(3) \times 10^{-1}$
1.7925	10	$532(2) \times 10^{-3}$	$176(3) \times 10^{-1}$	$174(3) \times 10^{-1}$
1.795	10	$538(2) \times 10^{-3}$	$170(3) \times 10^{-1}$	$168(3) \times 10^{-1}$
1.7975	10	$545(2) \times 10^{-3}$	$160(3) \times 10^{-1}$	$159(3) \times 10^{-1}$
1.8	10	$552(2) \times 10^{-3}$	$151(3) \times 10^{-1}$	$149(3) \times 10^{-1}$
1.8025	10	$558(2) \times 10^{-3}$	$145(3) \times 10^{-1}$	$144(3) \times 10^{-1}$
1.805	10	$568(2) \times 10^{-3}$	$133(3) \times 10^{-1}$	$131(3) \times 10^{-1}$
1.8075	10	$570(3) \times 10^{-3}$	$130(4) \times 10^{-1}$	$128(4) \times 10^{-1}$
1.81	10	$578(2) \times 10^{-3}$	$119(2) \times 10^{-1}$	$118(2) \times 10^{-1}$
1.8125	10	$586(2) \times 10^{-3}$	$110(2) \times 10^{-1}$	$109(2) \times 10^{-1}$
1.815	10	$590(2) \times 10^{-3}$	$102(3) \times 10^{-1}$	$101(3) \times 10^{-1}$
1.8175	10	$594(2) \times 10^{-3}$	$102(2) \times 10^{-1}$	$101(2) \times 10^{-1}$
1.82	10	$600(2) \times 10^{-3}$	$95(2) \times 10^{-1}$	$94(2) \times 10^{-1}$
1.83	10	$618(1) \times 10^{-3}$	$74(2) \times 10^{-1}$	$72(2) \times 10^{-1}$
1.84	10	$635(1) \times 10^{-3}$	$59(1) \times 10^{-1}$	$58(1) \times 10^{-1}$
1.85	10	$649(1) \times 10^{-3}$	$48(1) \times 10^{-1}$	$47(1) \times 10^{-1}$
1.86	10	$6622(9) \times 10^{-4}$	$406(6) \times 10^{-2}$	$392(6) \times 10^{-2}$
1.87	10	$6718(9) \times 10^{-4}$	$348(6) \times 10^{-2}$	$334(6) \times 10^{-2}$
1.9	10	$7012(7) \times 10^{-4}$	$236(3) \times 10^{-2}$	$223(3) \times 10^{-2}$
1.95	10	$7379(6) \times 10^{-4}$	$153(1) \times 10^{-2}$	$141(1) \times 10^{-2}$
2.0	10	$7658(4) \times 10^{-4}$	$1151(8) \times 10^{-3}$	$1029(8) \times 10^{-3}$
1.4	12	$903(1) \times 10^{-4}$	$949(9) \times 10^{-3}$	$782(8) \times 10^{-3}$
1.5	12	$1150(2) \times 10^{-4}$	$154(2) \times 10^{-2}$	$139(2) \times 10^{-2}$
1.55	12	$1316(3) \times 10^{-4}$	$244(4) \times 10^{-2}$	$228(4) \times 10^{-2}$
1.56	12	$1359(3) \times 10^{-4}$	$272(6) \times 10^{-2}$	$257(5) \times 10^{-2}$
1.57	12	$1398(3) \times 10^{-4}$	$306(6) \times 10^{-2}$	$291(6) \times 10^{-2}$
1.58	12	$1452(3) \times 10^{-4}$	$373(9) \times 10^{-2}$	$358(8) \times 10^{-2}$
1.59	12	$1502(4) \times 10^{-4}$	$46(1) \times 10^{-1}$	$45(1) \times 10^{-1}$
1.5925	12	$1515(4) \times 10^{-4}$	$46(1) \times 10^{-1}$	$45(1) \times 10^{-1}$
1.595	12	$1526(4) \times 10^{-4}$	$50(1) \times 10^{-1}$	$48(1) \times 10^{-1}$
1.5975	12	$1535(4) \times 10^{-4}$	$50(1) \times 10^{-1}$	$48(1) \times 10^{-1}$
1.6	12	$1558(4) \times 10^{-4}$	$53(1) \times 10^{-1}$	$52(1) \times 10^{-1}$
1.6025	12	$1567(5) \times 10^{-4}$	$58(2) \times 10^{-1}$	$56(2) \times 10^{-1}$
1.605	12	$1592(5) \times 10^{-4}$	$61(1) \times 10^{-1}$	$59(1) \times 10^{-1}$
1.6075	12	$1616(6) \times 10^{-4}$	$67(2) \times 10^{-1}$	$65(2) \times 10^{-1}$
1.61	12	$1619(4) \times 10^{-4}$	$68(2) \times 10^{-1}$	$66(2) \times 10^{-1}$
1.62	12	$1716(7) \times 10^{-4}$	$96(3) \times 10^{-1}$	$94(3) \times 10^{-1}$
1.63	12	$1819(8) \times 10^{-4}$	$127(4) \times 10^{-1}$	$125(4) \times 10^{-1}$
1.64	12	$194(1) \times 10^{-3}$	$163(4) \times 10^{-1}$	$162(4) \times 10^{-1}$

Continued on next page

Table F.1 – *Continued from previous page*

U	L	ρ_m	χ_1	χ_2
1.65	12	$2057(10) \times 10^{-4}$	$202(5) \times 10^{-1}$	$200(5) \times 10^{-1}$
1.66	12	$2255(9) \times 10^{-4}$	$264(4) \times 10^{-1}$	$263(4) \times 10^{-1}$
1.67	12	$242(1) \times 10^{-3}$	$312(4) \times 10^{-1}$	$311(5) \times 10^{-1}$
1.68	12	$2623(10) \times 10^{-4}$	$362(5) \times 10^{-1}$	$361(4) \times 10^{-1}$
1.69	12	$282(1) \times 10^{-3}$	$406(4) \times 10^{-1}$	$404(4) \times 10^{-1}$
1.7	12	$302(2) \times 10^{-3}$	$440(6) \times 10^{-1}$	$439(6) \times 10^{-1}$
1.71	12	$324(2) \times 10^{-3}$	$469(5) \times 10^{-1}$	$468(5) \times 10^{-1}$
1.72	12	$348(2) \times 10^{-3}$	$490(4) \times 10^{-1}$	$489(4) \times 10^{-1}$
1.73	12	$371(1) \times 10^{-3}$	$500(4) \times 10^{-1}$	$499(4) \times 10^{-1}$
1.74	12	$393(1) \times 10^{-3}$	$505(5) \times 10^{-1}$	$503(5) \times 10^{-1}$
1.75	12	$422(2) \times 10^{-3}$	$483(4) \times 10^{-1}$	$482(4) \times 10^{-1}$
1.76	12	$445(1) \times 10^{-3}$	$468(5) \times 10^{-1}$	$466(5) \times 10^{-1}$
1.77	12	$475(2) \times 10^{-3}$	$433(5) \times 10^{-1}$	$431(5) \times 10^{-1}$
1.78	12	$504(2) \times 10^{-3}$	$371(6) \times 10^{-1}$	$370(6) \times 10^{-1}$
1.79	12	$529(2) \times 10^{-3}$	$316(5) \times 10^{-1}$	$314(5) \times 10^{-1}$
1.7925	12	$539(2) \times 10^{-3}$	$285(5) \times 10^{-1}$	$284(5) \times 10^{-1}$
1.795	12	$541(2) \times 10^{-3}$	$279(8) \times 10^{-1}$	$278(8) \times 10^{-1}$
1.7975	12	$549(2) \times 10^{-3}$	$258(7) \times 10^{-1}$	$256(7) \times 10^{-1}$
1.8	12	$557(1) \times 10^{-3}$	$235(4) \times 10^{-1}$	$234(4) \times 10^{-1}$
1.8025	12	$561(2) \times 10^{-3}$	$230(5) \times 10^{-1}$	$228(5) \times 10^{-1}$
1.805	12	$570(2) \times 10^{-3}$	$202(5) \times 10^{-1}$	$201(5) \times 10^{-1}$
1.8075	12	$576(2) \times 10^{-3}$	$184(6) \times 10^{-1}$	$183(6) \times 10^{-1}$
1.81	12	$5841(9) \times 10^{-4}$	$163(3) \times 10^{-1}$	$161(3) \times 10^{-1}$
1.8125	12	$590(2) \times 10^{-3}$	$153(5) \times 10^{-1}$	$152(5) \times 10^{-1}$
1.815	12	$596(1) \times 10^{-3}$	$135(4) \times 10^{-1}$	$133(4) \times 10^{-1}$
1.8175	12	$598(1) \times 10^{-3}$	$128(5) \times 10^{-1}$	$127(5) \times 10^{-1}$
1.82	12	$6068(9) \times 10^{-4}$	$111(2) \times 10^{-1}$	$110(2) \times 10^{-1}$
1.83	12	$6228(9) \times 10^{-4}$	$83(2) \times 10^{-1}$	$81(2) \times 10^{-1}$
1.84	12	$640(1) \times 10^{-3}$	$62(2) \times 10^{-1}$	$60(2) \times 10^{-1}$
1.85	12	$6520(10) \times 10^{-4}$	$49(1) \times 10^{-1}$	$48(1) \times 10^{-1}$
1.9	12	$7023(6) \times 10^{-4}$	$235(2) \times 10^{-2}$	$222(2) \times 10^{-2}$
1.95	12	$7378(4) \times 10^{-4}$	$157(1) \times 10^{-2}$	$144(1) \times 10^{-2}$
2.0	12	$7654(4) \times 10^{-4}$	$1158(7) \times 10^{-3}$	$1035(7) \times 10^{-3}$
1.75	14	$416(2) \times 10^{-3}$	$88(1) \times 10^{0}$	$88(1) \times 10^{0}$

Bibliography

[1] F. Wilczek, Central Eur. J. Phys. **10**, 1021 (2012), arXiv:1206.7114 [hep-ph] .

[2] M. D. Schwartz, *Quantum Field Theory and the Standard Model* (Cambridge University Press, 2014).

[3] F. Halzen and A. D. Martin, *QUARKS AND LEPTONS: AN INTRODUCTORY COURSE IN MODERN PARTICLE PHYSICS* (1984).

[4] H. J. Munczek, Zeitschrift für Physik C Particles and Fields **32**, 585 (1986).

[5] B. Rosenstein, B. Warr, and S. H. Park, Phys. Rept. **205**, 59 (1991).

[6] M. E. Peskin and D. V. Schroeder, *An Introduction to quantum field theory* (1995).

[7] I.-H. Lee, J. Shigemitsu, and R. E. Shrock, Nucl.Phys. **B330**, 225 (1990).

[8] A. Hasenfratz and T. Neuhaus, Phys.Lett. **B220**, 435 (1989).

[9] A. Hasenfratz, W.-q. Liu, and T. Neuhaus, Phys.Lett. **B236**, 339 (1990).

[10] I.-H. Lee, J. Shigemitsu, and R. E. Shrock, Nucl.Phys. **B334**, 265 (1990).

[11] W. Bock, A. K. De, K. Jansen, J. Jersak, T. Neuhaus, and J. Smit, Nucl.Phys. **B344**, 207 (1990).

[12] Y. Nambu and G. Jona-Lasinio, Phys. Rev. **124**, 246 (1961).

[13] B. Rosenstein, B. J. Warr, and S. H. Park, Phys. Rev. **D39**, 3088 (1989).

[14] S. Chandrasekharan, Phys. Rev. **D82**, 025007 (2010), arXiv:0910.5736 [hep-lat] .

[15] S. Chandrasekharan, Eur. Phys. J. **A49**, 90 (2013), arXiv:1304.4900 [hep-lat] .

[16] S. Catterall, JHEP **01**, 121 (2016), arXiv:1510.04153 [hep-lat] .

[17] K. Slagle, Y.-Z. You, and C. Xu, Phys. Rev. B **91**, 115121 (2015).

[18] Y.-Y. He, H.-Q. Wu, Y.-Z. You, C. Xu, Z. Y. Meng, and Z.-Y. Lu, Phys. Rev. **B93**, 115150 (2016), arXiv:1508.06389 [cond-mat.str-el] .

[19] Y.-Y. He, H.-Q. Wu, Y.-Z. You, C. Xu, Z. Y. Meng, and Z.-Y. Lu, (2016), arXiv:1603.08376 [cond-mat.str-el] .

[20] H. J. Rothe, World Sci. Lect. Notes Phys. **43**, 1 (1992), [World Sci. Lect. Notes Phys.82,1(2012)].

[21] D. B. Kaplan, Phys. Lett. **B288**, 342 (1992), arXiv:hep-lat/9206013 [hep-lat] .

[22] D. B. Kaplan, in *Modern perspectives in lattice QCD: Quantum field theory and high performance computing. Proceedings, International School, 93rd Session, Les Houches, France, August 3-28, 2009* (2009) pp. 223–272, arXiv:0912.2560 [hep-lat] .

[23] J. Kogut and L. Susskind, Phys. Rev. D **11**, 395 (1975).

[24] H. Sharatchandra, H. Thun, and P. Weisz, Nucl.Phys. **B192**, 205 (1981).

[25] C. van den Doel and J. Smit, Nucl.Phys. **B228**, 122 (1983).

[26] N. Goldenfeld, *Lectures on phase transitions and the renormalization group* (1992).

[27] J. Zinn-Justin, Int. Ser. Monogr. Phys. **77**, 1 (1989).

[28] S. Dürr, Z. Fodor, J. Frison, C. Hoelbling, R. Hoffmann, S. D. Katz, S. Krieg, T. Kurth, L. Lellouch, T. Lippert, K. K. Szabo, and G. Vulvert, Science **322**, 1224 (2008), http://science.sciencemag.org/content/322/5905/1224.full.pdf .

[29] C. T. H. Davies, E. Follana, A. Gray, G. P. Lepage, Q. Mason, M. Nobes, J. Shigemitsu, H. D. Trottier, M. Wingate, C. Aubin, C. Bernard, T. Burch, C. DeTar, S. Gottlieb, E. B. Gregory, U. M. Heller, J. E. Hetrick, J. Osborn, R. Sugar, D. Toussaint, M. D. Pierro, A. El-Khadra, A. S. Kronfeld, P. B. Mackenzie, D. Menscher, and J. Simone (HPQCD and UKQCD Collaborations and MILC Collaboration and HPQCD and Fermilab Lattice Collaborations), Phys. Rev. Lett. **92**, 022001 (2004).

[30] C. Aubin, C. Bernard, C. T. H. Davies, C. DeTar, S. A. Gottlieb, A. Gray, E. B. Gregory, J. Hein, U. M. Heller, J. E. Hetrick, G. P. Lepage, Q. Mason, J. Osborn, J. Shigemitsu, R. Sugar, D. Toussaint, H. Trottier, and M. Wingate, Phys. Rev. D **70**, 031504 (2004).

[31] I. F. Allison, C. T. H. Davies, A. Gray, A. S. Kronfeld, P. B. Mackenzie, and J. N. Simone (HPQCD, Fermilab Lattice, and UKQCD Collaborations), Phys. Rev. Lett. **94**, 172001 (2005).

[32] H.-W. Lin, Chin. J. Phys. **49**, 827 (2011), arXiv:1106.1608 [hep-lat] .

[33] M. A. Stephanov and M. Tsypin, Phys.Lett. **B236**, 344 (1990).

[34] M. A. Stephanov and M. Tsypin, Phys.Lett. **B242**, 432 (1990).

[35] V. Ayyar and S. Chandrasekharan, Phys. Rev. **D91**, 065035 (2015), arXiv:1410.6474 [hep-lat] .

[36] M. F. Golterman and J. Smit, Nucl.Phys. **B245**, 61 (1984).

[37] V. Ayyar and S. Chandrasekharan, (2016), arXiv:1606.06312 [hep-lat] .

[38] C. M. Bender, F. Cooper, and G. S. Guralnik, Annals Phys. **109**, 165 (1977).

[39] R. T. Scalettar, D. J. Scalapino, and R. L. Sugar, Phys. Rev. **B34**, 7911 (1986).

[40] S. Chandrasekharan and A. Li, Phys. Rev. Lett. **108**, 140404 (2012), arXiv:1111.7204 [hep-lat] .

[41] S. Chandrasekharan and A. Li, Phys. Rev. **D85**, 091502 (2012), arXiv:1202.6572 [hep-lat] .

[42] S. Chandrasekharan and A. Li, *Proceedings, 29th International Symposium on Lattice field theory (Lattice 2011)*, PoS **LATTICE2011**, 058 (2011), arXiv:1111.5276 [hep-lat] .

[43] E. Huffman, (2016), private communication .

[44] M. Maggiore, *A Modern Introduction to Quantum Field Theory*, Oxford Master Series in Physics (OUP Oxford, 2004).

[45] K. Riley, M. Hobson, and S. Bence, *Mathematical Methods for Physics and Engineering: A Comprehensive Guide* (Cambridge University Press, 2006).

[46] M. Creutz, L. Jacobs, and C. Rebbi, Phys. Rev. Lett. **42**, 1390 (1979).

[47] C. M. Bishop, *Pattern Recognition and Machine Learning (Information Science and Statistics)* (Springer-Verlag New York, Inc., Secaucus, NJ, USA, 2006).

[48] K. P. Murphy, *Machine Learning: A Probabilistic Perspective* (The MIT Press, 2012).

[49] E. F. Huffman and S. Chandrasekharan, Phys. Rev. **B89**, 111101 (2014), arXiv:1311.0034 [cond-mat.str-el] .

[50] W. Bietenholz, A. Pochinsky, and U. J. Wiese, Phys. Rev. Lett. **75**, 4524 (1995).

[51] S. Chandrasekharan and U.-J. Wiese, Phys. Rev. Lett. **83**, 3116 (1999), arXiv:cond-mat/9902128 [cond-mat] .

[52] S. Chandrasekharan, J. Cox, J. C. Osborn, and U. J. Wiese, Nucl. Phys. **B673**, 405 (2003), arXiv:cond-mat/0201360 [cond-mat.str-el] .

[53] G. Parisi and Y.-s. Wu, Sci. Sin. **24**, 483 (1981).

[54] M. Cristoforetti, F. Di Renzo, A. Mukherjee, and L. Scorzato, Phys. Rev. **D88**, 051501 (2013), arXiv:1303.7204 [hep-lat] .

[55] V. Azcoiti, G. Di Carlo, A. Galante, and V. Laliena, Phys. Rev. Lett. **89**, 141601. 4 p (2002).

[56] L. Bongiovanni, *Numerical methods for the sign problem in Lattice Field Theory*, Ph.D. thesis, Swansea U. (2015), arXiv:1603.06458 [hep-lat] .

[57] M. Newman and G. Barkema, *Monte Carlo Methods in Statistical Physics* (Clarendon Press, 1999).

[58] N. Prokof'ev and B. Svistunov, in *Understanding Quantum Phase Transitions, Lincoln D. Carr,ed. Taylor & Francis, Boca Raton, 2010* (2009) arXiv:0910.1393 [cond-mat.stat-mech] .

[59] Q. Liu, Y. Deng, and T. M. Garoni, Nucl. Phys. **B846**, 283 (2011), arXiv:1011.1980 [cond-mat.stat-mech] .

[60] R. Pordes *et al.*, J. Phys. Conf. Ser. **78**, 012057 (2007).

[61] I. Sfiligoi, D. C. Bradley, B. Holzman, P. Mhashilkar, S. Padhi, and F. Wurthwein, WRI World Congress on Computer Science and Information Engineering **2**, 428 (2009).

[62] H. Ricardo, *A Modern Introduction to Linear Algebra*, A Chapman & Hall book (CRC Press, 2009).

[63] V. Ayyar and S. Chandrasekharan, Phys. Rev. D **93**, 081701 (2016).

[64] M. F. L. Golterman, D. N. Petcher, and E. Rivas, Nucl. Phys. **B395**, 596 (1993), arXiv:hep-lat/9206010 [hep-lat] .

[65] E. Eichten and J. Preskill, Nucl. Phys. **B268**, 179 (1986).

Biography

Venkitesh Padmanabha Ayyar was born on October 22 1985 in Mumbai, India. He received a Bachelor of Science degree in Physics from Mumbai University in June 2008. He received a Master of Science degree in Physics from Indian Institute of Technology (IIT) Bombay in June 2010. He graduated from Duke University in 2016 with his PhD in Physics.

Publications

1. **V. Ayyar**, S. Chandrasekharan, Fermion masses through four-fermion condensates, arXiv:1606.06312, (2016).
2. **V. Ayyar**, S. Chandrasekharan, Origin of fermion masses without spontaneous symmetry breaking, Phys. Rev. D 93, 081701(R) (2016).
3. **V. Ayyar**, S. Chandrasekharan, Massive fermions without fermion bilinear condensates, Phys. Rev. D 91, 065035 (2015).
4. **V. Ayyar**, Berndt Muller, Approach to equilibrium in the Caldeira-Leggett Model, Int.J.Mod.Phys. E22, 1350016 (2013).